Performance Evaluation and Enhancement in 5G Networks : A Stochastic Geometry Approach

by

Anqi He

Doctor of Philosophy

School of Electronic Engineering and Computer Science
Queen Mary University of London
United Kingdom

2016

Abstract

The deployment of heterogeneous networks (HetNets), in which low power nodes (LPNs) and high power nodes (HPNs) coexist, has become a promising solution for extending coverage and increasing capacity in wireless networks. Meanwhile, several advanced technologies such as massive multi-input multi-output (MIMO), cloud radio access networks (C-RAN) and device-to-device (D2D) communications have been proposed as competent candidates for supporting the next generation (5G) network. Since single technology cannot solely achieve the envisioned 5G requirements, the effect of integrating multiple technologies in one system is worth to be investigated. In this thesis, a thoroughly theoretical analysis is conducted to evaluate the network performance in different scenarios, where two or more 5G techniques are employed.

First, the downlink performance of massive MIMO enabled HetNets is fully evaluated. The exact and asymptotic expressions for the probability of a user being associated with a macro cell or a small cell are presented. The analytical expressions for the spectrum efficiency (SE) and energy efficiency (EE) in the K-tier network are also derived. The analysis reveals that the implementation of massive MIMO in the macro cell can considerably improve the network performance and decrease the demands for small cells in HetNets, which simplifies the network deployment.

Then, the downlink performance of a massive MIMO enabled heterogeneous C-RAN is investigated. The exact expressions for the SE and EE of the remote radio heads (RRHs) tier and a tractable approximation approach for evaluating the SE and EE of the macrocell tier are obtained. Numerical results collaborate the analysis and prove that massive MIMO with dense deployment of RRHs can significantly enhance the performance of heterogeneous C-RAN theoretically.

Next, the uplink performance of massive MIMO enabled HetNets is exploited with interference management via derived SE and EE expressions. The numerical results show that the uplink performance in the massive MIMO macrocells can be significantly improved through uplink power control in the small cells, while more uplink transmissions in the macrocells have mild adverse effect on the uplink performance of the small cells. In addition, the SE and EE of the massive MIMO macrocells with heavier load can be improved by expanding the small cell range.

Lastly, the uplink performance of the D2D underlaid massive MIMO network is investigated and a novel D2D power control scheme is proposed. The average uplink achievable SE and EE expressions for the cellular and D2D are derived and results demonstrate that the proposed power control can efficiently mitigate the interference from the D2D. Moreover, the D2D scale properties are obtained, which provide the sufficient conditions for achieving the anticipated SE. The results demonstrate that there exists the optimal D2D density for maximizing the area SE of D2D tier. In addition, the achievable EE of a cellular user can be comparable to that of a D2D user.

Stochastic geometry is applied to model all of the systems mentioned above. Monte Carlo simulations are also developed and conducted to validate the derived expressions and the theoretical analysis.

Acknowledgments

First and foremost, I would like to express my greatest gratitude to my supervisor Prof. Yue Chen for her strongest support to my Ph.D life. As an excellent role model, she presented huge enthusiasms towards work and life which encouraged me all the time. I would also like to thank her valuable technical guidance and priceless suggestions on both my research and daily lives. I feel extremely lucky to be her student because she is the best supervisor can be ever imagined.

I would also like to use this opportunity to express my sincere gratitude to my family who always supports me selflessly. My parents gave me infinite courage and energy to insist on my work and to overcome every difficulty I encountered.

I would like to express my special thanks to Dr. Kok Keong Chai, Dr. Miles Hansard, Dr. Maged Elkashlan, Dr. Tiankui Zhang (Beijing University of Posts and Telecommunications) and Prof. Kai-Kit Wong (University of College London) for their valuable comments and advices on my research work in terms of both technical development and writing skills.

I would like to thank Prof. Zhiguo Ding (Lancaster University) and Dr. Vasilis Friderikos (King's College London) for serving as my Ph.D examiners.

Last but not least,I would like to express my warm thanks to my colleagues and friends: Dr. Lifeng Wang, Dr. Dan Zhao, Dr. Dantong Liu, Dr. Lexi Xu, Dr. Yuanwei Liu, Dr. Xinyue Wang, Dr. Yansha Deng, Dr. Xingyu Han, Dr. Yun Li, Dr. Xueke Lv, Dr. Zhijin Qin, Shenglan Huang, Liumeng Song, Aini Li, Jie Deng, Jingjing Zhao, Bingyu Xu, Yanru Wang, Yiming Wang and Yuhang Dai among others. I feel really thankful for their selfless helps and supports during my Ph.D lives. I wish all of them the best in their future career and life.

Table of Contents

List of Figures

List of Tables

List of Abbreviations

5G	Fifth Generation
AP	Access Point
BBU	Base Band Unit
BS	Base Station
CA	Carrier Aggregation
CAPEX	Capital Expenditure
CLPC	Close Loop Power Control
CoMP	Coordinated Multipoint
CRAN	Cloud Radio Access Network
CRE	Cell Range Expansion
CSI	Channel State Information
D2D	Device-to-Device
DUE	D2D User
EE	Energy Efficiency
FFR	Fractional Frequency Reuse
HetNet	Heterogeneous Network
HCN	Heterogeneous Cellular Network
HC-RAN	Heterogeneous Cloud Radio Access Network
HPN	High Power Node
HPPP	Homogeneous Poisson Point Process

ICT	Information and Communications Technologies
KPI	Key Performance Indicator
LPN	Low Power Node
LTE	Long Term Evolution
LTE-A	Long Term Evolution Advanced
MBS	Macro Base Stations
MC	Monte Carlo
MIMO	Multi-input Multi-output
MUE	Macro User
OFDM	Orthogonal Frequency Division Multiplexing
OLPC	Open Loop Power Control
OPEX	Operating Expenditure
PBS	Pico Base Station
PGFL	Probability Generating Functional
PPP	Poisson Point Process
PUE	Pico User
RRH	Remote Radio Head
RB	Resource Block
SBS	Small Base Station
SE	Spectrum Efficiency
S-FFR	Soft Fractional Frequency Reuse
SINR	Signal to noise plus interference ratio
TDD	Time Division Duplexing
UE	User Equipment
VT	Voronoi Tessellation
ZFBF	Zero-forcing Beamforming

Chapter 1

Introduction

1.1 Background

Attributed to the proliferation of smart phones and thousands of instant social networking services, the wireless industry has taken on the challenge of supporting a 1000-fold increase in traffic demand with 10-fold increase in spectrum efficiency (SE) and energy efficiency (EE) [WHG+14]. Nevertheless, existing network deployment and radio technology such as carrier aggregation (CA), multiple-input multiple-output (MIMO) with up to 8×8 antenna arrays are approaching their theoretical limits, which cannot satisfy the user requirements envisioned before 2020 [SSD+09]. Moreover, the energy consumption from the industry of telecommunications keeps at a high level, EE must be regarded as one of the key performance indicators (KPIs) in the network design in addition to traditional emphasis on maximising data rate or SE [CZXL11, HQ14, CLRH+14]. In order to address the issues raised by wireless traffic explosion and energy consumption escalation over the next decade, the next generation mobile and wireless communication architecture and technologies are emerging into research fields.

From the perspective of the architecture, both the heterogeneous network (HetNet) and cloud radio access network (C-RAN) are envisioned as candidates for achieving 5G network requirements. Specifically, the HetNets, with the co-deployment of high power nodes (HPNs) and low power nodes (LPNs), have been introduced in the long term evolu-

tion advanced (LTE-A) standardization and promise a solution to provide great capacity gains and coverage extensions [LPGdlR+11]. Thus the next generation, as known as the fifth generation (5G) network should continue to be deployed as a heterogeneous one. As for the C-RAN, which separates the network into baseband unit (BBU) pool and remote radio heads (RRHs), becomes a trending network. This kind of architecture can provide high network efficiency while reduce capital expenditure (CAPEX) and operating expenditure (OPEX) based on the cloud computing technology [PLZW15].

At the same time, a series of advanced techniques, which are capable of enabling 5G wireless communications such as massive multiple input multiple output (MIMO) transmission and device-to-device (D2D) communications [BHL+14, GJ15, HH15a, JMZ+14], have been highlighted in both academic and industry area. The benefits and challenges of these technologies have been solely investigated in amounts of research works but the effects of integrating two or more techniques in one network scenario have not been fully studied. Moreover, it is necessary to quantify the KPIs such as SE and EE as mathematical expressions in such a highly integrative network, for providing the 5G network deployment with theoretical basis.

1.2 Research Motivations

Although the HetNet has been viewed and deployed as a powerful architecture since the 4G (LTE) network, its complexity brings challenges on both network planning and performance evaluation. On the one hand, base stations (BSs) in multi-tier networks are likely to have distinctly different features in terms of transmit power, tower height and user density. Their locations are also subject to uncertainties. On the other hand, the dense network deployment will lead to strong inter-tier and intercell interference resulting in large network performance loss, which limits the heterogeneous architecture to achieve the stringent 5G requirements. Therefore, the design of the 5G network should be based on a combination of network topology innovations and radio technology

evolutions [BTAS14].

A series of advanced techniques have been proposed and regarded as 5G enablers [CZXL11, ABC+14]. For instance, the C-RAN is envisioned as another candidate architecture that can make dense networks possible along with HetNets; a massive MIMO enabled network, in which macro BSs are equipped with large number of antennas, can achieve high SE and EE gain without jeopardizing existing investments; underlying D2D communication in cellular networks enables the devices in proximity to communicate directly for traffic offloading, whereby further enhance the network performance. Due to the fact that none of the above mentioned technology can solely achieve the stringent 5G requirements, it is necessary to integrate two or more of them in one system. However, few performance evaluations in such a complex network can be found in existing literatures.

To conduct a theoretical performance evaluation, network simulations are limited by the calculation power to be developed on a large scale. Therefore, it is necessary to quantify the network KPIs via deriving mathematical expressions. Based on the expressions, the performance of a system model can be evaluated via varying the related parameters. While the conventional hexagonal system models are hard to accurate depict a multi-tier architecture, the stochastic geometry approach, which based on point process distributions, has gained increasing popularity for modelling wireless networks. Moreover, using the mathematical tools from the stochastic geometry is able to derive tractable expressions for the network performance metrics such as coverage, SE and EE.

Motivated by above mentioned technical issues, a further investigation on the 5G network in which integrates cutting-edge architectures and technologies is conducted in this thesis. Exact or approximated closed-form expressions of KPIs in different scenarios are derived in a stochastic geometry approach. The impact of various parameters related to the network infrastructure and underlying system assumptions on network performance are clearly addressed.

1.3 Research Contributions

This research work theoretically evaluates and enhances network performance mainly in terms of SE and EE in 5G networks. To provide a thoroughly analysis, different system models incorporating with avant-garde technologies and architectures are proposed and compared. A series of theorems, corollaries are obtained and provided for performance evaluation. Specifically, based on a stochastic geometry approach, the performance metrics such as SE and EE of massive MIMO, C-RAN or D2D communications enabled networks are characterized through derived tractable theoretical expressions. Then the effectiveness of these techniques can be addressed via varying the parameters such as tiers' density, number of antennas and power consumption. In addition, interference management mechanisms are applied in different scenarios to figure out the trade-offs when multiple technologies coexist. Observations from the derived expressions and numerical results can provide operators with a guidance to deploy the next generation networks. The contributions in each chapter are summarised as follows:

- The potentials of massive MIMO in downlink K-tier HetNets for enhancing coverage, SE and EE are explored thoroughly. Exact and asymptotic expressions for the probability of a user being associated with a macro base station (MBS) or small base station (SBS) are first derived. Then, an exact expression for examining SE and EE of massive MIMO enabled HetNets without cell range expansion (CRE) is derived and analysed. Next, lower bound expressions of SE and EE of massive MIMO enabled HetNets with CRE applied in small cells are derived and verified. The impact of system parameters such as tier's density and BS transmit power on user association is explicitly identified.

- A massive MIMO enabled heterogeneous C-RAN (HC-RAN) is proposed for improving SE and EE during the downlink transmission. In this network, the soft fractional frequency reuse (S-FFR) is employed for interference mitigation. Tractable expressions are derived for evaluating the lower bounds of area throughput and

EE in the specific scenario. The obtained results can well characterize the impacts of key system parameters such as number of MBS antennas, remote radio head (RRH) tiers density, and S-FFR factor on the network design.

- The uplink performance of the proposed massive MIMO aided HCNs is evaluated in terms of SE and EE. The open loop power control (OLPC) for interference coordination and CRE for traffic offloading are exploited. Theoretical expressions of SE and EE are derived for the macrocell users and picocell users. Results clearly demonstrate the effectiveness of applying uplink power control and CRE in the small cells.

- A spatially dynamic power control policy for mitigating the cellular-to-D2D and D2D-tocellular interference is introduced. In particular, the proposed D2D power control policy is rather flexible including the special cases of no D2D links or using maximum transmit power. Under the considered power control, the exact expressions of SE for a cellular user or D2D transmitter are derived, which quantify the impacts of key system parameters such as massive MIMO antennas and D2D density. Moreover, the D2D scale properties are obtained, which provide the sufficient conditions for achieving the anticipated SE. Numerical results show that the proposed power control solution can efficiently mitigate interference between the cellular and D2D tier. The results demonstrate that there exists the optimal D2D density for maximizing the area SE of D2D tier.

1.4 Thesis Outline

The rest of the thesis is organised as follows:

Chapter 2 introduces the commonly used system models, channel model and performance metrics as well as principles of stochastic geometry for performance evaluation. Then, it gives the definitions of the cutting-edge architectures and techniques that have

potentials for enabling 5G wireless networks. Interference management mechanisms in 5G networks are also introduced. The benefits and challenges of each technology are summarised and relative technical literatures are reviewed.

Chapter 3 gives in detail about the downlink performance of massive MIMO enabled HetNets. The first section explores the impact of massive MIMO on users association, coverage and SE in a K-tier HetNet based on the derived expressions. The second section considers the CRE in the small cells for offloading macro cells. New tractable expressions for performance metrics are derived and the impact of bias factor and massive MIMO on SE and EE are addressed respectively.

Chapter 4 conducts in a statistical system model where the massive MIMO incorporates with heterogeneous C-RAN. S-FFR is employed to mitigate the inter-tier interference. Exact and approximated expressions are derived for the throughput and EE of RRHs tier and MBSs tier. The co-effect of massive MIMO and C-RAN in such a heterogeneous architecture is comprehensively demonstrated. The impact of S-FFR on the network throughput is also explained.

Chapter 5 accounts for the uplink transmission in massive MIMO enabled HetNets. Since the macrocell users' (MUEs') uplink performance will be hampered seriously by inter-tier interference from small cells, both OLPC and CRE are applied on the LPNs. With the derived expressions for network SE, the influence of OLPC and CRE on performance in such a network is clearly illustrated.

Chapter 6 considers the co-existence of massive MIMO cellular networks and D2D transmission. The interplay between massive MIMO and D2D after applying power control on both CUEs and DUEs are analysed comprehensively, where the power control mechanism applied on DUEs is originally proposed. Exact and asymptomatic expressions are both derived to support the analysis. The impact of D2D density, user numbers and power control compensation factors on SE and EE are demonstrated.

Chapter 7 gives the conclusion of this thesis and discusses the future work directions.

1.5 Publications List

Journal Paper

1. **Anqi He**, Lifeng Wang, Yue Chen, Kai-Kit Wong, and Maged Elkashlan. " Spectral and Energy Efficiency of Uplink D2D Underlaid Massive MIMO Cellular Networks", *IEEE Transactions on Communications*.

2. **Anqi He**, Lifeng Wang, Yue Chen, Kai-Kit Wong, and Maged Elkashlan. "Uplink Interference Management in Massive MIMO Heterogeneous Cellular Networks", in *IEEE Wireless Communications Letters*, vol. 5, no. 5, pp. 560-563, Oct. 2016.

3. **Anqi He**, Lifeng Wang, Yue Chen, Maged Elkashlan, and Kai-Kit Wong. "Spectrum and Energy Efficiency in Massive MIMO Enabled HetNets: A Stochastic Geometry Approach", in *IEEE Communications Letters*, vol.19, no.12, pp.2294-2297, Dec. 2015.

Conference Papers

1. **Anqi He**, Lifeng Wang, Yue Chen, Kai-Kit Wong and Maged Elkashlan. "SE and EE of Uplink D2D Underlaid Massive MIMO Cellular Networks with Power Control", *IEEE Wireless Communications and Networking Conference (WCNC),2017* .

2. Xiangyu He, **A.He**, Yue Chen, K.K.Chai, Tiankui Zhang, "Energy Efficient Resource Allocation in Heterogeneous Cloud Radio Access Networks", *IEEE Wireless Communications and Networking Conference (WCNC), 2017* .

3. **Anqi He**, Lifeng Wang, Yue Chen, Kai-Kit Wong and Maged Elkashlan. "Throughput and Energy Efficiency for S-FFR in Massive MIMO enabled Heterogeneous C-RAN", *IEEE Global Communications Conference (GLOBECOM), 2016* .

4. **Anqi He**, Lifeng Wang, Yue Chen, Maged Elkashlan, and Kai-Kit Wong."Massive

MIMO in K-tier Heterogeneous Cellular Networks: Coverage and Rate", *IEEE Global Communications Conference (GLOBECOM)*, San Diego, CA, 2015, pp. 1-6.

5. **Anqi He**, Lifeng Wang, Yue Chen, Miles Hansard and Tiankui Zhang. "Comparison of CoMP and MISO for Energy Efficiency in HetNets",*IEEE Wireless Communications and Networking Conference (WCNC)Workshops*, New Orleans, LA, 2015, pp. 352-357.

6. **Anqi He**, Dantong Liu, Yue Chen and Tiankui Zhang. "Stochastic Geometry Analysis of Energy Efficiency in HetNets with Combined CoMP and BS Sleeping", *IEEE 25th Annual International Symposium on Personal, Indoor, and Mobile Radio Communication (PIMRC)*, Washington DC, 2014, pp. 1798-1802.

Chapter 2

Fundamental Concepts and State-of-the-Art

2.1 Overview

This chapter first introduces the commonly used system models, channel model and performance metrics for performance evaluation. Then the fundamentals of stochastic geometry analysis are presented. Next, the concepts of several candidate architectures and technologies for enabling 5G networks are demonstrated. Meanwhile, the recent related research achievements are reviewed and summarised.

2.2 Modelling and Analysis in Cellular networks

2.2.1 System Model

System modelling is the first step to conduct network analysis and performance evaluation. An appropriate system model can characterise the network with the best estimation while simplify the experiment process for theoretical analysis. Meanwhile, the insights given from theoretical analysis can provide operators with a reliable and effective guidance for network planning in practical scenarios.

2.2.1.1 Single-Cell Model

A single cell system model usually contains one base station (BS) (or one typical user) centred at the origin point and has circular coverage with a radius R. Then multiple users (or BSs) are distributed inside and outside the circular disk. For example, Figure 2.1 from [BSHD15] shows a BS centric single cell model, where a BS with large-scale antennas is located at the origin and user locations therein are selected from an arbitrary random distribution.

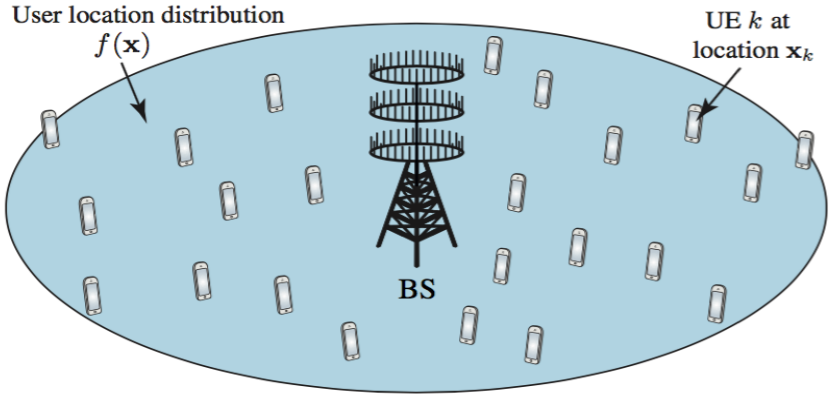

Figure 2.1: A base station centric single cell system model [BSHD15]

Figure 2.2 from [KHXR15] shows a user centric single cell model where a typical user is located at the origin while a MBS is located at a distance R away from the user. Then a group of radio access heads (RRHs) are distributed randomly around the user within its coverage region to provide service. Note that the distribution of the distance between the user and RRHs will change when distance R between the user and the MBS changes.

Single centred models are simple to implement in simulation process but the inter cell interference and inter tier interference are ignored. For example, signal-to-noise ratio (SNR) instead of signal-to-interference-plus-noise ratio (SINR) is considered in [KHXR15] for outage probability analysis. Therefore, single-cell system models are preferred in interference-limited scenarios or utilised at the early stage of research when a technology or a concept is newly introduced [PZJ+15, ZDO+14, LLAH15, SBK+15].

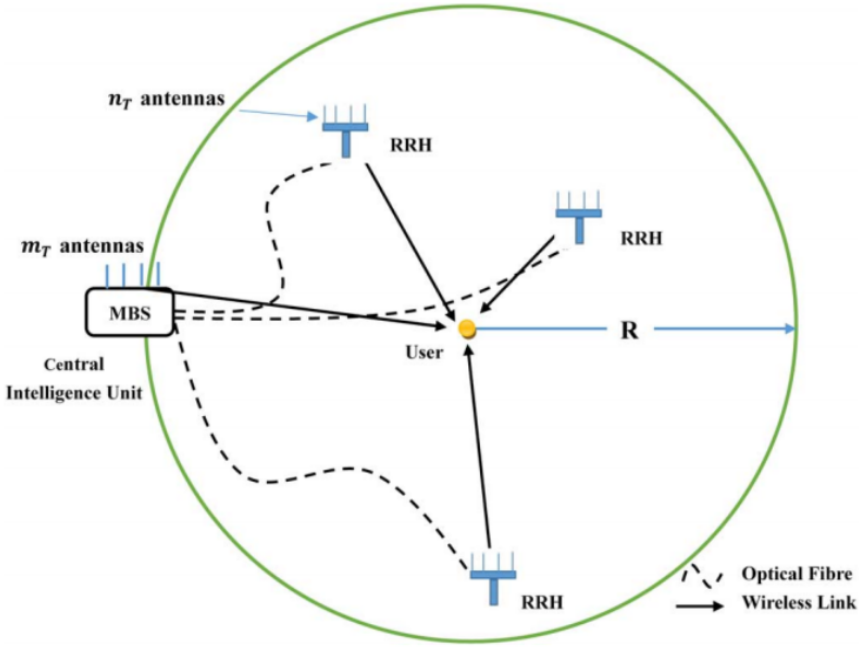

Figure 2.2: A user centric single cell system model [KHXR15]

2.2.1.2 Multi-Cell Model with Symmetric Distribution

Square-based (Figure 2.3) or honeycomb-based (Figure 2.4) system models, where multiple MBSs are placed deterministically, are normally regarded as symmetric system models. Taking a multi-cell simulation scenario from [BSHD15] as an example, each MBS in Figure 2.3 has a fixed location and each macrocell has the same size. Users are distributed uniformly in each cell and the distance between the serving BSs and users are defined as constant values. Only the interference that arrives from the two closest cells (in each direction) are considered.

After determining the appropriate parameters, a symmetric multi-cell system model is easy to be implemented in Monte Carlo simulations. However, the obtained numerical results are too idealised and can only provide upper bounds of the related performance metrics. Moreover, Monte Carlo simulated results are not very tractable since the fundamental properties cannot be separated from behaviours induced by parameter selection. Hence, the symmetric distributions are preferred for studying the network potential gains

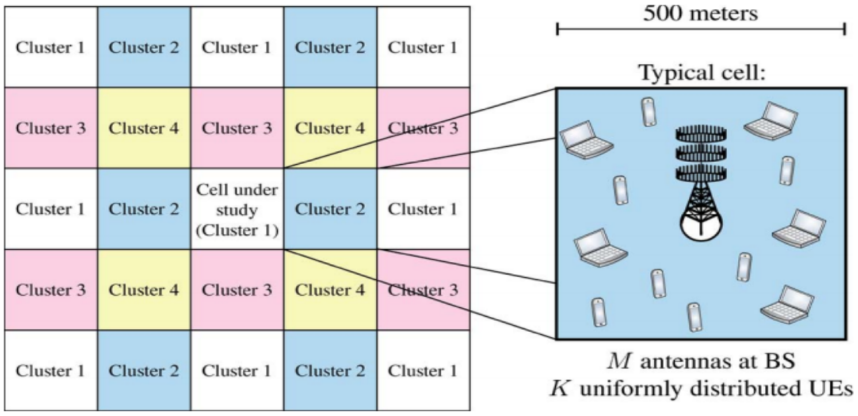

Figure 2.3: A grid-based multi cell system model [BSHD15]

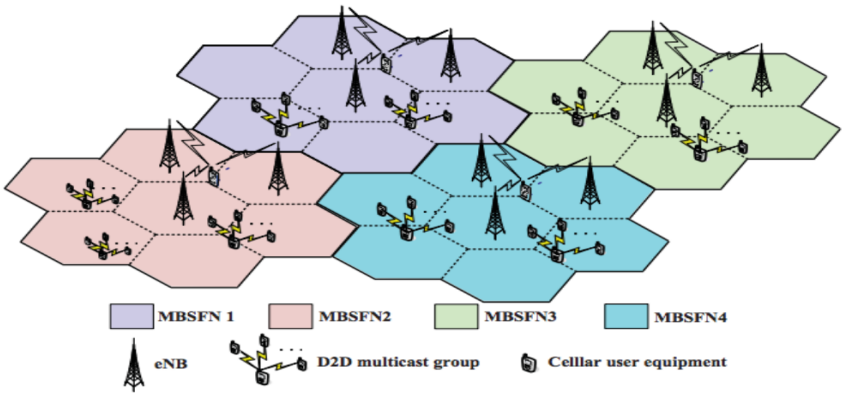

Figure 2.4: A honeycombe-based multi cell system model [GWLH14]

in homogeneous networks, but far from realistic when it comes to HetNets.

2.2.1.3 Multi-Cell Model with Random Distribution

In a multi-cell model with random distribution, locations of BSs can be modelled as a homogeneous Poisson point process (HPPP) [1]. Instead of using parameters empirically perceived by experts, the network deployment for BSs and users who based on PPP is absolutely autonomous and uncoordinated. Such an approach for BS modelling has been

[1] A point process $\prod = \{x_i; i = 1, 2, 3, ...\} \subset R_d$ is a PPP if and only if the number of points inside any compact set $B \subset R_d$ is a Poisson random variable, and the numbers of points in disjoint sets are independent.

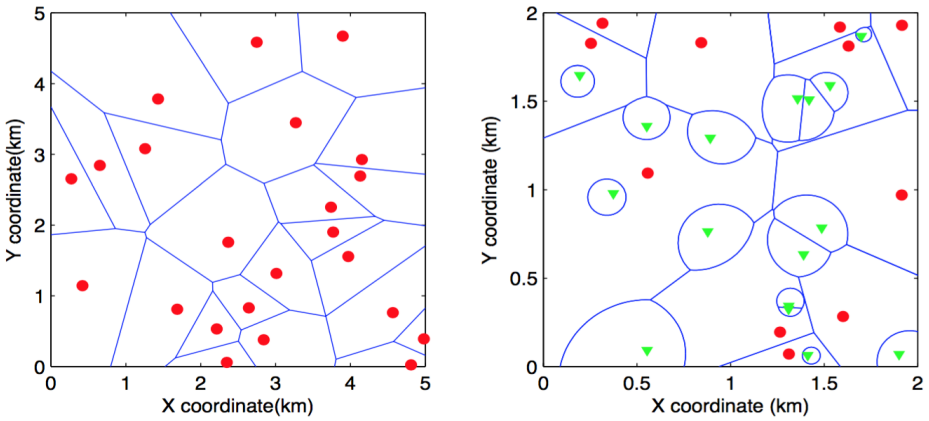

Figure 2.5: This figure compares the deployment of a homogeneous network and a two-tier HetNet where red points represent HPNs and green triangles represent LPNs. The cell boundaries are shown and form a Voronoi Tessellation.

considered as early as 1997 in [BKLZ97], which is suitable for HetNets modelling where the deployment of small cells are far from symmetric distribution.

In PPP based spatial distribution, the network performance is basically characterised through the density, which is the expected number of points of the process per unit area. Take the Figure 2.5 as an example, a homogeneous network and a heterogeneous network are shown in which the BSs are distributed following PPP. This figure clearly reflects the randomness of BSs locations and the differences in the coverage among different tiers. Moreover, compared to the real data in terms of BS distributions in Figure 2.6 from [DGBA12b], the PPP based system model can well characterise the actual 4G macro cells deployment.

Another benefit of PPP based system model is that the intercell interference can be well characterised with the assistance of tools from stochastic geometry, which will be explained in detail in Section 2.2.3. The main limitation of the Poisson model is that because of the independence of the PPP, BSs will in some cases be located very close together but with a significant coverage area [ABG11]. However, this weakness is balanced by two strengths: the natural inclusion of different cell sizes and shapes and

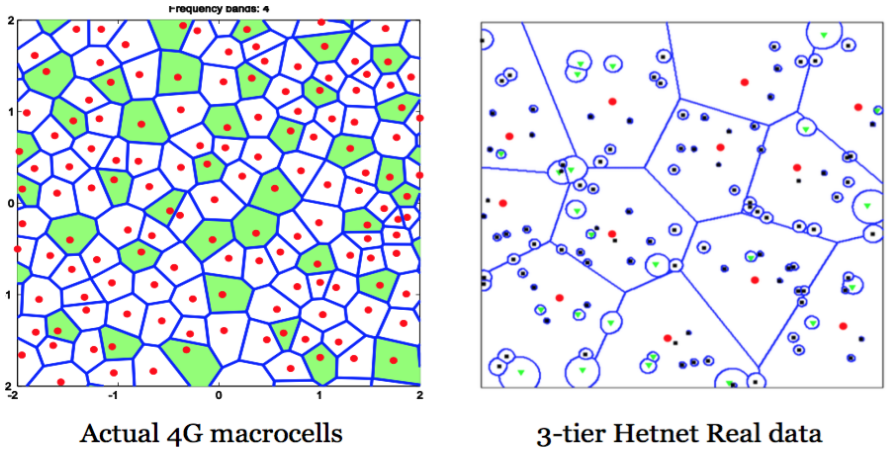

Figure 2.6: The actual macrocells distribution in 4G and 3-tier HetNets distribution with real data [DGBA12b]

the lack of edge effects, i.e. the network extends indefinitely in all directions. To break into a new area, more point process models such as hard core point process, Poisson cluster process [EHH13] can be applied in the future work.

2.2.2 Channel Model and Performance Metrics

The signal-to-noise-plus-interference ratio (SINR) is used to measure the signal power compared to the noise and interference power. It can also reflect the quality of the transmission channel. Take the downlink transmission as an example. Without any loss of generality, the typical user is assumed to be located at the origin. Then, the SINR of the typical user, at a random distance d from its associated BS can be expressed as

$$\text{SINR} = \frac{P_t h d^{-\alpha}}{I_r + \sigma^2} \tag{2.1}$$

where $I_r = \sum_{i \in \Phi / b_o} P_i g_i d_i^{-\alpha}$ is the cumulative interference from all the other BSs (except the serving BS for the typical user at the origin denoted by b_o). P_t and P_i are the transmitted signal power of the serving BS and interfering BSs respectively. $d^{-\alpha}$ is the large-scale fading caused by signal attenuation during the signal transmission

over large distances and α is the path loss exponent. d_i [2] is the distance between the interfering BS and the typical user. h and g_i represents the value of the small-scale fading and shadowing [3]. σ^2 is regarded as additive Gaussian white noise with a constant value.

It is indicated from the above equation that the received signal strength of a typical user is substantially affected by the transmit power, distance between users and BSs as well as the interference from other cells.

The spectrum efficiency (SE) refers to the data rate that can be transmitted over a given bandwidth with unit $bits/s/Hz$. It measures the quantity of users and services can be transmitted simultaneously supported by a limited radio frequency bandwidth. Theoretically, the SE R of a typical user can be derived based upon the SINR, which is also known as the Shannon formula.

$$R = \log_2\{1 + \text{SINR}\} \tag{2.2}$$

Due to the physical scarcity of spectrum, the SE enhancement is extremely important in the research of wireless networks.

The energy efficiency (EE) with unit $bps/Hz/J$ is another KPI to be discussed in this thesis. It refers to the data rate that can be achieved within a given power consumption. It is commonly defined as the ratio between the SE and the total power consumption of a base station (downlink) or a user (uplink) P within a given period.

$$EE = \frac{R}{P} \tag{2.3}$$

EE enhancement is especially significant in the 5G network research since environ-

[2] In this thesis, both d and d_i are assumed to be larger than 1 to avoid singularity.

[3] In this thesis, it is assumed that the target user and target base station experience only Rayleigh fading with mean 1. A detailed description of Rayleigh fading can be found in Appendix 1.

ment protection has become one of the major societal and economical concerns.

2.2.3 Stochastic Geometry Analysis

At the heart of the stochastic geometry approach lies the study of random point patterns in terms of mathematics and point process theory. By using stochastic geometry, one of the main goals of network designers has been to find the closed-form expressions for the SINR accounting for the spatial node distribution, the channel propagation characteristics, and the path-loss coefficient [QdlRGK13]. As mentioned in the previous section, a few critical theorems are addressed in this section for featuring the interference.

1. Sums and Products over PPP [QdlRGK13]

   The Campell Theorem gives the mean of a sum for a homogeneous PPP [4].

   Theorem 1. *Let ϕ be a PPP with density λ and $f(x)$: $R^d \to [0, \infty)$ be a measurable (non-negative) function, then can have:*

$$\mathrm{E}(\sum_{x \in \Phi} f(x)) = \lambda \int_{R^d} \mathrm{E}(f(x)) dx \tag{2.4}$$

   The probability generating functional (PGFL) gives the mean of a product over a homogeneous PPP.

   Theorem 2. *Let Φ be a PPP with density λ and $f(x) : R^d \to [0, 1]$ be a real valued function, then can have*

$$\mathrm{E}\{\prod_{x \in \Phi} f(x)\} = \exp(-\lambda \int_{R^d} (1 - \mathrm{E}(f(x))) dx) \tag{2.5}$$

2. Laplace Functional

   The Laplace Functional of a PPP Φ is defined by

[4] A PPP is called homogeneous when the intensity function $\lambda(x) = \lambda > 0$. In the rest of the thesis, homogeneous PPP based distribution is applied for system modelling.

$$\mathcal{L}_{\Phi}(sf) = \exp(-\lambda \int_{R^d} (1 - \mathrm{e}^{-sf(x)}) dx) = \mathrm{E}[\mathrm{e}^{s \sum_{x \in \Phi} f(x)}] \tag{2.6}$$

Based on the properties of PPP and Laplace functional addressed above, the statistical behaviour of the aggregate interference can be characterised through its Laplace function [HKB13]. Assuming that $I(y)$ is the sum of a set of interference who follows the exponential distribution in Φ, then the mean value of the aggregate interference can be derived as

$$\begin{aligned} \mathrm{E}\{\exp(-sI(y))\} &= \mathrm{E}\{\exp(-s \sum_{x \in \Phi} l(x-y))\} \\ &= \mathrm{E}\{\prod_{x \in \Phi} \exp(-sl(x-y))\} \\ &= \exp(-\lambda \int_{R^2} (1 - \mathrm{e}^{-sl(x-y)}) \mathrm{d}x) \end{aligned} \tag{2.7}$$

where $x-y$ is the distance between the interfering BSs (downlink) or users (uplink) to the receiver. Without the loss of generality, it can be assumed that the typical user or BS is located as the origin, then $x - y \to x$ and

$$\mathcal{L}_I(s) = \exp(-\lambda \int_{R^2} (1 - \mathrm{e}^{-sl(x)}) \mathrm{d}x). \tag{2.8}$$

3. Poisson-Voronoi tessellation

Theorem 3 gives the definition of Voronoi Tessellation (VT)[ABG11].

Theorem 3. *Given a collection of points $\Phi = \{X_i\}$ and a given point x, the Voronoi cell $C_x(\Phi)$ of this point is defined as the subset of the plane of all locations that are closer to x than to any point in Φ. Using equation to present it as:*

$$C_x(\Phi) = \{y \in R^d : \|y - x\| < \inf_{x_i \in \Phi, x_i \neq x} \|y - x_i\|\} \tag{2.9}$$

When $\Phi = \{X_i\}$ is a Poisson point process, the (random) collection of cells

$\{C_{xi}(\Phi)\}$ is called as the Poisson-Voronoi Tessellation (PVT).

If the receiver is associated with the nearest transmitter with density λ, that is deployed in the Voronoi cell, the probability density function (pdf) of the distance between the transmitter and the receiver r can be expressed as

$$f_{R(r)} = 2\pi\lambda r \exp(-\pi\lambda r^2) \tag{2.10}$$

Proof. The pdf of the distance between the transmitter and the receiver can be derived using the simple fact that the null probability of a 2-D Poisson process in an area A is $\exp(\lambda A)$ [ABG11].

$$\mathrm{P[r > R]} = \mathrm{e}^{-\lambda\pi\mathrm{R}^2} \tag{2.11}$$

Therefore, the CDF is $\mathrm{P}[r \leqq R] = F_r(R) = 1 - e^{-\lambda\pi R^2}$ and the pdf can be found as

$$f_r r = \frac{\mathrm{d}F_r(R)}{\mathrm{d}r} = e^{-\lambda\pi r^2} 2\pi\lambda r. \tag{2.12}$$

□

Since the single-cell models [LLAH15, SBK+15] and symmetric multi-cell models [BSHD15] cannot well characterise the 5G network architecture and the intercell interference, especially for HetNets, more and more research works have been conducted via a stochastic geometry approach [PTHX13, NDA13b, EHH13, TSAJ14]. A tractable analysis for network performance in terms of coverage and rate is first introduced in homogeneous networks in [ABG11]. Then authors in [EHH13] extended the work in [ABG11] to HetNets scenario. Moreover, users can be associated with the nearest BS [QCK11] or with the BS providing the strongest signal in terms of received power or

SINR [JSXA12, DGBA12a]. The derived theoretical expressions in existing literatures are all verified by Monte Carlo simulations.

To conclude, using mathematical tools from stochastic process to derive the theoretical expressions of network performance metrics, is worth to be further conducted in a random distributed system model. In this way, the performance in the 5G networks can be analysed more tractably and accurately.

2.3 State-of-the-Art in 5G wireless networks

The 5G network will be dense either by deploying large scale small cells or employing large amounts of antennas on a macro base station (MBS). An envisioned 5G network model equipped with multiple advanced technologies including HetNets, massive multiple input multiple output (MIMO), cloud radio access network (C-RAN) and device and device (D2D) is shown in Figure 2.7.

2.3.1 Heterogeneous networks

A heterogeneous network (HetNet), featuring with a large number of cell splitting, transmission power disparity between high power nodes (HPNs) and low power nodes (LPNs), is a promising solution to deal with challenges resulting from the explosive rising data demands in the 5G networks.

In HetNets, HPNs are normally macro base stations (MBSs) whose coverage range is at the level of thousands metres and transmit power is at the level of tens of watts. They are deployed by operators with fixed locations to serve amounts of users ranging from tens to thousands each. LPNs with smaller coverage, as table **2-A** from [QdlRGK13] shows, usually consume less power and can be deployed in a more targeted manner to alleviate coverage dead zones and traffic hot zones.

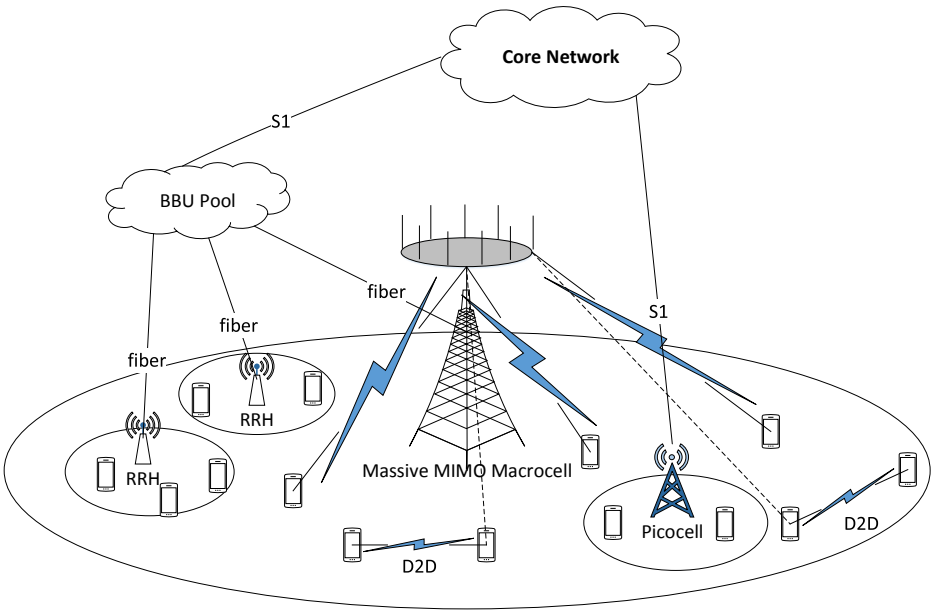

Figure 2.7: An envisioned 5G HetNet architecture integrated with C-RAN, massive MIMO and D2D communications

Types of nodes	Transmit power	Coverage	Backhaul
Macrocell	46 dBm	Few km	S1 interface
Picocell	23-30 dBm	<300m	X2 interface
Femtocell	<23dBm	<50m	Internet IP
Relay	30dBm	300m	Wireless
RRH	46dBm	Few km	Fiber

Table 2-A: The comparison of power consumption and coverage area among different BS types [QdlRGK13].

Deploying more small base stations (SBSs) underlaid with MBS brings loads of enhancement to the network performance. First of all, more SBSs can serve more users, whereby provides great capacity gain. Secondly, the frequency reuse among HPNs and LPNs can well utilise the resource, which in further provide high spectrum efficiency (SE). Thirdly, deploying LPNs as an energy-efficient replacement to MBSs opens the possibility to the use of alternative energy sources (e.g. solar and wind power), which

are potentially more sustainable and cost-effective [KTV12].

However, the multi-tier topology brings technical challenges to network design and analysis in terms of system modelling, user association and resource allocation. Firstly, dense and unplanned small cell deployment leads to strong inter-cell interference and intra-cell interference jeopardising the network performance [And13]. Secondly, in spite of LPNs consume less power than conventional MBSs, the large scale deployment of small cells and advanced wireless technologies gives rise to the whole network energy consumption. Thirdly, network modelling becomes significantly more complex due to each tier of access points (APs) is likely to have distinctly different characteristics. The conventional system modelling methods such as hexagonal grid cannot accurately depict a HetNet topology any more. These limitations have seriously hampered the development and deployment of HetNets technology.

2.3.2 Massive MIMO transmission

A massive multiple input multiple output (MIMO) equipped system can use a large number of antennas to serve a much smaller number of end users simultaneously. Due to the high SE and EE gain, it has become a key technology candidate for supporting 5G networks in recent years [RPL+13]. The shift from MIMO to massive MIMO is shown in Figure 2.8 [Jun15].

Massive MIMO transmission can bring large performance gain to the networks. Specifically, after employing large scale antennas on one BS, the significant array gain can be achieved. Then, as more data streams are transmitted from the same radio resource in separate spatial dimensions, multiplexing gains will be enhanced [LETM14]. Also, the intra-cell interference can be efficiently mitigated when an appropriate precoding processing such as zero forcing (ZF) beamforming is applied. Moreover, massive MIMO is expected to increase the EE because the transmit power can be reduced by an order of magnitude with the very large antenna array [NLM13b].

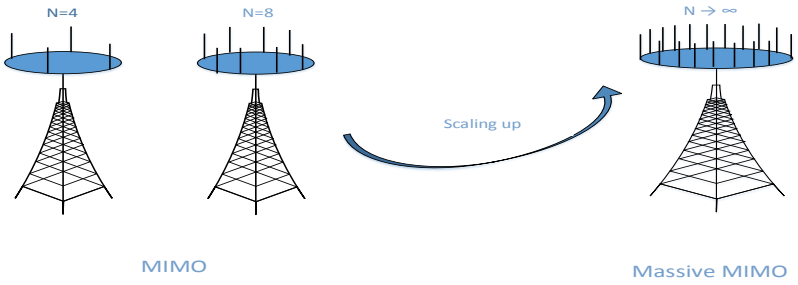

Figure 2.8: Scaling up the MIMO to massive MIMO

Although users experience better quality of service under a large scale MIMO, the performance of this highlighted technology is limited by a few constraints. Firstly, the large-scale antennas deployment will lead to the increased complexity of the hardware and signal processing at both ends. Then, the high reuse of pilots with adjacent cells contaminates the pilots and results in impairments to the channel estimation, even in a time division duplexing (TDD) [5] system [HTBD13]. Different from the uncorrelated noise and small-scale fading, the pilot contamination will not vanish as the number of antennas grows without limit [Mar10].

2.3.3 Cloud radio access networks

In a cloud radio access network (C-RAN), as shown in Figure 2.7, baseband units (BBUs) are centralised into one entity to form a BBU pool. This architecture was first proposed by IBM [LSZ+10] and described in detail by China Mobile in [Mob11]. Actually, a network with remote radio heads (RRHs) architecture, where the BS is separated into a radio unit and a signal processing unit, was introduced in 3G networks and now has been generally deployed in 4G networks. In 5G, to optimise BBU utilisation between heavily and lightly loaded BS, the baseband data path processing as well as radio resource control

[5] TDD mode exploits the channel reciprocity for the channel estimation information (CSI) acquisition.

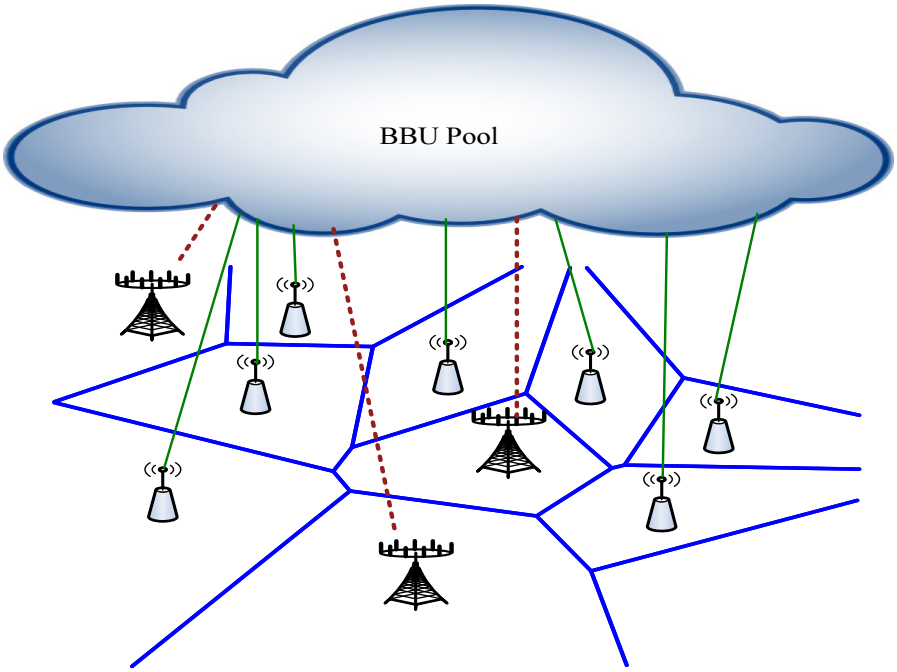

Figure 2.9: System architecture for HC-RAN, where the red dash lines represent the backhaul links between the MBSs and BBU pool via X2/S1 interfaces, and the green solid lines represent the fronthaul links between the RRHs and BBU pool via optical fibre link.

for RRHs are moved to cloud server to take advantages of cloud computing capabilities.

Attributed to the cloud computing capability, a C-RAN can efficiently deal with large-scale control/data processing with less operating expenditure (OPEX) [CCY+15], e.g. the inter-cell interference coordination (ICIC) mechanism is feasible to be realized. Thus, the network maintenance is eased and the scalability is much improved in contrast to the conventional architecture.

However, operators who pay higher cost for fibre bandwidth such as China Unicom will suffer from a high transportation cost if C-RAN is deployed and they prefer small cells architecture [Mad13]. As such, the concept of heterogeneous C-RAN (HC-RAN), which can take full advantage of both HetNets and C-RANs, is proposed as a new paradigm in [PLJ+14a]. The HC-RAN different from the C-RAN in that the HPNs are interfaced with BBU pool via air interface. In this way, HC-RAN can alleviates the fronthaul requirements. However, the inter-tier interference between the RRHs and

macrocell BSs may be problematic in the HC-RAN, due to the limited radio resources.

2.3.4 D2D communications

In a device-to-device (D2D) underlaid communication network, two users in vicinity can communicate with each other directly using a cellular frequency and instructed by MBSs, as shown in Figure 2.7. This function is specifically useful in heavy traffic zones for offloading from MBSs. As devices are LPNs compared to MBSs, D2D communication can serve as another tier in the 5G networks, where clusters of devices cooperate with each other can dramatically increase SE [BTAS14].

Featuring with small path loss resulting from the short transmission distance, D2D communications have potentials to ensure the content delivery, regardless of the low transmit power from the device who plays the role as a transmitter. Thus, D2D communication has a profound impact on both the SE and EE in such a scenario. Note that the advantages of D2D communications are not only limited to enhance SE and EE but also improve delay and fairness [AWM14], but they are out of scope in this thesis.

However, challenges addressed by D2D underlaid cellular networks cannot be ignored. On the one hand, interference generated in the same cells and other cell is hard to quantified during the interact of D2D and cellular networks [She15]. On the other hand, since terminals are usually hand-held devices with limited battery life in practical implementation, how to improve the EE in D2D underlaid cellular networks needs to be figured out. Due to the fact that massive MIMO can provide high SE and EE while mitigating interference, the interplay between D2D and massive MIMO on network performance is worth to be analysed.

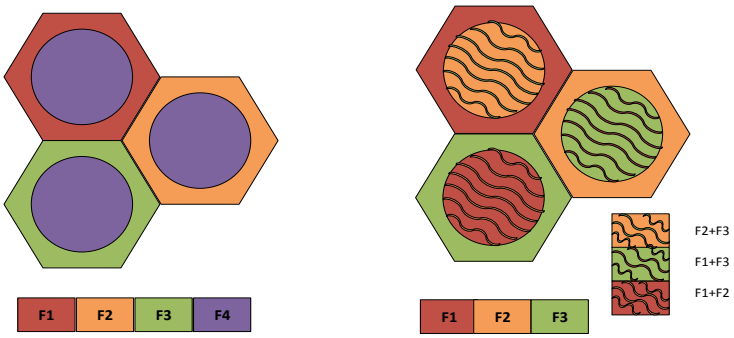

Figure 2.10: a) Strict FFR and b) soft FFR deployments with N=3 cell-edge reuse factor.

2.3.5 Interference Management Mechanisms

Although the intra-cell interference in the 5G HetNet can be well mitigated via adopting Orthogonal Frequency Division Multiplexing (OFDMA) [DHL12], massive MIMO or coordination in the BBU pool in a C-RAN, the inter-cell interference and inter-tier interference still degrade the network performance. To face this challenge, two commonly used interference mitigation mechanisms are introduced in this section.

2.3.5.1 Fractional frequency reuse

Fractional frequency reuse (FFR) is to partition the bandwidth of the cell, so that cell-edge users do not interfere with each other. The FFR has been proposed as an inter-cell interference coordination technique in OFDMA based wireless networks and defined in the LTE release 8 [BPG+09].

There are two commonly used fractional frequency reuse (FFR) schemes in existing

literatures: strict FFR and soft FFR [NAS+10]. Figure 2.10 a) illustrates a strict FFR deployment with a cell-edge reuse factor of N = 3. Users in each cell interior are allocated a common sub-band of frequencies while cell-edge users bandwidth is partitioned across cells based on a reuse factor of N. In total, strict FFR requires a total of N + 1 sub-bands. In this way, interior users do not share any spectrum with exterior users, which reduces interference for both interior users and cell-edge users. Figure 2.10 b) illustrates a soft FFR deployment with a reuse factor of N = 3 on the cell-edge. The same cell-edge bandwidth partitioning strategy as strict FFR is employed, but the interior users are allowed to share sub-bands of edge users in other cells. Because cell interior users share the bandwidth with neighbouring cells, they typically transmit at lower power levels than the cell-edge users. Comparatively speaking, soft FFR is more bandwidth efficient than strict FFR but suffers stronger interference to both cell interior and edge users.

2.3.5.2 Power control

The uplink power control is defined by 3GPP in [R1-11] as a combination of open loop power control (OLPC) and closed loop power control (CLPC). It has been used as a simple but effective interference mitigation method in long term evolution (LTE) networks. Specifically, the OLPC allows for full or partial compensation of the path loss and each user controls its power by itself. Whereas in CLPC, evolved Node B (eNodeB) adjusts users power according to channel variation by sending transmit power control (TPC) commands and compensates for the generated inter-cell interference (ICI). In most cases, the OLPC method is more attractive for its simplicity and ease of implementation to avoid the SINR differences resulting in different throughput for users in different locations. Such an approach, while not optimal from an aggregate throughput or spectral efficiency perspective, assures fairness to cell edge users.

Downlink/Uplink	Involved Technologies	Interference Management	Network Tiers
Downlink	Massive MIMO and HetNets	No	K-tier
Downlink	Massive MIMO and HC-RAN	An Enhanced S-FFR	Two-tier
Uplink	Massive MIMO and HetNets	Power control	Two-tier
Uplink	Massive MIMO and D2D transmission	Power control	One-tier

Table 2-B: The comparison of the proposed scenarios.

2.4 Summary

While the cutting-edge architectures and technologies such as massive MIMO, D2D or C-RAN have been extensively solely studied in the existing literatures, their co-effects on enhancing network performance in HetNets have not been quantified and analysed in a relatively practical scenario. Moreover, performance loss caused by the strong inter-tier interference needs to be well managed. Compared to the traditional system models, the PPP based models are more reliable for characterising a complex network architecture.

Therefore, the thesis quantifies and addresses the co-effects of the highlighted technologies in the 5G networks through a stochastic geometry approach. The proposed scenarios are compared in the Table **2-B**.

Chapter 3

Downlink Performance Evaluation in Massive MIMO enabled Heterogeneous Cellular Networks

3.1 Overview

To meet such large traffic demand, the fifth generation (5G) network is underway [ABC+14]. Although there is no preliminary 5G standard yet, the benefits of HCNs and massive MIMO have attracted considerable attention. For example, the coverage probability and average rate of the K-tier downlink HCNs was investigated in [DGBA12a], where each user was associated with the BS with strongest signal-to-interference-plus-noise ratio (SINR). In [JSXA12], the effect of cell expansion on the cell load and the average rate in HCNs was analysed and a flexible user association was proposed. Energy efficient HCNs was proposed in [SQKS13] by deploying more small cells and switching off high-power macro cell services based on sleep mode polices. The implementation of massive MIMO in cellular networks was first examined in [Mar10], where each cellular BS is equipped with very large antenna arrays. It was demonstrated in [Mar10] that the effects of uncorrelated noise and small-scale fading disappear as the number of antennas at the BS grows without limit. In [WNE+15], massive MIMO in cognitive radio networks was examined, which showed that interference power constraint can be significantly relieved.

In [NLM13b], the uplink achievable rate in the multi-cell multi-user systems with a very large antenna array at the BS was derived, and the performance comparisons between the maximal-ratio combining and zero-forcing were evaluated. A multi-cell network MIMO system with inter-cell cooperation was considered in [HTC12], where BSs in the same cooperation cluster employed joint transmission with linear zero-forcing beamforming. An important conclusion given in [HTC12] was that in most cases cooperation among BSs with large antenna arrays is not necessary, in order to reduce channel estimation cost. Because users experience better quality of service under a large scale MIMO than network MIMO multi-cell networks, it was confirmed in [HYA14] that large scale MIMO system could be the preferred route toward interference mitigation in cellular networks. Recently, user association for massive MIMO heterogeneous networks was investigated in terms of long-term average rate in [BBPC16] and energy efficiency in [LWC$^+$15a].

While the aforementioned literature laid a solid foundation for the efficiency of massive MIMO in providing large array gain and mitigating interference, an analytical approach to address the impact of massive MIMO on the user association, coverage, SE and EE in HCNs is not investigated yet. Therefore, this chapter presents a comprehensive analysis in massive multiple input multiple output (MIMO) aided heterogeneous cellular networks (HCNs) on the downlink performance in terms of the user association probability, coverage probability, spectrum efficiency (SE) as well as energy efficiency (EE).

In section 3.2, the impact of massive MIMO on downlink user association in K-tier HCNs was examined. Such a stochastic model can well characterize the practical HCNs deployment [DGBA12a, JSXA12, ABG11], compared to the conventional hexagonal grid model [NLM13b]. Firstly, the impact of massive MIMO on user association in HCNs is examined. According to the asymptotic analysis, the transmit power of macrocell BS can be reduced proportionally to $\frac{S}{N-S+1}$. The exact and asymptotic expressions for the probability that a user is associated with a macro cell or a small cell are derived. Based

on the asymptotic analysis, the effects of density ratio and transmit power on user association are explicitly shown. The coverage probability and SE of HCNs with massive MIMO are derived. Numerical results corroborate the analysis and show that the implementation of massive MIMO in macro cells can significantly enhance the performance of HCNs in terms of coverage and SE. A guideline for practical cellular deployment is reached that macro base stations (MBSs) with large antenna arrays can decrease the demands for small cells.

In section 3.3, the cell range expansion (CRE) that allows tier selection for cell load balancing is considered, and the potential SE and EE improvement it brings is evaluated. An analytical approach to examine SE and EE of heterogeneous networks (HetNets)[1] is developed and results show that serving moderate number of users in the macro cells with massive MIMO can boost both SE and EE. Moreover, it is confirmed that using CRE can improve the EE of HetNets by offloading data traffic to small cells.

3.2 Spectrum Efficiency without Cell Range Expansion

3.2.1 System Model

3.2.1.1 Spatial Distribution

As shown in Figure 3.1, the time-division duplex (TDD) downlink transmission in K-tier HCNs was considered, which consist of macro cells and small cells such as picocells and femtocells. Without loss of generality, it is assumed that the first tier represents the class of MBSs. The MBSs are located following a Homogeneous Poisson Point Process (HPPP) Φ_{M} with density λ_{M}, while small cell base stations (SBSs) in the i-th tier ($i = 2, \ldots, K$) are located following a HPPP Φ_i with density λ_i. Massive MIMO is adopted in the macro cells [JMZ+14], where each MBS is equipped with N antennas and simultaneously communicate with S users with $N \gg S \geq 1$. Each SBS and user are

[1] In this chapter, HetNets are defaulted as heterogeneous cellular networks.

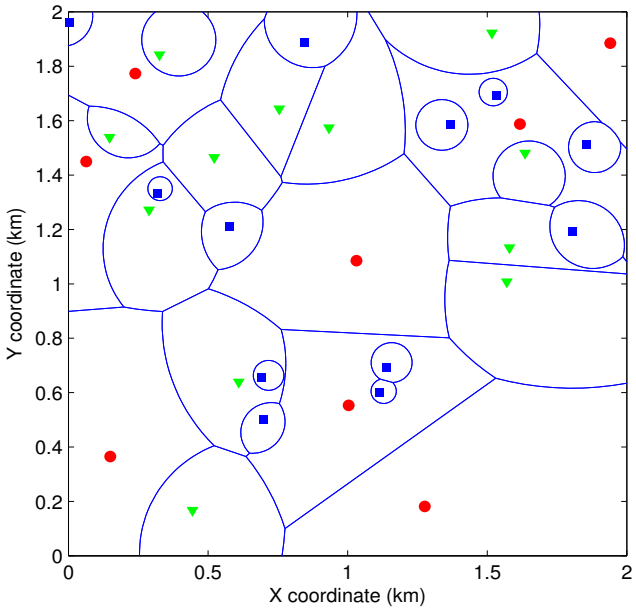

Figure 3.1: An illustration of downlink three-tier HCNs, where macro cell base stations (red circle) are deployed in combination with picocell base stations (green triangle) and femtocell base stations (blue square).

single-antenna nodes. Each MBS uses zero forcing beamforming (ZFBF) to transmit S data streams with equal power assignment. Such a transmission scheme has been widely used in the existing multiuser MIMO literature such as [HTC12, NLM13b, HYA14]. Assuming that perfect downlink channel state information (CSI) is known at the MBS[2]. The universal frequency reuse i.e. all tiers share the same spectrum, is took into account

.

3.2.1.2 User Association

In the macro cell, a MBS provides its served users with large array gains, whereby has an effect on the user association. Assuming that a typical served user is located at the origin o, user association based on the maximum receive power is employed, where a user is associated with the BS that provides the largest average receive power. The

[2]In the practical TDD massive MIMO systems, the downlink CSI can be obtained through channel reciprocity based on uplink training [Mar10].

long-term average receive power at a user that is connected with the MBS belongs to Φ_{M} is expressed as

$$P_{r,M} = G_a \frac{P_{\mathrm{M}}}{S} L\left(|X_{o,\mathrm{M}}|\right), \tag{3.1}$$

where G_a is the array gain, P_{M} is the MBS's transmit power, $L\left(|X_{o,\mathrm{M}}|\right) = \beta |X_{o,\mathrm{M}}|^{-\alpha_{\mathrm{M}}}$ is the path loss function, β is a unitless constant value depends on the antenna characteristics and the average channel attenuation[3]. $|X_{o,\mathrm{M}}|$ is the distance between the user and its associated MBS, and α_{M} is the path loss exponent[4]. The array gain G_a of zero-forcing beamforming (ZFBF) transmission is $N - S + 1$ [HTC12, BBPC16, HYA14]. It is implied by (3.1) that the large array gain brought by massive MIMO can have a big impact on tier selection and load distribution between different types of BSs.

In the small cell, the long-term average receive power at a user that is connected with the SBS k ($k \in \Phi_i$) in the i-th tier is expressed as

$$P_{r,k} = P_i L\left(|X_{o,k}|\right), \tag{3.2}$$

where P_i is the SBS's transmit power in the i-th tier and $L\left(|X_{o,k}|\right) = \beta (|X_{o,k}|)^{-\alpha_i}$ with path loss exponent α_i and distance $|X_{o,k}|$ between the user and its associated SBS k from tier i.

3.2.1.3 Channel Model

All channels undergo the independent and identically distributed (i.i.d.) quasi-static Rayleigh fading. The receive signal-to-interference-plus-noise ratio (SINR) of a typical

[3]The value of $\beta < 1$ is set to the free-space path gain assuming omnidirectional antennas [Gol05]: $\beta = (\frac{\text{wavelength}}{4\pi})^2$.

[4]The large-scale fading between a UE and the BS is assumed to be the same for all BS antennas. This is reasonable since the distances between UEs and the BS are much larger than the distance between the antennas.

served user at a distance $|X_{o,\mathrm{M}}|$ from its associated MBS $B_{o,\mathrm{M}}$ is given by

$$\mathrm{SINR}_{\mathrm{M}} = \frac{\frac{P_{\mathrm{M}}}{S} h_{o,\mathrm{M}} L\left(|X_{o,\mathrm{M}}|\right)}{I_1 + \delta^2}, \tag{3.3}$$

where inter-cell interference $I_1 = I_{\mathrm{M},1} + I_{\mathrm{S},1}$, $I_{\mathrm{M},1} = \sum_{\ell \in \Phi_{\mathrm{M}} \backslash B_{o,\mathrm{M}}} \frac{P_{\mathrm{M}}}{S} h_{\ell,\mathrm{M}} L\left(|X_{\ell,\mathrm{M}}|\right)$, and $I_{\mathrm{S},1} = \sum_{i=2}^{K} \sum_{j \in \Phi_i} P_i h_{j,i} L\left(|X_{j,i}|\right)$, $h_{o,\mathrm{M}}$ is the small-scale fading channel power gain between the typical user and its associated MBS, $h_{o,\mathrm{M}} \sim \Gamma\left(N - S + 1, 1\right)$ [HYA14], $h_{j,i} \sim \exp(1)$, $h_{\ell,\mathrm{M}}$ and $|X_{\ell,\mathrm{M}}|$ are the equivalent small-scale fading interfering channel power gain and distance between the typical user and MBS $\ell \in \Phi_{\mathrm{M}} \backslash B_{o,\mathrm{M}}$ (except the serving BS $B_{o,\mathrm{M}}$), respectively, $h_{\ell,\mathrm{M}} \sim \Gamma\left(S, 1\right)$, $h_{j,i}$ and $|X_{j,i}|$ are the small-scale fading interfering channel power gain and distance between the typical user and BS j in the i-th tier, respectively. δ^2 is the noise power.

Remark 1. *From* (3.3)*, it can be seen that when the number of antennas at MBS grows large,* $h_{o,\mathrm{M}} \approx N - S + 1$*. Compared with the conventional MBS with single antenna, the transmit power of MBS can be reduced proportionally to* $\frac{S}{N-S+1}$ *while maintaining the same quality of service (QoS) per user in terms of SINR.*

The SINR of a typical user at a random distance $|X_{o,k}|$ from its associated SBS $B_{o,k}$ in the k-th tier is given by

$$\mathrm{SINR}_k = \frac{P_k g_{o,k} L\left(|X_{o,k}|\right)}{I_k + \delta^2}, \tag{3.4}$$

where $I_k = I_{\mathrm{M},k} + I_{\mathrm{S},k}$, $I_{\mathrm{M},k} = \sum_{\ell \in \Phi_{\mathrm{M}}} \frac{P_{\mathrm{M}}}{S} g_{\ell,\mathrm{M}} L\left(|X_{\ell,\mathrm{M}}|\right)$, $I_{\mathrm{S},k} = \sum_{i=2}^{K} \sum_{j \in \Phi_i \backslash B_{o,k}} P_i g_{j,i} L\left(|X_{j,i}|\right)$, $g_{o,k}$, which follows the exponential distribution, is the small-scale fading channel power gain between the typical user and its serving BS, $g_{o,k} \sim \exp(1)$, $g_{\ell,\mathrm{M}}$ and $|X_{\ell,\mathrm{M}}|$ are the equivalent small-scale fading interfering channel power gain and distance between the typical user and MBS ℓ, respectively, $g_{\ell,\mathrm{M}} \sim \Gamma\left(S, 1\right)$, and $g_{j,i}$ and $|X_{j,i}|$ are the small-scale fading interfering channel power gain and distance between the typical user and BS $j \in \Phi_i \backslash B_{o,k}$, respectively, and $g_{j,i} \sim \exp(1)$.

Remark 2. *Based on* **Remark** 1*, it can be obtained that decreasing the MBS transmit*

power reduces the interference from the macro-cells. While from (3.3) *and* (3.4)*, it can be seen that for a given transmit power at the MBS, massive MIMO with adding more antennas at MBSs has no effect on the existing interference environment.*

3.2.2 User Association Probability

Based on user association in section 3.2.1.2, the probability density function (PDF) of the distance between a typical user and its serving BS is first presented. In an effort to assess the performance of HCNs with massive MIMO, the coverage probability and rate of the network scenario are derived then.

The PDF of the distance between a typical user and its serving BS is derived as the following two lemmas.

Lemma 1. The PDF of the distance $|X_{o,\mathrm{M}}|$ between a typical user and its serving MBS $B_{o,\mathrm{M}}$ is given by

$$f_{|X_{o,\mathrm{M}}|}(x) = \frac{2\pi\lambda_{\mathrm{M}}}{\mathcal{A}_{\mathrm{M}}} x \exp\left\{ -\pi\lambda_{\mathrm{M}} x^2 - \pi \sum_{i=2}^{K} \lambda_i \left(\frac{P_i S}{P_{\mathrm{M}}(N-S+1)} \right)^{2/\alpha_i} x^{2\alpha_{\mathrm{M}}/\alpha_i} \right\}. \quad (3.5)$$

Here, $\mathcal{A}_{\mathrm{M}}$ is the probability that a typical user is associated with the MBS, which is given by

$$\mathcal{A}_{\mathrm{M}} = 2\pi\lambda_{\mathrm{M}} \int_0^{\infty} r \exp\left\{ -\pi\lambda_{\mathrm{M}} r^2 - \pi \sum_{i=2}^{K} \lambda_i \left(\frac{P_i S}{P_{\mathrm{M}}(N-S+1)} \right)^{2/\alpha_i} r^{2\alpha_{\mathrm{M}}/\alpha_i} \right\} dr. \quad (3.6)$$

Lemma 2. The PDF of the distance $|X_{o,k}|$ between a typical user and its serving SBS in the k-th tier $B_{o,k}$ is given by

$$f_{|X_{o,k}|}(x) = \frac{2\pi\lambda_k}{\mathcal{A}_k} x \exp\left\{ -\pi\lambda_{\mathrm{M}} \left(\frac{P_{\mathrm{M}}(N-S+1)}{P_k S} \right)^{2/\alpha_{\mathrm{M}}} x^{2\alpha_k/\alpha_{\mathrm{M}}} - \pi \sum_{i=2}^{K} \lambda_i \left(\frac{P_i}{P_k} \right)^{2/\alpha_i} x^{2\alpha_k/\alpha_i} \right\}. \quad (3.7)$$

Here, $\mathcal{A}_k$ is the probability that a typical user is associated with the SBS in the k-th tier, which is given by

$$\mathcal{A}_k = 2\pi\lambda_k \int_0^\infty r \exp\left\{ -\pi\lambda_{\mathrm{M}} \left(\frac{P_{\mathrm{M}} \left(N - S + 1\right)}{P_k S} \right)^{2/\alpha_{\mathrm{M}}} r^{2\alpha_k/\alpha_M} - \pi \sum_{i=2}^{K} \lambda_i \left(\frac{P_i}{P_k} \right)^{2/\alpha_i} r^{2\alpha_k/\alpha_i} \right\} dr. \tag{3.8}$$

Proof. In a heterogeneous network (HetNet) with flexible cell association, as shown in the Lemma 1 of [JSXA12], the probability that a typical user is associated with the kth tier is

$$\mathcal{A}_k = 2\pi\lambda_k \int_0^\infty r \exp\left\{ -\pi \sum_{j=1}^{K} \lambda_j \left(\hat{P}_j \hat{B}_j \right)^{2/\alpha_j} r^{2/\hat{\alpha}_j} \right\} \tag{3.9}$$

and Lemma 3 therein shows the PDF $f_{X_k}(x)$ of a distance X_k between a typical user and its serving BS is

$$f_{X_k}(x) = \frac{2\pi\lambda_k}{\mathcal{A}_k} x \exp\left\{ -\pi \sum_{j=1}^{K} \lambda_j \left(\hat{P}_j \hat{B}_j \right)^{2/\alpha_j} x^{2/\hat{\alpha}_j} \right\} \tag{3.10}$$

where $\hat{P}_j \triangleq \frac{P_j}{P_k}$, $\hat{B}_j \triangleq \frac{B_j}{B_k}$ and $\hat{\alpha}_j \triangleq \frac{\alpha_j}{\alpha_k}$, which respectively characterize transmit power ratio, bias power ratio and path loss exponent ratio of interfering to serving BS. Note that $\hat{P}_k = \hat{B}_k = \hat{\alpha}_k = 1$.

Based on the above equations, the probability that a typical user is associated with the macrocell tier $\mathcal{A}_{\mathrm{M}}$ and the PDF of the distance $|X_{o,\mathrm{M}}|$ between a typical user and its serving MBS $B_{o,\mathrm{M}}$ are obtained via the following steps:

1. The massive MIMO large array gain $\frac{\mathrm{N-S+1}}{\mathrm{S}}$ is regarded as the bias B_j for the first

tier and $B_k = 1$ (no range expansion) for the rest of tiers;

2. When $i = 1$, $\hat{P}_k = \hat{B}_k = \hat{\alpha}_k = 1$;

3. When $i > 1$, $\hat{P}_k = \frac{P_i}{P_{\mathrm{M}}}$, $\hat{\alpha}_k = \frac{\alpha_i}{\alpha_{\mathrm{M}}}$ and $\hat{B}_k = \frac{\mathrm{S}}{\mathrm{N-S+1}}$;

□

Similarly, the probability that a typical user is associated with the SBS $\mathcal{A}_k$ and the PDF of the distance $|X_{o,k}|$ between a typical user and its serving SBS $B_{o,k}$ can be also obtained.

Base on these two lemmas, the following remark and corollary are presented.

Remark 3. *From $\mathcal{A}_{\mathrm{M}}$ in* **Lemma** 1 *and $\mathcal{A}_k$ in* **Lemma** 2*, it can be seen that increasing the number of antennas at the MBS increases the probability that a user is associated with the MBS, which in turn decreases the probability that a user is associated with the SBS.*

Corollary 1. For very large number of antennas with $N \to \infty$, using $e^{-x} \to 1 - x\,(x \to 0)$, the probability that a typical user is associated with the MBS is asymptotically derived as

$$\begin{aligned}\mathcal{A}_{\mathrm{M}}^{\infty} &= 2\pi\lambda_{\mathrm{M}}\left[\int_0^{\infty} r\exp\left\{-\pi\lambda_{\mathrm{M}}r^2\right\}dr - \pi\sum_{i=2}^{K}\lambda_i\right.\\ &\left.\left(\frac{P_i S}{P_{\mathrm{M}}\left(N-S+1\right)}\right)^{2/\alpha_i}\int_0^{\infty} r^{1+2\alpha_{\mathrm{M}}/\alpha_i}\exp\left\{-\pi\lambda_{\mathrm{M}}r^2\right\}dr\right]\\ &= 1 - \pi\sum_{i=2}^{K}\lambda_i\left(\frac{P_i S}{P_{\mathrm{M}}\left(N-S+1\right)}\right)^{2/\alpha_i}\frac{\Gamma\left(1+\alpha_{\mathrm{M}}/\alpha_i\right)}{\left(\pi\lambda_{\mathrm{M}}\right)^{\alpha_{\mathrm{M}}/\alpha_i}}. \end{aligned} \tag{3.11}$$

Note that the probability that a typical user is associated with the SBS is $1 - \mathcal{A}_{\mathrm{M}}^{\infty}$. From (3.11), it is explicitly shown that the probability that a typical user is associated with the MBS increases with increasing the density of MBS and decreases with increasing the density of SBS.

3.2.3 Performance Metrics

In an effort to assess the performance of HCNs with massive MIMO, the coverage probability and the downlink data rate of K-tier HCNs are then derived.

3.2.3.1 Coverage Probability Analysis

Theorem 4. The coverage probability of a typical user that is associated with MBS is derived as

$$P_{\text{cov}}^{\text{M}}(\gamma) = \int_0^{\infty} P_{\text{cov}}^{\text{M}}(x,\gamma) f_{|X_{o,\text{M}}|}(x)\, dx, \tag{3.12}$$

where $f_{|X_{o,\text{M}}|}(x)$ is given by (3.5), and $P_{\text{cov}}^{\text{M}}(x,\gamma)$ is the conditional coverage probability given a distance x between a typical user and its serving MBS, which is given by

$$P_{\text{cov}}^{\text{M}}(x,\gamma) = \sum_{n=0}^{N-S} \frac{(x^{\alpha_{\text{M}}})^n}{n!(-1)^n} \sum \frac{n!}{\prod_{q=1}^{n} m_q!(q!)^{m_q}} \times$$
$$\exp\left(-\frac{\gamma S \delta^2 x^{\alpha_{\text{M}}}}{P_{\text{M}}\beta} - \Xi\left(\frac{\gamma S x^{\alpha_{\text{M}}}}{P_{\text{M}}\beta}\right)\right) \prod_{q=1}^{n} \left(\Lambda^{(q)}(x^{\alpha_{\text{M}}})\right)^{m_q}, \tag{3.13}$$

where $\sum_{q=1}^{n} q \cdot m_q = n$. In (3.13), $\Xi(\cdot)$ and $\Lambda^{(q)}(\cdot)$ are given by (3.14), (3.15), and (3.16) at the top of the next page. In (3.14)-(3.16), $R_i^{\text{M}}(x) = \left(\frac{P_i S}{(N-S+1)P_{\text{M}}}\right)^{\frac{1}{\alpha_i}} x^{\frac{\alpha_{\text{M}}}{\alpha_i}}$, $\text{B}_{(\cdot)}[\cdot,\cdot]$ is the incomplete beta function [GR07, (8.391)], and ${}_2F_1[\cdot,\cdot;\cdot;\cdot]$ is the Gauss hypergeometric function [GR07, (9.142)].

Proof. The coverage probability represents the probability that the receive SINR at a

$$\Xi(s) = \lambda_{\mathrm{M}} 2\pi \sum_{\mu=1}^{S} \binom{S}{\mu} \left(\frac{P_{\mathrm{M}}}{S}\beta\right)^{\mu} s^{\mu} \frac{\left(-s\frac{P_{\mathrm{M}}}{S}\beta\right)^{-\mu+\frac{2}{\alpha_{\mathrm{M}}}}}{\alpha_{\mathrm{M}}} \mathrm{B}_{\left(-s\frac{P_{\mathrm{M}}}{S}\beta x^{-\alpha_{\mathrm{M}}}\right)}\left[\mu - \frac{2}{\alpha_{\mathrm{M}}}, 1-S\right] + \sum_{i=2}^{K} \lambda_i 2\pi s P_i \beta \frac{\left(R_i^{\mathrm{M}}(x)\right)^{2-\alpha_i}}{\alpha_i - 2} {}_2F_1\left[\frac{\alpha_i - 2}{\alpha_i}, 1; 2 - \frac{2}{\alpha_i}; -sP_i\beta\left(R_i^{\mathrm{M}}(x)\right)^{-\alpha_i}\right], \quad (3.14)$$

$$\Lambda^{(1)}(z) = -\frac{\gamma S \delta^2}{P_{\mathrm{M}}\beta} - \lambda_{\mathrm{M}} 2\pi S\gamma \frac{x^{2-\alpha_{\mathrm{M}}}}{\alpha_{\mathrm{M}} - 2} {}_2F_1\left[\frac{\alpha_{\mathrm{M}} - 2}{\alpha_{\mathrm{M}}}, S+1; 2 - \frac{2}{\alpha_{\mathrm{M}}}; -\gamma z x^{-\alpha_{\mathrm{M}}}\right] - \sum_{i=2}^{K} \lambda_k 2\pi \frac{\gamma S}{P_{\mathrm{M}}} P_i \frac{\left(R_i^{\mathrm{M}}(x)\right)^{2-\alpha_i}}{\alpha_i - 2} {}_2F_1\left[\frac{\alpha_i - 2}{\alpha_i}, 2; 2 - \frac{2}{\alpha_i}; -\frac{\gamma S z}{P_{\mathrm{M}}} P_i \left(R_i^{\mathrm{M}}(x)\right)^{-\alpha_i}\right], \quad (3.15)$$

$$\Lambda^{(q)}(z) = \lambda_{\mathrm{M}} 2\pi \frac{(S+q-1)!}{(S-1)!} (-\gamma)^{\frac{2}{\alpha_{\mathrm{M}}}} \frac{(z)^{-q+\frac{2}{\alpha_{\mathrm{M}}}}}{\alpha_{\mathrm{M}}} \mathrm{B}_{(-\gamma z x^{-\alpha_{\mathrm{M}}})}\left[q - \frac{2}{\alpha_{\mathrm{M}}}, 1 - S - q\right] + \sum_{i=2}^{K} \lambda_i 2\pi q! \left(-\frac{\gamma S}{P_{\mathrm{M}}} P_i\right)^{\frac{2}{\alpha_{\mathrm{M}}}} \frac{(z)^{-q+\frac{2}{\alpha_{\mathrm{M}}}}}{\alpha_{\mathrm{M}}} B_{\left(-\frac{\gamma S z}{P_{\mathrm{M}}} P_i \left(R_i^{\mathrm{M}}(x)\right)^{-\alpha_{\mathrm{M}}}\right)}\left[q - \frac{2}{\alpha_{\mathrm{M}}}, -q\right], \qquad q = 2, \ldots, n \quad (3.16)$$

---

typical user is larger than the threshold γ, which is written as

$$\begin{aligned} P_{\mathrm{cov}}^{\mathrm{M}}(\gamma) &= \Pr\left(\mathrm{SINR}_{\mathrm{M}} > \gamma\right) \\ &= \int_0^{\infty} \underbrace{\Pr\left(\mathrm{SINR}_{\mathrm{M}} > \gamma \mid |X_{o,\mathrm{M}}| = x\right)}_{P_{\mathrm{cov}}^{\mathrm{M}}(x,\gamma)} f_{|X_{o,\mathrm{M}}|}(x)\, dx. \end{aligned} \quad (3.17)$$

First calculate the conditional coverage probability $P_{\mathrm{cov}}^{\mathrm{M}}(x,\gamma)$ given a distance x as

$$\begin{aligned} P_{\mathrm{cov}}^{\mathrm{M}}(x,\gamma) &= \Pr\left(\frac{\frac{P_{\mathrm{M}}}{S} h_{o,\mathrm{M}} L(x)}{I_1 + \delta^2} > \gamma\right) \\ &= \int_0^{\infty} \Pr\left(h_{o,\mathrm{M}} > \frac{\gamma S x^{\alpha_{\mathrm{M}}}\left(\tau + \delta^2\right)}{P_{\mathrm{M}}\beta}\right) d\Pr\left(I_1 \le \tau\right) \\ &\overset{(a)}{=} \int_0^{\infty} e^{-\frac{\gamma S x^{\alpha_{\mathrm{M}}}\left(\tau+\delta^2\right)}{P_{\mathrm{M}}\beta}} \sum_{n=0}^{N-S} \frac{\left(\frac{\gamma S x^{\alpha_{\mathrm{M}}}}{P_{\mathrm{M}}\beta}\left(\tau + \delta^2\right)\right)^n}{n!} d\Pr\left(I_1 \le \tau\right). \end{aligned} \quad (3.18)$$

where (a) is due to that the complementary cumulative distribution function (CCDF)

of Gamma distribution is $e^{-x}\sum_{m=0}^{N}\frac{x^m}{m!}$.

Note that

$$\begin{aligned}&\left.\frac{d^n\left(\exp\left(-\frac{\gamma Sz\left(\tau+\delta^2\right)}{P_{\mathrm{M}}\beta}\right)\right)}{dz^n}\right|_{z=x^{\alpha_{\mathrm{M}}}}\\&=\left(-\frac{\gamma S\left(\tau+\delta^2\right)}{P_{\mathrm{M}}\beta}\right)^n\exp\left(-\frac{\gamma Sx^{\alpha_{\mathrm{M}}}\left(\tau+\delta^2\right)}{P_{\mathrm{M}}\beta}\right).\end{aligned}\tag{3.19}$$

By using (3.19), (3.18) can be written in an elegant form as follows [HKB13, (13)]

$$P_{\mathrm{cov}}^{\mathrm{M}}\left(x,\gamma\right)=\sum_{n=0}^{N-S}\frac{\left(x^{\alpha_{\mathrm{M}}}\right)^n}{n!(-1)^n}\left.\frac{d^n\left(e^{-\frac{\gamma Sz\delta^2}{P_{\mathrm{M}}\beta}}\mathcal{L}_{I_1}\left(\frac{\gamma Sz}{P_{\mathrm{M}}\beta}\right)\right)}{dz^n}\right|_{z=x^{\alpha_{\mathrm{M}}}},\tag{3.20}$$

where $\mathcal{L}_{I_1}\left(s\right)$ is the Laplace transform of the PDF of I_1. Then has

$$\mathcal{L}_{I_1}\left(s\right)=\mathcal{L}_{I_{\mathrm{M},1}}\left(s\right)\mathcal{L}_{I_{\mathrm{S},1}}\left(s\right),\tag{3.21}$$

where $\mathcal{L}_{I_{\mathrm{M},1}}\left(s\right)$ is the Laplace transform of the PDF of $I_{\mathrm{M},1}$, which is calculated as

$$\begin{aligned}\mathcal{L}_{I_{\mathrm{M},1}}\left(s\right)&=\mathrm{E}\left[\exp\left(-\mathrm{s}\sum\nolimits_{\ell\in\Phi_{\mathrm{M}}\setminus\mathrm{B}_{\mathrm{o,M}}}\frac{\mathrm{P_M}}{\mathrm{S}}\mathrm{h}_{\ell,\mathrm{M}}\mathrm{L}\left(|\mathrm{X}_{\ell,\mathrm{M}}|\right)\right)\right]\\&=\mathrm{E}_{\Phi_{\mathrm{M}}}\left[\prod_{\ell\in\Phi_{\mathrm{M}}\setminus B_{o,\mathrm{M}}}\mathrm{E}_{\mathrm{h}_{\ell,\mathrm{M}}}\left[\exp\left(-s\frac{P_{\mathrm{M}}}{S}h_{\ell,\mathrm{M}}\beta|X_{\ell,\mathrm{M}}|^{-\alpha_{\mathrm{M}}}\right)\right]\right]\\&\overset{(a)}{=}\exp\left(-\int_x^\infty\left(1-\mathrm{E}_{\mathrm{h}_{\ell,\mathrm{M}}}\left[\exp\left(-s\frac{P_{\mathrm{M}}}{S}h_{\ell,\mathrm{M}}\beta r^{-\alpha_{\mathrm{M}}}\right)\right]\right)\lambda_{\mathrm{M}}2\pi rdr\right)\\&=\exp\left(-\int_x^\infty\left(1-\frac{1}{\left(1+s\frac{P_{\mathrm{M}}}{S}\beta r^{-\alpha_{\mathrm{M}}}\right)^S}\right)\lambda_{\mathrm{M}}2\pi rdr\right)\\&\overset{(b)}{=}\exp\left(-\lambda_{\mathrm{M}}2\pi\sum_{\mu=1}^{S}\binom{S}{\mu}\int_x^\infty\frac{\left(\frac{P_{\mathrm{M}}}{S}\beta\right)^\mu s^\mu\left(r^{-\alpha_{\mathrm{M}}}\right)^\mu}{\left(1+s\frac{P_{\mathrm{M}}}{S}\beta r^{-\alpha_{\mathrm{M}}}\right)^S}rdr\right),\end{aligned}\tag{3.22}$$

where (a) is obtained by using the generating functional of PPP [Hae12], (b) results

from using Binomial expansion. Likewise, $\mathcal{L}_{I_{\mathrm{S},1}}(s)$ is the Laplace transform of the PDF of $I_{\mathrm{S},1}$, which is calculated as

$$\begin{aligned}\mathcal{L}_{I_{\mathrm{S},1}}(s) &= \mathrm{E}\left[\exp\left(-\mathrm{s}\sum_{\mathrm{i}=2}^{\mathrm{K}}\sum\nolimits_{\mathrm{j}\in\Phi_{\mathrm{i}}}\mathrm{P_i h_{j,i}}\mathcal{L}\left(|\mathrm{X_{j,i}}|\right)\right)\right] \\ &= \exp\left(-\sum_{i=2}^{K}\lambda_i 2\pi\int_{R_i^{\mathrm{M}}(x)}^{\infty}\left(\frac{sP_i\beta r^{-\alpha_i}}{1+sP_i\beta r^{-\alpha_i}}\right)rdr\right), \end{aligned} \tag{3.23}$$

where $R_i^{\mathrm{M}}(x)$ denotes the distance between the closest interfering BS in the i-th tier and the typical user.

By plugging (3.22) and (3.23) into (3.21), after some manipulations, $\mathcal{L}_{I_1}(s)$ is derived as

$$\mathcal{L}_{I_1}(s) = e^{-\Xi(s)}, \tag{3.24}$$

where $\Xi(s)$ is given by (3.14). Substituting (3.24) into (3.20), and using the Faà di Bruno's formula, (3.13) obtained. □

Similarly, the coverage probability of a typical user that is associated with SBS in the k-th tier is derived as

$$P_{\mathrm{cov}}^{k}(\gamma) = \int_0^{\infty} P_{\mathrm{cov}}^{k}(x,\gamma) f_{|X_{o,k}|}(x)\, dx, \tag{3.25}$$

where $f_{|X_{o,k}|}(x)$ is given by (3.7), $P_{\mathrm{cov}}^{k}(x,\gamma)$ is the conditional coverage probability given

a distance x between a typical user and its serving SBS in the k-tier, which is given by

$$P_{\text{cov}}^{k}(x,\gamma) = \exp\Bigg\{ -\frac{\gamma x^{\alpha_k}\delta^2}{P_k\beta} - \lambda_{\text{M}} 2\pi \sum_{\mu=1}^{S} \binom{S}{\mu} \left(\frac{\gamma x^{\alpha_k} P_{\text{M}}}{P_k S}\right)^{\mu}$$
$$\times \frac{\left(-\frac{\gamma x^{\alpha_k} P_{\text{M}}}{P_k S}\right)^{-\mu+\frac{2}{\alpha_{\text{M}}}}}{\alpha_{\text{M}}} B_{\left(-\frac{\gamma x^{\alpha_k} P_{\text{M}}}{P_k S}\left(R_{\text{M}}^{k}(x)\right)^{-\alpha_{\text{M}}}\right)}\left[\mu - \frac{2}{\alpha_{\text{M}}}, 1-S\right]$$
$$- \sum_{i=2}^{K} \lambda_i 2\pi \frac{\gamma x^{\alpha_k}}{P_k} P_i \frac{(R_i^k(x))^{2-\alpha_i}}{\alpha_i - 2}$$
$$\times {}_2F_1\left[\frac{\alpha_i - 2}{\alpha_i}, 1; 2 - \frac{2}{\alpha_i}; -\frac{\gamma}{P_k} P_i (R_i^k(x))^{\alpha_k - \alpha_i}\right] \Bigg\}, \tag{3.26}$$

where $R_{\text{M}}^{k}(x) = \left(\frac{N-S+1}{SP_k} P_{\text{M}}\right)^{\frac{1}{\alpha_{\text{M}}}} x^{\frac{\alpha_k}{\alpha_{\text{M}}}}$ is the distance between the closest interfering MBS and the typical user, $R_i^k(x) = \left(\frac{P_i}{P_k}\right)^{\frac{1}{\alpha_i}} x^{\frac{\alpha_k}{\alpha_i}}$ is the distance between the closest interfering BS in the i-th tier and the typical user.

Based on (3.12) and (3.25), and using the law of total probability, the coverage probability of a typical user in HCNs is obtained as

$$P_{\text{cov}}^{\text{HCN}}(\gamma) = \mathcal{A}_{\text{M}} P_{\text{cov}}^{\text{M}}(\gamma) + \sum_{k=2}^{K} \mathcal{A}_k P_{\text{cov}}^{k}(\gamma). \tag{3.27}$$

3.2.3.2 Spectrum Efficiency Analysis

Next, the network SE is derived based on the coverage probability.

The downlink SE between a typical user and its serving MBS is calculated as [ABG11]

$$\begin{aligned} \tau_{\text{M}} &= \mathbb{E}\left\{\log_2(1+\text{SINR}_{\text{M}})\right\} \\ &\overset{(c)}{=} \frac{1}{\ln 2} \int_0^{\infty} \frac{P_{\text{cov}}^{\text{M}}(\gamma)}{1+\gamma} d\gamma, \end{aligned} \tag{3.28}$$

where (c) is used the integration by parts and derivations detail can found in Appendix

B.2. Similarly, the downlink SE between a typical user and its serving SBS in the k-th tier is derived as

$$\tau_k = \mathbb{E}\left\{\log_2\left(1+\mathrm{SINR}_k\right)\right\} = \frac{1}{\ln 2}\int_0^{\infty}\frac{P_{\mathrm{cov}}^k\left(\gamma\right)}{1+\gamma}d\gamma. \tag{3.29}$$

Finally, the downlink SE of K-tier HCNs can be obtained as

$$\mathrm{SE}_{\mathrm{HetNets}} = \mathcal{A}_{\mathrm{M}} \times \mathrm{SE}_{\mathrm{M}} + \sum_{k=2}^{K}\mathcal{A}_k \times \mathrm{SE}_k, \tag{3.30}$$

where $\mathrm{SE}_{\mathrm{M}} = S \times \tau_{\mathrm{M}}$ is the SE of macro cell, and $\mathrm{SE}_k = \tau_k$ is the SE of small cell in the k-th tier.

3.2.4 Numerical Results

Numerical results are provided to understand the impact of massive MIMO and BS density on the user association, coverage and SE. This analysis considers a two-tier network consisting of macro cells with density $\lambda_{\mathrm{M}} = \left(500^2 \times \pi\right)^{-1}$ and picocells with density λ_2. Such a network is assumed to operate at 1 GHz (carrier frequency), and the bandwidth is BW = 10 MHz, the path loss exponents $\alpha_{\mathrm{M}} = 3.5$ and $\alpha_2 = 4$, the transmit power at the picocell base station is $P_2 = 30$ dBm, the noise figure is Nf = 10 dB, hence the noise power is $\delta^2 = -170 + 10 \times \log_{10}\left(\mathrm{BW}\right) + \mathrm{Nf} = -90$ dBm.

Figure 3.2 shows the probability that a user is associated with MBS. The number of active users in each macro cell is $S = 5$. The solid and dash curves represent the exact and asymptotic expressions given by (3.6) and (3.11), respectively. The exact curves have a good match with Monte Carlo simulation marked with 'o' and the asymptotic curves well approximate the exact ones at high number of antennas N. It can be observed that even when MBS cuts its transmit power by the same level as the picocell BS (PBS) (e.g. $P_{\mathrm{M}} = 30$ dBm), a user is still much more likely to be associated with the MBS than

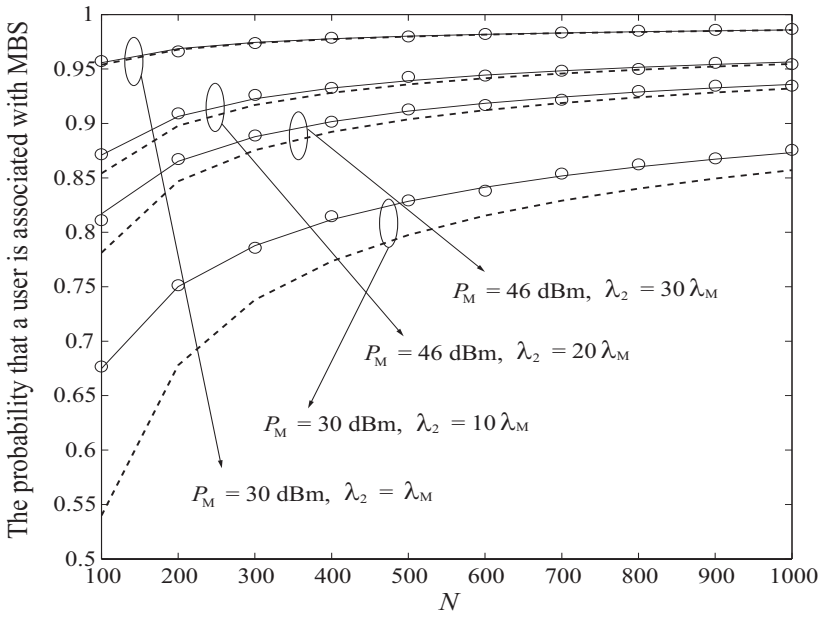

Figure 3.2: The probability that a user is associated to MBS versus the antenna numbers N with different MBS transmit power P_{M} and different PBS density λ_2, where $S = 5$.

with the PBS, due to the large array gain. It can also be observed that increasing the number of antennas at the MBS improves the probability that a user is associated with MBS, which indicates that MBSs with large antenna arrays have potential to carry more traffic load and decrease the number of required small cells in practice.

Figure 3.3 shows the coverage probability for different SINR thresholds in a conventional MIMO system. The number of active users in each macro cell is $S = 2$, the transmit power of the MBSs are assumed as $P_{\mathrm{M}} = 46$ dBm and antenna number is set as $N = 4$. The analytical curves are obtained from (3.12), (3.25), and (3.27), respectively, and they have a precise match with the Monte Carlo simulation marked with 'o'. Note that without massive MIMO, the coverage probability of a user in the macro cell is close to that in the picocell, and the picocell outperforms the macro cell when the SINR threshold is high. The reason is that a large amount of PBSs are deployed such that the distance between the user and the PBS is shortened, which decreases the path loss.

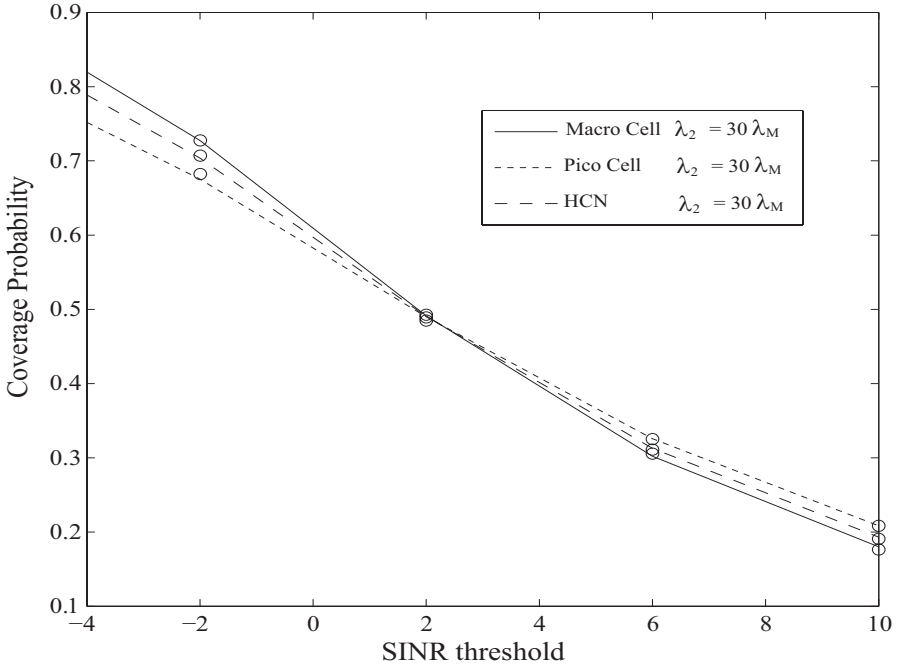

Figure 3.3: Coverage probability of macrocell, picocell and the overall network versus SINR thresholds with unit dB, where $P_{\mathrm{M}} = 46$ dBm, $N = 4$ and $S = 2$.

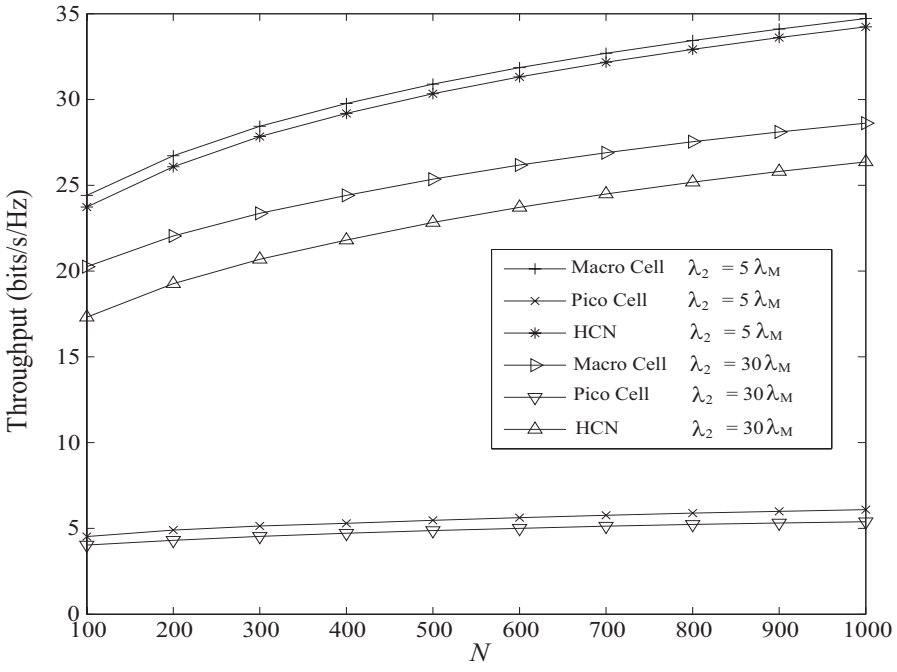

Figure 3.4: The downlink SE versus number of MBS antennas N with different PBS density λ_2, where $P_{\mathrm{M}} = 46$ dBm and $S = 5$.

Figure 3.4 shows the SE for different numbers of antennas at the MBS with different density ratios. The number of active users in each macro cell is $S = 5$ and the MBS transmit power is $P_{\mathrm{M}} = 46$ dBm. It is noticeable that increasing the MBS antennas can enhance the SE and the main contribution on the SE of this two-tier network is made by the MBS. Also, it can be seen that decreasing the PBS density can achieve higher SE. The reason is that deploying more small cells brings severer inter-cell interference. Thus the demand of small cells can be decreased after employing massive MIMO in HCNs. Another observation is that the SE between the user and its serving PBS slightly increases with increasing the number of MBS antennas. The reason is that the averaged distance between the active user and its serving PBS becomes smaller than before such that the received signal from the PBS is stronger, otherwise the user will be served by MBS, as suggested in Figure 3.2.

3.3 Spectrum Efficiency and Energy Efficiency with Cell Range Expansion

In HCNs, there is a significant difference in maximum downlink transmit power between macro BSs (MBSs) and low power nodes; e.g. the maximum transmit power of a macro BS in long term evolution (LTE) networks is standardized as 46dBm while a pico BS is 30dBm. Therefore, users are preferred to be associated with the MBSs when the maximum receive power association strategy is applied, which leads to heavy loaded macrocells. In order to offload the data traffic to small cells, the idea of CRE was utilised in [JSXA12]. The rational behind CRE is to impact the cell selection process by adding the predefined offset to the received power from small BS (SBS) in order to facilitate macro-layer offload. The small cell range expands when bias is larger than 1.

In this section, SBSs are designed to have a bias towards admitting users and then the SE and EE in K-tier massive MIMO aided HCNs are analysed.

3.3.1 System Model

3.3.1.1 Spatial Distribution

Similarly to the Section 3.2, TDD downlink transmission in K-tier HetNets consisting of macro cells and small cells such as picocells and femtocells are considered. It is assumed that the first tier represents the class of MBSs, where each MBS is equipped with a large antenna array. The positions of the MBSs are modeled following a HPPP Φ_{M} with density λ_{M}. The positions of the SBSs in the i-th tier ($i = 2, \ldots, K$) are modeled following an independent HPPP Φ_i with density λ_i. Massive MIMO is applied in the macro cells [JMZ+14], where each MBS has N antennas and simultaneously communicates with S users over the same time and frequency band, $N \gg S \geq 1$, while each SBS and user are single antenna nodes. Each MBS uses linear ZFBF to transmit S data streams with equal power assignment. The perfect downlink CSI and the universal frequency reuse are considered such that all of the tiers share the same bandwidth. All the channels undergo independent and identically distributed (i.i.d.) quasi-static Rayleigh fading.

3.3.1.2 User Association

The flexible cell association based on maximum received power is considered. Since users in the macro cell have large array gains, the long-term average receive power at a user which is connected with the MBS ℓ ($\ell \in \Phi_{\mathrm{M}}$) is expressed as

$$P_{r,\mathrm{M}} = G_a \frac{P_{\mathrm{M}}}{S} L\left(|X_{\ell,\mathrm{M}}|\right), \tag{3.31}$$

where G_a is the array gain, P_{M} is the MBS's transmit power, $L\left(|X_{\ell,\mathrm{M}}|\right) = \beta |X_{\ell,\mathrm{M}}|^{-\alpha_{\mathrm{M}}}$ is the path loss function, β is the frequency dependent constant value, $|X_{\ell,\mathrm{M}}|$ is the distance, and α_{M} is the path loss exponent. The array gain G_a obtained by the ZFBF transmission is $N - S + 1$ [XM15, HYA14]. It can be seen that the long-term average receive power is scaled by $(N - S + 1)/S$, compared to the single-antenna systems.

Due to the CRE is considered in the small cells, that is the bias factor $\hat{B}_k \neq 1$, the long-term average receive power at a user which is connected with the SBS k ($k \in \Phi_i$) in the i-th tier is expressed as

$$P_{r,i} = P_i L\left(|X_{k,i}|\right) B_i, \tag{3.32}$$

where P_i is the SBS's transmit power in the i-th tier and $L\left(|X_{k,i}|\right) = \beta(|X_{k,i}|)^{-\alpha_i}$ with distance $|X_{k,i}|$ and path loss exponent α_i, and B_i is the biasing factor, which is useful for offloading the data traffic to small cells in conventional HetNets.

3.3.1.3 Channel Model

Assuming that a typical user is located at the origin o, the receive SINR of a typical user, at a random distance $|X_{o,\mathrm{M}}|$ from its associated MBS is given by

$$\mathrm{SINR}_{\mathrm{M}} = \frac{\frac{P_{\mathrm{M}}}{S} h_{o,\mathrm{M}} L\left(|X_{o,\mathrm{M}}|\right)}{I_1 + \delta^2}, \tag{3.33}$$

where $I_1 = I_{\mathrm{M},1} + I_{\mathrm{S},1}$, $I_{\mathrm{S},1} = \sum_{i=2}^{K} \sum_{j \in \Phi_i} P_i h_{j,i} L\left(|X_{j,i}|\right)$, $I_{\mathrm{M},1} = \sum_{\ell \in \Phi_{\mathrm{M}} \backslash B_{o,\mathrm{M}}} \frac{P_{\mathrm{M}}}{S} h_{\ell,\mathrm{M}} L\left(|X_{\ell,\mathrm{M}}|\right)$, P_{M} is the transmit power of the MBS, P_i is the transmit power of the interfering SBS from the ith tier. $h_{o,\mathrm{M}} \sim \Gamma\left(N - S + 1, 1\right)$as is the small-scale fading channel power gain between the typical user and its associated MBS, $h_{j,i} \sim \exp(1)$ and $|X_{j,i}|$ are the small-scale fading interfering channel power gain and distance between the typical user and SBS j in the i-th tier, respectively, $h_{\ell,\mathrm{M}} \sim \Gamma\left(S, 1\right)$ and $|X_{\ell,\mathrm{M}}|$ are the equivalent small-scale fading interfering channel power gain and distance between the typical user and MBS $\ell \in \Phi_{\mathrm{M}} \backslash \mathrm{B}_{o,\mathrm{M}}$ (except the serving MBS $B_{o,\mathrm{M}}$), respectively, and δ^2 is the noise power.

The SINR of a typical user at a random distance $|X_{o,k}|$ from its associated SBS $B_{o,k}$

in the k-th tier is given by

$$\mathrm{SINR}_k = \frac{P_k g_{o,k} L\left(|X_{o,k}|\right)}{I_k + \delta^2}, \tag{3.34}$$

where $I_k = I_{\mathrm{M},k} + I_{\mathrm{S},k}$, $I_{\mathrm{M},k} = \sum_{\ell \in \Phi_{\mathrm{M}}} \frac{P_{\mathrm{M}}}{S} g_{\ell,\mathrm{M}} L\left(|X_{\ell,\mathrm{M}}|\right)$, $I_{\mathrm{S},k} = \sum_{i=2}^{K} \sum_{j \in \Phi_i \backslash B_{o,k}} P_i g_{j,i} L\left(|X_{j,i}|\right)$, P_k is the transmit power of the serving SBS. $g_{o,k} \sim \exp(1)$ is the small-scale fading channel power gain between the typical user and its serving SBS, $g_{\ell,\mathrm{M}} \sim \Gamma\left(S, 1\right)$ and $|X_{\ell,\mathrm{M}}|$ are the equivalent small-scale fading interfering channel power gain and distance between the typical user and MBS ℓ, respectively, and $g_{j,i} \sim \exp(1)$ and $|X_{j,i}|$ are the small-scale fading interfering channel power gain and distance between the typical user and SBS $j \in \Phi_i \backslash B_{o,k}$, respectively.

3.3.1.4 Power Consumption Model

Apart from the power consumed by the power amplifier, the circuit power consumption from digital signal processing and analog filters used for radio frequency and baseband processing cannot be ignored at a massive MIMO equipped MBS. Therefore, the total power consumption model at the MBS in each channel use is given by [BSHD14]

$$P_{\mathrm{M}}^{total} = P_{\mathrm{M}}^0 + \frac{P_{\mathrm{M}}}{\varepsilon_{\mathrm{M}}} + \sum_{t=1}^{3} \Big((S)^t \Delta_t + (S)^{(t-1)} N \Lambda_t \Big), \tag{3.35}$$

where P_{M}^0 is the MBS's static hardware power consumption, $\varepsilon_{\mathrm{M}} \left(0 < \varepsilon_{\mathrm{M}} \leq 1\right)$ is the efficiency of the power amplifier, the parameters Δ_t and Λ_t depends on the transceiver chains, coding and decoding, precoding, etc.[5], which are detailed set in the Section 3.3.4.

In the small cell, the total power consumption at the SBS in ith tier in each channel use is given by

$$P_i^{total} = P_i^0 + \frac{P_i}{\varepsilon_i}, \tag{3.36}$$

[5]The exact coefficient setting under ZF precoding can be found in Table I in [BSHD15]

where P_i^0 is the static hardware power consumption of the SBS in the i-th tier, and ε_i is the efficiency of the power amplifier.

3.3.2 User Association Probability

Based on the user association described in the previous section, new probability density function (PDF) of the distance between a typical user and its serving base station is provided as the following two lemmas.

Lemma 3. The PDF of the distance $|X_{o,\mathrm{M}}|$ between a typical user and its serving MBS $B_{o,\mathrm{M}}$ is given by

$$f_{|X_{o,\mathrm{M}}|}(x) = \frac{2\pi\lambda_{\mathrm{M}}}{\mathcal{A}_{\mathrm{M}}} x \exp\left\{ -\pi\lambda_{\mathrm{M}} x^2 - \pi \sum_{i=2}^{K} \lambda_i \left(\frac{P_i B_i S x^{\alpha_{\mathrm{M}}}}{P_{\mathrm{M}} (N - S + 1)} \right)^{2/\alpha_i} \right\}. \tag{3.37}$$

Here, $\mathcal{A}_{\mathrm{M}}$ is the probability that a typical user is associated with the MBS, which is given by

$$\mathcal{A}_{\mathrm{M}} = 2\pi\lambda_{\mathrm{M}} \int_0^{\infty} r \exp\left\{ -\pi\lambda_{\mathrm{M}} r^2 - \pi \sum_{i=2}^{K} \lambda_i \left(\frac{P_i B_i S r^{\alpha_{\mathrm{M}}}}{P_{\mathrm{M}} (N - S + 1)} \right)^{2/\alpha_i} \right\} dr. \tag{3.38}$$

Lemma 4. The PDF of the distance $|X_{o,k}|$ between a typical user and its serving SBS in the k-th tier $\mathrm{B}_{o,k}$ is given by

$$f_{|X_{o,k}|}(x) = \frac{2\pi\lambda_k}{\mathcal{A}_k} x \exp\left\{ -\pi\lambda_{\mathrm{M}} \left(\frac{P_{\mathrm{M}} (N - S + 1) x^{\alpha_k}}{P_k B_k S} \right)^{2/\alpha_{\mathrm{M}}} - \pi \sum_{i=2}^{K} \lambda_i \left(\frac{P_i B_i x^{\alpha_k}}{P_k B_k} \right)^{2/\alpha_i} \right\}. \tag{3.39}$$

Here, $\mathcal{A}_k$ is the probability that a typical user is associated with the SBS in the k-th

tier, which is given by

$$\mathcal{A}_k = 2\pi\lambda_k \int_0^\infty r \exp\left\{ -\pi\lambda_{\mathrm{M}} \left(\frac{P_{\mathrm{M}} \left(N - S + 1\right) r^{\alpha_k}}{P_k B_k S} \right)^{2/\alpha_{\mathrm{M}}} - \pi \sum_{i=2}^{K} \lambda_i \left(\frac{P_i B_i r^{\alpha_k}}{P_k B_k} \right)^{2/\alpha_i} \right\} dr. \tag{3.40}$$

Note that **Lemma 3** and **Lemma 4** can be easily obtained following the similar approach in the section 3.2.2.

Remark 4. *From* $\mathcal{A}_{\mathrm{M}}$ *in* **Lemma** 3 *and* $\mathcal{A}_k$ *in* **Lemma** 4*, it can be seen that increasing the bias factor in SBS increases the probability that a user is associated with the SBS, which in turn decreases the probability that a user is associated with the MBS.*

3.3.3 Spectrum Efficiency and Energy Efficiency

SE and EE are principal performance metrics in HetNets to be explored. Using the statistical property, analytical expressions for SE and EE in massive MIMO enabled HetNets are presented.

In the following theorem, a tractable lower bound on the SE when a typical user is associated with MBS is first derived.

Theorem 5. The lower bound on the SE when a typical user is associated with MBS is given by

$$\tau_{\mathrm{M}}^{\mathrm{L}} = \log_2 \left(1 + (N - S + 1) \frac{P_{\mathrm{M}}}{S} \beta \Upsilon^{-1} \right), \tag{3.41}$$

where

$$\Upsilon = \int_0^\infty x^{\alpha_{\mathrm{M}}} \left(\overline{I}(x) + \delta^2 \right) f_{|X_{o,\mathrm{M}}|}(x)\, dx$$

with $\overline{I}(x) = \frac{P_{\mathrm{M}} \beta 2\pi\lambda_{\mathrm{M}}}{\alpha_{\mathrm{M}} - 2} x^{2-\alpha_{\mathrm{M}}} + \sum_{i=2}^{K} \frac{P_i \beta 2\pi\lambda_i}{\alpha_i - 2} \left(R_i^{\mathrm{M}}(x) \right)^{2-\alpha_i}$, $R_i^{\mathrm{M}}(x) = \left(\frac{P_i B_i S}{(N-S+1) P_{\mathrm{M}}} \right)^{\frac{1}{\alpha_i}} x^{\frac{\alpha_{\mathrm{M}}}{\alpha_i}}$,

and $f_{|X_{o,\mathrm{M}}|}(x)$ is given by (3.37).

Proof. The SE is defined as $\mathbb{E}\{\log_2(1+\mathrm{SINR}_{\mathrm{M}})\}$. Using Jensen's inequality, the lower bound can be obtained [NLM13a] [6]

$$\tau_{\mathrm{M}}^{\mathrm{L}} = \log_2\left(1+\frac{1}{\mathbb{E}\left\{(\mathrm{SINR}_{\mathrm{M}})^{-1}\right\}}\right). \tag{3.42}$$

Based on (3.33), $\mathbb{E}\left\{(\mathrm{SINR}_{\mathrm{M}})^{-1}\right\}$ is calculated as

$$\begin{aligned}
\mathbb{E}\left\{(\mathrm{SINR}_{\mathrm{M}})^{-1}\right\} &= \mathbb{E}\left\{\frac{I_1+\delta^2}{\frac{P_{\mathrm{M}}}{S}h_{o,\mathrm{M}}\beta x^{-\alpha_{\mathrm{M}}}}\right\} \\
&\overset{(a)}{\approx} \left(P_{\mathrm{M}}\frac{N-S+1}{S}\beta\right)^{-1}\mathbb{E}\left\{\left(I_1+\delta^2\right)x^{\alpha_{\mathrm{M}}}\right\} \\
&= \left(P_{\mathrm{M}}\frac{N-S+1}{S}\beta\right)^{-1}\int_0^{\infty} x^{\alpha_{\mathrm{M}}}\left(\overline{I}(x)+\delta^2\right)f_{|X_{o,\mathrm{M}}|}(x)\,dx,
\end{aligned} \tag{3.43}$$

where (a) is obtained by using the law of large numbers, i.e., $h_{o,\mathrm{M}} \approx N-S+1$ as N is large. In (3.43), $\overline{I}(x) = \mathbb{E}\{I_1\}$ is the expectation of the sum of interference, which can be derived as

$$\begin{aligned}
\overline{I}(x) =& \mathbb{E}\left\{\sum\nolimits_{\ell\in\Phi_{\mathrm{M}}\setminus \mathrm{B}_{o,\mathrm{M}}}\frac{P_{\mathrm{M}}}{S}h_{\ell,\mathrm{M}}\beta x^{-\alpha_{\mathrm{M}}}\right\} + \mathbb{E}\left\{\sum_{i=2}^{K}\sum\nolimits_{j\in\Phi_i}P_i h_{j,i}\beta x^{-\alpha_i}\right\} \\
\overset{(b)}{=}& P_{\mathrm{M}}\beta 2\pi\lambda_{\mathrm{M}}\int_x^{\infty} t^{-\alpha_{\mathrm{M}}}t dt + \sum_{i=2}^{K}P_i\beta 2\pi\lambda_i\int_{R_i^{\mathrm{M}}(x)}^{\infty} t^{-\alpha_i}t dt \\
=& \frac{P_{\mathrm{M}}\beta 2\pi\lambda_{\mathrm{M}}}{\alpha_{\mathrm{M}}-2}x^{2-\alpha_{\mathrm{M}}} + \sum_{i=2}^{K}\frac{P_i\beta 2\pi\lambda_i}{\alpha_i-2}\left(R_i^{\mathrm{M}}(x)\right)^{2-\alpha_i},
\end{aligned} \tag{3.44}$$

where (b) is obtained by using Campbell's theorem [BB09]. In (3.44), $R_i^{\mathrm{M}}(x)$ is the closest distance between the interfering SBS in the i-th tier and the typical user. Substituting (3.43) and (3.44) into (3.42), (3.41) obtained. □

From Theorem 5, it can be found that the SE per user in the macro cell increases

[6] We note that the exact expression for the SE can be written in a general-form following the approach in [DRGC13], however, it is very difficult to compute the SE by using such approach in this chapter.

with increasing the number of antennas. However, it decreases with increasing number of users served by the MBS, since the transmit power assigned to each user is reduced, and the intra-cell interference is cancelled at the cost of decreasing array gain.

Then derive the SE τ_k when a typical user is associated with SBS in the k-th tier, which is given by

$$\tau_k = \mathbb{E}\left\{\log_2\left(1+\mathrm{SINR}_k\right)\right\} = \frac{1}{\ln 2}\int_0^\infty \frac{P_{\mathrm{cov}}^k\left(\gamma\right)}{1+\gamma}d\gamma, \tag{3.45}$$

where $P_{\mathrm{cov}}^k\left(\gamma\right) = \int_0^\infty P_{\mathrm{cov}}^k\left(x,\gamma\right) f_{|X_{o,k}|}\left(x\right)dx$. Here, $P_{\mathrm{cov}}^k\left(x,\gamma\right)$ is the conditional coverage probability given a distance x between a typical user and its serving SBS in the k-tier, which is given by

$$\begin{aligned} P_{\mathrm{cov}}^k\left(x,\gamma\right) &= \Pr\left(\frac{P_k g_{o,k}\beta x^{-\alpha_k}}{I_k+\delta^2} > \gamma\right) \\ &= \exp\left(-\frac{\gamma x^{\alpha_k}\delta^2}{P_k\beta}\right)\mathcal{L}_{I_k}\left(\frac{\gamma x^{\alpha_k}}{P_k\beta}\right), \end{aligned} \tag{3.46}$$

where $\mathcal{L}_{I_k}\left(\cdot\right)$ is the Laplace transform of the PDF of I_k. Using the generating functional of PPP, we derive $\mathcal{L}_{I_k}\left(\cdot\right)$ as

$$\begin{aligned} \mathcal{L}_{I_k}\left(s\right) = \exp\Bigg\{ &-\lambda_{\mathrm{M}} 2\pi \sum_{\mu=1}^{S}\binom{S}{\mu}\left(s\frac{P_{\mathrm{M}}}{S}\beta\right)^{\mu}\frac{\left(-s\frac{P_{\mathrm{M}}}{S}\beta\right)^{-\mu+\frac{2}{\alpha_{\mathrm{M}}}}}{\alpha_{\mathrm{M}}} \\ &B_{\left(-s\frac{P_{\mathrm{M}}}{S}\beta\left(R_{\mathrm{M}}^k(x)\right)^{-\alpha_{\mathrm{M}}}\right)}\left[\mu-\frac{2}{\alpha_{\mathrm{M}}}, 1-S\right] - \sum_{i=2}^{K}\lambda_i 2\pi s P_i\beta \\ &\frac{\left(R_i^k(x)\right)^{2-\alpha_i}}{\alpha_i-2}{}_2F_1\left[\frac{\alpha_i-2}{\alpha_i}, 1; 2-\frac{2}{\alpha_i}; -sP_i\beta\left(R_i^k(x)\right)^{-\alpha_i}\right]\Bigg\}, \end{aligned} \tag{3.47}$$

where $R_{\mathrm{M}}^k\left(x\right) = \left(\frac{P_{\mathrm{M}}(N-S+1)}{P_k B_k S}\right)^{1/\alpha_{\mathrm{M}}} x^{\alpha_k/\alpha_{\mathrm{M}}}$ and $R_i^k\left(x\right) = \left(\frac{P_i B_i}{P_k B_k}\right)^{1/\alpha_i} x^{\alpha_k/\alpha_i}$, $\mathrm{B}_{(\cdot)}\left[\cdot,\cdot\right]$ is the incomplete beta function [GR07, (8.391)], and ${}_2F_1\left[\cdot,\cdot;\cdot;\cdot\right]$ is the Gauss hypergeometric function [GR07, (9.142)].

Based on the above analysis, using the law of total expectation, a tractable lower

bound on the SE of K-tier HetNets with massive MIMO is given by

$$\mathrm{SE}_{\mathrm{HetNets}}^{\mathrm{L}} = \mathcal{A}_{\mathrm{M}} \times \mathrm{SE}_{\mathrm{M}} + \sum_{k=2}^{K} \mathcal{A}_k \times \mathrm{SE}_k, \tag{3.48}$$

where $\mathrm{SE}_{\mathrm{M}} = S \times \tau_{\mathrm{M}}^{\mathrm{L}}$ is the SE of macro cell, and $\mathrm{SE}_k = \tau_k$ is the SE of small cell in the k-th tier. The lower bound on the EE of K-tier HetNets with massive MIMO is given by

$$\mathrm{EE}_{\mathrm{HetNets}}^{\mathrm{L}} = \mathcal{A}_{\mathrm{M}} \times \mathrm{EE}_{\mathrm{M}} + \sum_{k=2}^{K} \mathcal{A}_k \times \mathrm{EE}_k, \tag{3.49}$$

where $\mathrm{EE}_{\mathrm{M}} = \frac{S \times \tau_{\mathrm{M}}^{\mathrm{L}}}{P_{\mathrm{M}}^{total}}$ is the EE of macro cell, and $\mathrm{EE}_k = \frac{\tau_k}{P_k^{total}}$ is the EE of small cell in the k-th tier.

Note that higher SE means lower spectrum consumption and higher EE means lower energy consumption.

3.3.4 Numerical Results

Numerical results are provided to understand the impact of flexible user association and massive MIMO on the SE and EE. A two-tier network consisting of macro cells with density $\lambda_{\mathrm{M}} = \left(500^2 \times \pi\right)^{-1}$ and picocells with density $\lambda_2 = 20 * \lambda_{\mathrm{M}}$ is considered in a circular region with radius 1×10^4m. Such a network is assumed to operate at a carrier frequency of 1 GHz and a bandwidth of BW = 10 MHz, the path loss exponents $\alpha_{\mathrm{M}} = 3.5$ and $\alpha_2 = 4$, the transmit power at the MBS is $P_{\mathrm{M}} = 40$ dBm, the transmit power at the picocell base station is $P_2 = 30$ dBm, and the noise figure is Nf = 10 dB, hence the noise power is $\delta^2 = -170 + 10 \times \log_{10}(\mathrm{BW}) + \mathrm{Nf} = -90$ dBm. Set the coefficients for power consumption under LZFBF precoding in (3.35) as $P_{\mathrm{M}}^0 = 4$ W, $\Delta_1 = 4.8$, $\Delta_2 = 0$, $\Delta_3 = 2.08 \times 10^{-8}$, $\Lambda_0 = 1$, $\Lambda_1 = 9.5 \times 10^{-8}$ and $\Lambda_2 = 6.25 \times 10^{-8}$ [BSHD14]. The static power consumption of PBS is $P_2^0 = 13.6$ W [AGD+11]. In the figures, Monte Carlo simulated lower bounds of the SE and EE marked by 'o' are numerically obtained to

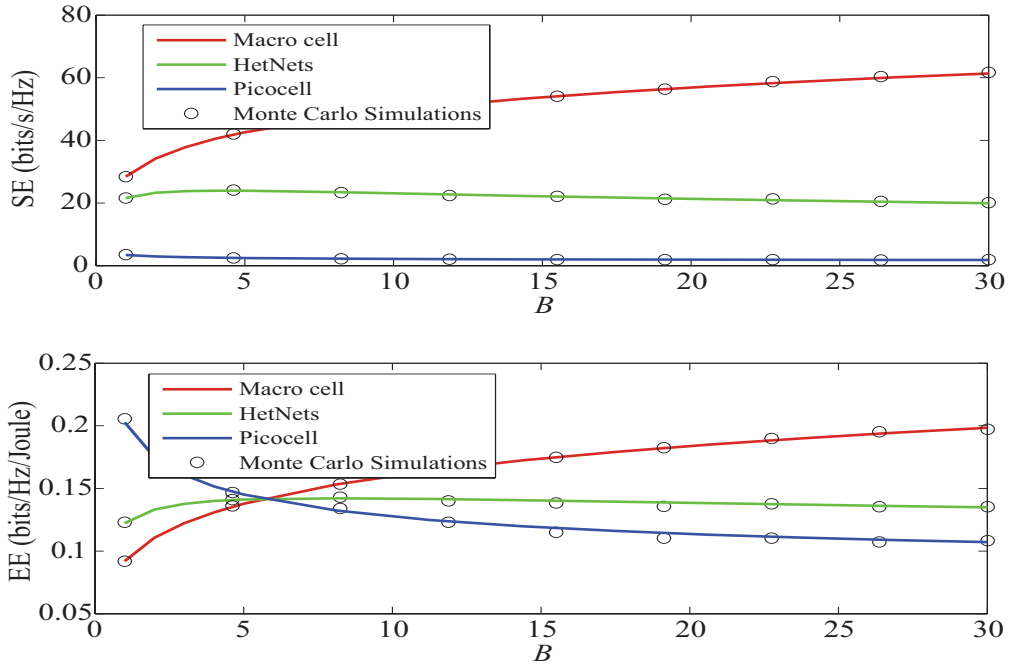

Figure 3.5: The SE and EE of macrocell, picocell and the overall network versus biasing factor B with unit dB.

validate the analytical ones, and the red, blue and green curves represent the SE and EE achieved by the macro cell, picocell, and HetNets, respectively.

Figure 3.5 shows the SE and EE for different biasing factor B. Here, we set $N = 200$ and $S = 15$. The analytical SE and EE curves are obtained from (3.41), (3.45), (3.48) and (3.49) respectively. Evidently, the analytical curves have a good match with the Monte Carlo simulations, which validates our theoretical analysis. The effects of different B are:

- **SE**. As the picocell biasing factor B increases, the SE of picocell decreases and the SE of macro cell increases. This is attributed to the fact that more macro cell users with low SINR are associated with the picocell, which in turn improves the SE of the macro cell but degrades the SE of picocell. The SE of HetNets decreases with increasing B, which can be explained by the fact that when macro cell users with low SINR are associated with the picocell, they obtain lower SINR.

- **EE**. By increasing B, the EE of macro cell improves but the EE of picocell degrades,

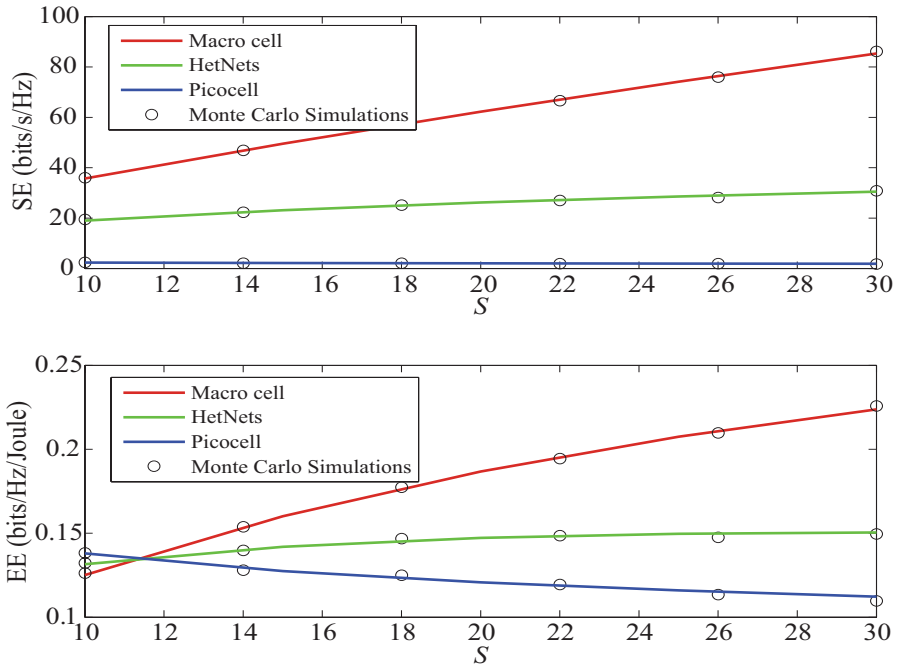

Figure 3.6: The SE and EE of macrocell, picocell and the overall network versus user numbers S.

this is due to the fact that the SE of the macro cell increases and the SE of picocell decreases over the identical power consumption. With increasing B, the EE of HetNet first increases, then it converges to the constant value, which indicates that selecting a suitable biasing factor is still useful for improving the EE of HetNets.

Figure 3.6 shows the SE and EE for different number of users S served by the MBS. Here, we set $N = 200$ and $B = 10$. The effects of different S are:

- **SE**. As the number of users served by the MBS increases, the SE of macro cell significantly increases, and the SE of HetNets also has a significant improvement. Meanwhile, increasing S has no big effect on the SE of picocell.

- **EE**. By increasing S, the EE of macro cell and HetNets also increases, because of increasing SE over the identical power consumption. The decrease of the EE in picocell can be explained by the fact that from (3.41), with increasing S, the SE per user in the macro cell decreases, which results in more macro cell users with low SINR being offloaded on the picocell.

3.4 Summary

In this chapter, the downlink network performance of massive MIMO enabled HCNs is analysed using a stochastic geometry approach. In section 3.2, a user association based on maximal average receive power was employed, and the impact of massive MIMO on the user association was addressed. The expressions for the probability of a user being associated with a macro cell or a small cell were derived. Then the analytical expressions for the coverage probability and SE in such HCNs were derived. It is shown that the implementation of massive MIMO in the macro cell can considerably improve the rate while the transmit power of macrocell BS can be reduced proportionally to $\frac{S}{N-S+1}$. Meanwhile, with the help of massive MIMO, the demands for small cells can be decreased in HCNs, which simplifies the network deployment.

In section 3.3, the impact of CRE was considered in small cells in the K-tier massive MIMO enabled HCNs. A novel asymptotic expression for MBS SE and an exact expression for SBS SE are derived for performance evaluation. EE are derived based on the SE expressions as well. After validated by the Monte Carlo simulations, important guidelines can be drawn from the results, indicating that the mixture of CRE and massive MIMO can achieve significant improvements to SE and EE in macrocells, while the density of small cells and the bias factor should be carefully chosen to enhance the whole network performance.

Chapter 4

Performance Evaluation in Massive MIMO enabled Heterogeneous Cloud Radio Access Networks with Interference Management

4.1 Overview

Heterogeneous C-RAN is a new paradigm by integrating cloud computing with heterogeneous networks (HetNets) [PLJ+14b, PZJ+15]. In heterogeneous C-RAN, severe inter-tier interference is mitigated for the enhancement of SE and EE. In addition, massive MIMO is another essential enabling 5G technology for improving SE and EE. In massive MIMO systems, BSs equipped with large antenna arrays accommodate a large number of users in the same time-frequency domain [NLM13a]. The architecture of heterogenous C-RAN with massive MIMO is envisioned as an appealing solution, since none of these techniques can solely achieve 5G targets [HH15b, PLJ+14b]. In [PLJ+14b], the opportunities and challenges for heterogenous C-RAN with massive MIMO were illustrated, in which it was mentioned that the proper densities of the massive MIMO empowered macrocell BSs and RRHs in the networks should be addressed. While the significance of heterogenous C-RAN with massive MIMO has been highlighted in the prior

works [PWLP15, PLJ+14b], more research efforts should be devoted for comprehensively understanding it.

Although C-RAN can well mitigate the inter-RRH interference by using the efficient interference management techniques such as coordinated multi-point (CoMP), the inter-tier interference between the RRHs and macrocell BSs may be problematic in the heterogeneous C-RAN, due to the limited radio resources. The work of [PZJ+15] considered soft fractional frequency reuse (S-FFR) in the heterogeneous C-RAN, and an energy-efficient resource allocation solution to jointly assign the resource block (RB) and transmit power was obtained by using Lagrange dual decomposition.

Motivated by the aforementioned, this chapter focuses on a two-tier HC-RAN, where RRHs coexist with massive MIMO aided macrocell BSs and the S-FFR is considered for interference management. To the best of my knowledge, this system model has not been investigated comprehensively before. Different from [PZJ+15], the spatially distributed RRHs and massive MIMO enabled macrocell BSs is considered with the help of stochastic geometry. While the aforementioned literature [DP13, KHXR15] considered only one single user existed in the network with multiple RRHs around the user coverage area and evaluated the performance from the standpoint of the user, this chapter analyses the throughput and EE of the entire network by addressing the impact of tier density and massive MIMO. Specifically, the exact expressions of the throughput and EE for RRHs tier are first derived. Then, closed-form lower bound expressions for the throughput and EE of the macrocell BSs tier are obtained. Numerical results show that although RRHs achieve higher EE, massive MIMO adopted by the macrocells can significantly improve the throughput of the entire network. Moreover, when the number of RRHs is not dense, increasing the S-FFR factor decreases the network throughput. When a large number of RRHs is deployed, both throughput and EE of the entire network have a substantial increase.

4.2 System Model

4.2.1 Spatial Distribution

As shown in Figure 4.1, the downlink transmission in a two-tier heterogeneous C-RAN is considered, where the BBU pool in the cloud is established to coordinate the entire network. Massive MIMO enabled macrocell BSs (MBSs) of the first tier, as high power nodes (HPNs), are connected with the BBU pool via backhaul link; and RRHs of the second tier, as low power nodes (LPNs), are connected with the BBU pool via fronthaul link (optical fibre link). Different from [PZJ+15] who considered only one single user existed in the network with multiple RRHs around, the locations of MBSs are modelled following a homogeneous HPPP Φ_{M} with density λ_{M}, and the locations of RRHs are modelled following an independent HPPP Φ_{R} with density λ_{R}. Using linear zero-forcing beam-forming (ZFBF), each MBS is equipped with N_{M} antennas and simultaneously communicates with S single-antenna users over the same RB ($N_{\mathrm{M}} \gg S \geq 1$) under equal power assignment. Each RRH is equipped with one single antenna and serves one single-antenna user [1] over one RB. The total number of RBs is K and B_o is the bandwidth per RB. All the channels are assumed to undergo independent identically distributed (i.i.d.) quasi-static Rayleigh block fading. In this network, each user is assumed to be connected with its nearest BS such that the Euclidean plane is divided into Poisson-Voronoi cells.

4.2.2 Channel Model

In this model, the S-FFR for inter-tier interference mitigation is took into account. Assuming that K is the total number of RBs, then αK RBs are only allocated to the RRH tier while $(1-\alpha)K$ can be shared by both RRH tier and MBS tier with a S-FFR factor $\alpha \in \{0, 1\}$.

[1] In reality, there may be more than one active users in a small cell and this can be dealt with using multiple access techniques.

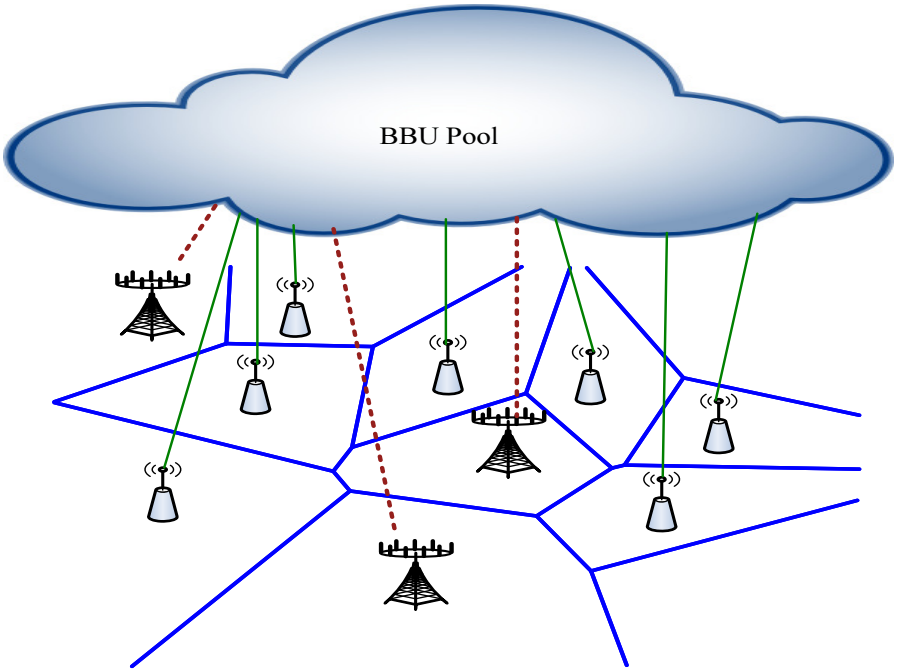

Figure 4.1: An illustration of a two-tier heterogeneous C-RAN, where the red dash lines represent the backhaul links between the macrocell base stations and BBU pool via X2/S1 interfaces, and the green solid lines represent the fronthaul links between the RRHs and BBU pool via optical fibre link.

Based on the proposed resource allocation strategy, if RBs are only allocated to the RRH tier, the signal-to-interference-plus-noise-ratio (SINR) of the typical RRH tier user is written as

$$\gamma_{\mathrm{R},k} = \frac{P_{\mathrm{R}}}{B_o N_o} h_{\mathrm{R},k} \beta \left| X_{o,\mathrm{R}} \right|^{-\eta_{\mathrm{R}}}, \tag{4.1}$$

Otherwise, the RRH tier shares RBs with MBS tier and the SINR is written as

$$\gamma_{\mathrm{R},\nu} = \frac{P_{\mathrm{R}} h_{\mathrm{R},\nu} \beta \left| X_{o,\mathrm{R}} \right|^{-\eta_{\mathrm{R}}}}{I_{\mathrm{M},\nu} + B_o N_o}. \tag{4.2}$$

where P_{R} is the RRH transmit power allocated to each RB, $h_{\mathrm{R},k} \sim \exp(1)$ and $h_{\mathrm{R},\nu} \sim \exp(1)$ are the small-scale fading channel power gains, β is the frequency dependent

constant value, η_{R} is the pathloss exponent, $|X_{o,\mathrm{R}}|$ is the distance between the typical RRH and its intended user. B_o is the bandwidth per RB, N_o is the power spectrum density of the noise and weak inter-RRH interference. In (4.2), $I_{\mathrm{M},\nu}$ is the inter-tier interference from MBSs, which is given by

$$I_{\mathrm{M},\nu} = \sum_{\ell \in \Phi_{\mathrm{M}}} \frac{P_{\mathrm{M}}}{S} h_{\ell,\nu} \beta \left| X_{\ell,\mathrm{M}} \right|^{-\eta_{\mathrm{M}}}, \tag{4.3}$$

where P_{M} is the MBS transmit power allocated to each RB, $h_{\ell,\nu} \sim \Gamma(S,1)$ is the small-scale fading interfering channel power gain. $|X_{\ell,\mathrm{M}}|$ is the distance between the interfering MBS $\ell \in \Phi_{\mathrm{M}}$ and the user associated with the typical RRH, and η_{M} is the path loss exponent.

Then the instantaneous achievable rate for a typical RRH can be derived based on the Shannon Formula

$$R_{\mathrm{RRH}} = \sum_{k=1}^{\alpha K} B_o \log_2 \left(1 + \gamma_{\mathrm{R},k}\right) + \sum_{\nu=1}^{(1-\alpha)K} B_o \log_2 \left(1 + \gamma_{\mathrm{R},\nu}\right), \tag{4.4}$$

In the C-RAN, the inter-MBS interference can be coordinated by the BBU pool through backhaul link [PLJ+14a]. Thus, the SINR $\gamma_{\mathrm{M},\nu}$ of a typical user connected to the MBS tier is given by

$$\gamma_{\mathrm{M},\nu} = \frac{\frac{P_{\mathrm{M}}}{S} g_{\mathrm{M},\nu} \beta \left| X_{o,\mathrm{M}} \right|^{-\eta_{\mathrm{M}}}}{I_{\mathrm{R},\nu} + B_o N_1}. \tag{4.5}$$

where $g_{\mathrm{M},\nu} \sim \Gamma(N_{\mathrm{M}} - S + 1, 1)$ is the small-scale fading channel power gain [HYA14], $|X_{o,\mathrm{M}}|$ is the distance between the typical MBS and its intended user, N_1 is the power spectrum density of the noise and weak inter-MBS interference, and $I_{\mathrm{R},\nu}$ is the inter-tier

interference from RRHs, which is given by

$$I_{\mathrm{R},\nu} = \sum_{j \in \Phi_{\mathrm{R}}} P_{\mathrm{R}} g_{j,\nu} \beta \left| X_{j,\mathrm{R}} \right|^{-\eta_{\mathrm{R}}}, \tag{4.6}$$

where $g_{j,\nu} \sim \exp(1)$ and $|X_{j,\mathrm{R}}|$ are the small-scale interfering channel power gain and the distance between interfering RRH $j \in \Phi_{\mathrm{R}}$ and the user associated with the typical MBS, respectively.

Similarly, the instantaneous achievable rate for a typical MBS can be written as

$$R_{\mathrm{MBS}} = \sum_{\nu=1}^{(1-\alpha)K} B_o S \log_2 \left(1 + \gamma_{\mathrm{M},\nu}\right), \tag{4.7}$$

4.2.3 Power Consumption Model

The total power consumption at each RRH is calculated as

$$P_{\mathrm{R}}^{total} = K \frac{P_{\mathrm{R}}}{\varepsilon_{\mathrm{R}}} + P_{\mathrm{R}}^{0} + P_{\mathrm{fh}}, \tag{4.8}$$

where ε_{R} is the efficiency of the power amplifier, P_{R}^{0} is the static hardware power consumption of the RRH and P_{fh} the power consumption of the fronthaul link.

The total power consumption at each MBS is calculated as [BSHD14]

$$P_{\mathrm{M}}^{total} = (1-\alpha) K \left(\frac{P_{\mathrm{M}}}{\varepsilon_{\mathrm{M}}} + \sum_{\rho=1}^{3} \left((S)^{\rho} \Delta_{\rho} + (S)^{(\rho-1)} N \Lambda_{\rho} \right) \right) + P_{\mathrm{M}}^{0} + P_{\mathrm{bh}}, \tag{4.9}$$

where $\varepsilon_{\mathrm{M}}\,(0 < \varepsilon_{\mathrm{M}} \leq 1)$ is the efficiency of the power amplifier, the parameters Δ_{ρ} and Λ_{ρ} depends on the transceiver chains, coding and decoding, precoding, etc., which are detailed in the Section 4.4, P_{M}^{0} is the MBS's static hardware power consumption, and P_{bh} is the power consumption of the backhaul link.

4.3 Throughput and Energy Efficiency

This section first derives the throughput in the massive MIMO enabled heterogeneous C-RAN. Using the derived results, the EE in this network can be evaluated, as shown in the following theorems.

4.3.1 Throughput

The average throughput for a typical RRH is first derived, which is as follows.

Theorem 6. *The throughput for a typical RRH is given by*

$$\overline{R}_{\mathrm{RRH}} = \frac{2\pi}{\ln 2}\left(\lambda_{\mathrm{R}} + \lambda_{\mathrm{M}}\right) \int_0^{\infty} \phi\left(x\right) x e^{-\pi(\lambda_{\mathrm{R}}+\lambda_{\mathrm{M}})x^2} dx \tag{4.10}$$

with

$$\begin{aligned}\phi\left(x\right) =& \alpha K B_o e^{\frac{B_o N_o}{P_{\mathrm{R}}\beta} x^{\eta_{\mathrm{R}}}} \Gamma\left(0, \frac{B_o N_o}{P_{\mathrm{R}}\beta} x^{\eta_{\mathrm{R}}}\right) + \\ & \left(1-\alpha\right) K B_o \int_0^{\infty} \frac{e^{-\frac{B_o N_o}{P_{\mathrm{R}}\beta} x^{\eta_{\mathrm{R}}}\gamma} \mathcal{L}_{I_{\mathrm{M},\nu}}\left(\frac{1}{P_{\mathrm{R}}\beta} x^{\eta_{\mathrm{R}}}\gamma\right)}{1+\gamma} d\gamma,\end{aligned} \tag{4.11}$$

where $\Gamma\left(\cdot,\cdot\right)$ *is the upper incomplete gamma function [GR07, (8.350)], and* $\mathcal{L}_{I_{\mathrm{M},\nu}}\left(\cdot\right)$ *is given in* (4.16).

Proof. Based on (4.4), $\overline{R}_{\mathrm{RRH}}$ is derived as

$$\overline{R}_{\mathrm{RRH}} = \alpha K B_o \underbrace{\mathrm{E}\left\{\log_2\left(1+\gamma_{\mathrm{R},k}\right)\right\}}_{\Xi_1} + \left(1-\alpha\right) K B_o \underbrace{\mathrm{E}\left\{\log_2\left(1+\gamma_{\mathrm{R},\nu}\right)\right\}}_{\Xi_2}. \tag{4.12}$$

In (4.12), Ξ_1 is calculated as

$$\begin{aligned}\Xi_1 &= \int_0^\infty \mathrm{E}_{h_{\mathrm{R},k}}\left\{\log_2\left(1+\frac{P_{\mathrm{R}}\beta}{B_oN_o}h_{\mathrm{R},k}x^{-\eta_{\mathrm{R}}}\right)\right\} f_{|X_{o,\mathrm{R}}|}(x)\,dx \\ &\overset{(a)}{=} \frac{1}{\ln 2}\int_0^\infty \left\{\int_0^\infty \frac{1}{1+t}e^{-\frac{B_oN_o}{P_{\mathrm{R}}\beta}x^{\eta_{\mathrm{R}}}t}dt\right\} f_{|X_{o,\mathrm{R}}|}(x)\,dx \\ &= \frac{1}{\ln 2}\int_0^\infty e^{\frac{B_oN_o}{P_{\mathrm{R}}\beta}x^{\eta_{\mathrm{R}}}}\Gamma\left(0,\frac{B_oN_o}{P_{\mathrm{R}}\beta}x^{\eta_{\mathrm{R}}}\right) f_{|X_{o,\mathrm{R}}|}(x)\,dx, \end{aligned} \tag{4.13}$$

where (a) is based on the integration by parts, details can be found in Appendix B.2, $f_{|X_{o,\mathrm{R}}|}(x)$ is the probability density function (PDF) of the distance between the typical RRH and its intended user, using the similar approach in [JSXA12], $f_{|X_{o,\mathrm{R}}|}(x)$ is given by

$$f_{|X_{o,\mathrm{R}}|}(x) = \frac{2\pi\lambda_{\mathrm{R}}}{\mathcal{A}_{\mathrm{R}}}xe^{-\pi(\lambda_{\mathrm{R}}+\lambda_{\mathrm{M}})x^2}, \tag{4.14}$$

where $\mathcal{A}_{\mathrm{R}} = \frac{\lambda_{\mathrm{R}}}{\lambda_{\mathrm{R}}+\lambda_{\mathrm{M}}}$ is the probability that a user is associated with the RRH.

For Ξ_2, first provide the complementary cumulative distribution function (CCDF) of $\gamma_{\mathrm{R},\nu}$ given a distance $|X_{o,\mathrm{R}}| = x$, which is calculated as

$$\begin{aligned}&\bar{F}_{\gamma_{\mathrm{R},\nu}|\{|X_{o,\mathrm{R}}|=x\}}(\gamma) = \Pr\left(\frac{P_{\mathrm{R}}h_{\mathrm{R},\nu}\beta x^{-\eta_{\mathrm{R}}}}{I_{\mathrm{M},\nu}+B_oN_o} > \gamma\right) \\ &= e^{-\frac{B_oN_o}{P_{\mathrm{R}}\beta}x^{\eta_{\mathrm{R}}}\gamma}\mathrm{E}_{\Phi_{\mathrm{M}}}\left\{e^{-\frac{1}{P_{\mathrm{R}}\beta}x^{\eta_{\mathrm{R}}}\gamma I_{\mathrm{M},\nu}}\right\} \\ &= e^{-\frac{B_oN_o}{P_{\mathrm{R}}\beta}x^{\eta_{\mathrm{R}}}\gamma}\mathcal{L}_{I_{\mathrm{M},\nu}}\left(\frac{1}{P_{\mathrm{R}}\beta}x^{\eta_{\mathrm{R}}}\gamma\right)\end{aligned} \tag{4.15}$$

where $\mathcal{L}_{I_{\mathrm{M},\nu}}(\cdot)$ is the Laplace transform of the PDF of $I_{\mathrm{M},\nu}$, and is given by

$$\begin{aligned}\mathcal{L}_{I_{\mathrm{M},\nu}}(s) &= \mathrm{E}\left\{\exp\left\{-\left(\sum_{\ell\in\Phi_{\mathrm{M}}}\frac{P_{\mathrm{M}}}{S}h_{\ell,\nu}\beta\left|X_{\ell,\mathrm{M}}\right|^{-\eta_{\mathrm{M}}}\right)s\right\}\right\}\\ &\overset{(a)}{=}\exp\left\{-\int_x^{\infty}\left(1-\frac{1}{\left(1+s\frac{P_{\mathrm{M}}}{S}\beta r^{-\eta_{\mathrm{M}}}\right)^{S}}\right)\lambda_{\mathrm{M}}2\pi r dr\right\}\\ &=\exp\left\{-\lambda_{\mathrm{M}}2\pi\sum_{\mu=1}^{S}\binom{S}{\mu}\left(s\frac{P_{\mathrm{M}}}{S}\beta\right)^{\mu}\frac{\left(-s\frac{P_{\mathrm{M}}}{S}\beta\right)^{-\mu+\frac{2}{\eta_{\mathrm{M}}}}}{\eta_{\mathrm{M}}}\right.\\ &\quad\left.B_{\left(-s\frac{P_{\mathrm{M}}}{S}\beta x^{-\eta_{\mathrm{M}}}\right)}\left[\mu-\frac{2}{\eta_{\mathrm{M}}},1-S\right]\right\},\end{aligned}\tag{4.16}$$

where (a) is obtained by using the generating functional of PPP [Hae12], $\mathrm{B}_{(\cdot)}[\cdot,\cdot]$ is the incomplete beta function [GR07, (8.391)]. Accordingly, Ξ_2 is given by

$$\Xi_2=\frac{1}{\ln 2}\int_0^{\infty}\left[\int_0^{\infty}\frac{\bar{F}_{\gamma_{\mathrm{R},\nu}|\{|X_{o,\mathrm{R}}|=x\}}(\gamma)}{1+\gamma}d\gamma\right]f_{|X_{o,\mathrm{R}}|}(x)\,dx.\tag{4.17}$$

Substituting (4.13) and (4.17) into (4.12), (4.10) is obtained. □

Next derive the average throughput $\overline{R}_{\mathrm{MBS}}$ for a typical MBS , which can be written in a general-form following the approach in [DRG14], however, using this approach for computing $\overline{R}_{\mathrm{MBS}}$ will lead to intractable solution in this work. As such, a tractable and tight lower bound expression is presented for $\overline{R}_{\mathrm{MBS}}$ as follows:

Theorem 7. *The average throughput for a typical MBS can be lower bounded as*

$$\overline{R}^{\mathrm{L}}_{\mathrm{MBS}}=(1-\alpha)\,KB_oS\log_2\left(1+e^{Z_1+\bar{Z}_2}\right),\tag{4.18}$$

where

$$Z_1=\ln\left(\frac{P_{\mathrm{M}}}{S}\beta\right)+\psi\left(N_{\mathrm{M}}-S+1\right)-\frac{\eta_{\mathrm{M}}}{2}\left(\psi(1)-\ln\left(\pi\left(\lambda_{\mathrm{R}}+\lambda_{\mathrm{M}}\right)\right)\right),\tag{4.19}$$

and

$$\bar{Z}_2 = -\ln\left(\frac{P_{\mathrm{R}}\beta 2\pi\lambda_{\mathrm{R}}\Gamma\left(2-\frac{\eta_{\mathrm{R}}}{2}\right)}{\left(\eta_{\mathrm{R}}-2\right)\left(\pi\lambda_{\mathrm{R}}+\pi\lambda_{\mathrm{M}}\right)^{1-\frac{\eta_{\mathrm{R}}}{2}}}+B_o N_1\right), \tag{4.20}$$

respectively, where $\psi(\cdot)$ is the digamma function [AS70].

Proof. Based on (4.7), the average throughput of a typical MBS is written as

$$\overline{R}_{\mathrm{MBS}} = (1-\alpha) K B_o S \underbrace{\mathrm{E}\left\{\log_2\left(1+\gamma_{\mathrm{M},\nu}\right)\right\}}_{\Xi_3}, \tag{4.21}$$

By using Jensen's inequality, a lower bound for Ξ_3 is given by

$$\Xi_3^{\mathrm{L}} = \log_2\left(1+e^{Z_1+Z_2}\right), \tag{4.22}$$

where

$$Z_1 = \mathrm{E}\left\{\ln\left(\frac{P_{\mathrm{M}}}{S} g_{\mathrm{M},\nu}\beta\left|X_{o,\mathrm{M}}\right|^{-\eta_{\mathrm{M}}}\right)\right\}, \tag{4.23}$$

and

$$Z_2 = \mathrm{E}\left\{\ln\left(\frac{1}{I_{\mathrm{R},\nu}+B_o N_1}\right)\right\}. \tag{4.24}$$

First calculate Z_1 as

$$Z_1 = \ln\left(\frac{P_{\mathrm{M}}}{S}\beta\right) + \mathrm{E}\left\{\ln\left(g_{\mathrm{M},\nu}\right)\right\} - \eta_{\mathrm{M}}\mathrm{E}\left\{\ln\left(\left|X_{o,\mathrm{M}}\right|\right)\right\}, \tag{4.25}$$

Considering that $g_{\mathrm{M},\nu} \sim \Gamma\left(N_{\mathrm{M}}-S+1,1\right)$, $\mathrm{E}\left\{\ln\left(g_{\mathrm{M},\nu}\right)\right\}$ is given by

$$\begin{aligned}\mathrm{E}\left\{\ln\left(g_{\mathrm{M},\nu}\right)\right\} &= \int_0^\infty \frac{x^{N_{\mathrm{M}}-S}e^{-x}}{(N_{\mathrm{M}}-S)!}\ln(x)\,dx \\ &\overset{(b)}{=} \psi\left(N_{\mathrm{M}}-S+1\right),\end{aligned} \tag{4.26}$$

where (b) is using $\int_0^\infty x^{v-1}e^{-\mu x}\ln x dx = \mu^{-v}\Gamma(v)(\psi(v)-\ln\mu)$ [GR07, (4.352.1)], and for large N_{M}, $\psi(N_{\mathrm{M}}-S+1)\approx\ln(N_{\mathrm{M}}-S+1)$ [WNE+15].

$$\begin{aligned}\mathrm{E}\left\{\ln\left(\left|X_{o,\mathrm{M}}\right|\right)\right\} &\overset{(c)}{=} \int_0^\infty \ln(x) f_{\left|X_{o,\mathrm{M}}\right|}(x)\,dx \\ &= \int_0^\infty \ln(x)\frac{2\pi\lambda_{\mathrm{M}}}{\mathcal{A}_{\mathrm{M}}} x e^{-\pi(\lambda_{\mathrm{R}}+\lambda_{\mathrm{M}})x^2}dx \\ &= \frac{1}{2}\left(\psi(1)-\ln\left(\pi\left(\lambda_{\mathrm{R}}+\lambda_{\mathrm{M}}\right)\right)\right). \end{aligned} \tag{4.27}$$

In the step (c), $f_{\left|X_{o,\mathrm{M}}\right|}(x)$ is the PDF of the distance between the typical MBS and its intended user, which can be directly obtained following (4.14), and $\mathcal{A}_{\mathrm{M}} = \frac{\lambda_{\mathrm{M}}}{\lambda_{\mathrm{R}}+\lambda_{\mathrm{M}}}$ is the probability that a user is associated with the MBS. By substituting (4.26) and (4.27) into (4.25), Z_1 as (4.19) is obtained.

From (4.24), considering the convexity of $\ln\left(\frac{1}{1+x}\right)$ and using Jensen's inequality, the lower bound on the Z_2 is derived as

$$Z_2 \geq \bar{Z}_2 = \ln\left(\frac{1}{\mathrm{E}\left\{I_{\mathrm{R},\nu}\right\}+B_o N_1}\right). \tag{4.28}$$

Then,

$$\begin{aligned}\mathrm{E}\left\{I_{\mathrm{R},\nu}\right\} &= \int_0^\infty \mathrm{E}\left\{\sum_{j\in\Phi_{\mathrm{R}}} P_{\mathrm{R}} g_{j,\nu}\beta\left|X_{j,\mathrm{R}}\right|^{-\eta_{\mathrm{R}}}\right\} f_{\left|X_{o,\mathrm{M}}\right|}(x)\,dx \\ &\overset{(d)}{=} \int_0^\infty \left(P_{\mathrm{R}}\beta 2\pi\lambda_{\mathrm{R}}\int_x^\infty r^{1-\eta_{\mathrm{R}}}dr\right) f_{\left|X_{o,\mathrm{M}}\right|}(x)\,dx \\ &= \int_0^\infty \frac{P_{\mathrm{R}}\beta 2\pi\lambda_{\mathrm{R}}}{\eta_{\mathrm{R}}-2} x^{2-\eta_{\mathrm{R}}} f_{\left|X_{o,\mathrm{M}}\right|}(x)\,dx \\ &= \frac{P_{\mathrm{R}}\beta 2\pi\lambda_{\mathrm{R}}\Gamma\left(2-\frac{\eta_{\mathrm{R}}}{2}\right)}{\left(\eta_{\mathrm{R}}-2\right)\left(\pi\lambda_{\mathrm{R}}+\pi\lambda_{\mathrm{M}}\right)^{1-\frac{\eta_{\mathrm{R}}}{2}}}, \end{aligned} \tag{4.29}$$

where (d) results from using Campbell's theorem [BB09]

Substituting (4.29) into (4.28), we obtain $\bar{Z}_2$ as (4.20). □

Thus, the overall throughput of the network is evaluated as

$$\mathcal{T}_{\text{Net}} = \mathcal{T}_{\text{R}} + \mathcal{T}_{\text{M}}^{\text{L}} = \lambda_{\text{R}} \overline{R}_{\text{RRH}} + \lambda_{\text{M}} \overline{R}_{\text{MBS}}^{\text{L}}. \tag{4.30}$$

4.3.2 Energy Efficiency

The EE for the RRHs tier is given by

$$\text{EE}_{\text{R}} = \frac{\mathcal{T}_{\text{R}}}{\lambda_{\text{R}} P_{\text{R}}^{total}} = \frac{\overline{R}_{\text{RRH}}}{P_{\text{R}}^{total}}, \tag{4.31}$$

where $\overline{R}_{\text{RRH}}$ and P_{R}^{total} are given by (4.10) and (4.8), respectively. In the RRH tier, transmission over RBs that are only allocated to RRHs plays a dominant role in the overall throughput [PZJ+15], compared to using RBs shared by the RRHs and MBSs. As a consequence, (4.31) can be approximately evaluated as

$$\text{EE}_{\text{R}} \overset{(e)}{\approx} \frac{\alpha B_o \Xi_1}{\frac{P_{\text{R}}}{\varepsilon_{\text{R}}}}, \tag{4.32}$$

where (e) is obtained by omitting the power consumptions from static hardware and fronthaul link, compared to the RRH transmit power, and Ξ_1 is given by (4.13). It is implied from (4.32) that the EE for RRH transmission can be linearly improved by allocating more RBs to the RRHs. The EE for the MBSs tier is lower bounded as

$$\text{EE}_{\text{M}}^{\text{L}} = \frac{\mathcal{T}_{\text{M}}^{\text{L}}}{\lambda_{\text{M}} P_{\text{M}}^{total}} = \frac{\overline{R}_{\text{MBS}}^{\text{L}}}{P_{\text{M}}^{total}}, \tag{4.33}$$

where $\overline{R}_{\text{MBS}}^{\text{L}}$ and P_{M}^{total} are given by (4.18) and (4.9), respectively. Lastly, the EE of the massive MIMO enabled heterogeneous C-RAN is calculated as

$$\begin{aligned} \text{EE}_{\text{Net}} &= \frac{\text{Area throughput of the network}}{\text{Area Power Consumption of the network}} \\ &= \frac{\lambda_{\text{R}} \overline{R}_{\text{RRH}} + \lambda_{\text{M}} \overline{R}_{\text{MBS}}^{\text{L}}}{\lambda_{\text{R}} P_{\text{R}}^{total} + \lambda_{\text{M}} P_{\text{M}}^{total}}. \end{aligned} \tag{4.34}$$

Parameter	Symbol	Value
Pathloss exponent to MBSs	η_{M}	3.0
Pathloss exponent to RRHs	η_{R}	3.6
The MBS transmit power	P_{M}	40 dBm
The RRH transmit power	P_{R}	30 dBm
Each RB bandwidth	B_o	200 KHz
Number of RBs	K	25
The noise power spectrum densities [PWLP15]	$N_0 = N_1$	-162 dBm/Hz
The RRH static hardware power consumption	P_{R}^0	100 mW
The MBS static hardware power consumption	P_{M}^0	10 W
Power amplifier efficiency	$\varepsilon_{\mathrm{R}} = \varepsilon_{\mathrm{M}}$	0.38
Power consumption of the fronthaul link and backhaul link	$P_{\mathrm{fh}} = P_{\mathrm{bh}}$	0.2 W

Table 4-A: Simulation Parameters.

4.4 Numerical Results and Analysis

This section presents numerical results to evaluate the area throughput and the average EE in the massive MIMO enabled heterogeneous C-RAN (HC-RAN). The density of MBSs is $\lambda_{\mathrm{M}} = \left(500^2 \times \pi\right)^{-1} \mathrm{m}^{-2}$ in a circular region with radius 1×10^4 m. Power consumption under LZFBF precoding in (4.9) are set as $\Delta_1 = 4.8$, $\Delta_2 = 0$, $\Delta_3 = 2.08 \times 10^{-8}$, $\Lambda_1 = 1$, $\Lambda_2 = 9.5 \times 10^{-8}$ and $\Lambda_3 = 6.25 \times 10^{-8}$ [BSHD14]. Such a network is assumed to operate at a carrier frequency of 1 GHz. Detailed parameter settings are shown in Table 4.4.

In the figures, Monte Carlo (MC) simulated exact values of the SE and EE marked by 'o' are numerically obtained to validate the analytical results, and the green, red and blue curves represent the area throughput and EE achieved by the MBSs tier, RRHs tier, and HC-RAN, respectively. The throughput curves for the RRHs tier, MBSs tier and HC-RAN are obtained from (4.10), (4.18), and (4.30), respectively. The EE curves for the RRHs tier, MBSs tier and HC-RAN are obtained from (4.31), (4.33), and (4.34), respectively.

4.4.1 The effects of Massive MIMO

Figure 4.2 shows the area throughput and EE versus number of MBS antennas for different S. Set the density of RRHs as $\lambda_{\mathrm{R}} = 10 \times \lambda_{\mathrm{M}}$ and the S-FFR factor $\alpha = 0.5$.

In Figure 4.2(a), it can be seen that the analytical area throughput expression for RRHs tier has a good match with MC simulation, and the derived lower bounds are tight, which can well predict the exact ones. The area throughput of the MBSs tier and HC-RAN increases with the number of MBS antennas, due to the increasing array gains. Moreover, serving more number of users in the massive MIMO macrocell can significantly improve the throughput of the MBSs tier and HC-RAN, because of achieving more multiplexing gains. In addition, increasing the number of MBS antennas has negligible effect on the throughput of RRHs tier.

In Figure 4.2(b), it can be seen that RRHs tier achieves higher EE than the MBSs tier. EE of the MBSs tier and HC-RAN decreases with increasing the number of MBS antennas, due to more power consumption from the precoding. However, serving more users in the macrocell can significantly improve EE, due to higher throughput as shown in Fig. 4.2(a). Again, increasing the number of MBS antennas has negligible effect on the EE of RRHs tier.

4.4.2 The effects of S-FFR and RRHs tier density

Figure 4.3 shows the area throughput and energy efficiency versus S-FFR factor for different RRH tier density. Set the number of MBS antennas as 200 and $S = 15$.

In Figure 4.3(a), it can be seen that the throughput of RRHs tier increases with the S-FFR factor α. When the density of RRHs tier is not dense (e.g. $\lambda_{\mathrm{R}} = 10\lambda_{\mathrm{M}}$ in this figure), the throughput of MBSs tier and HC-RAN decreases with α. The reason is that the MBSs tier plays a crucial role in the throughput of the entire network, and increasing α reduces the amount of RBs allocated to the MBSs tier. There is a critical

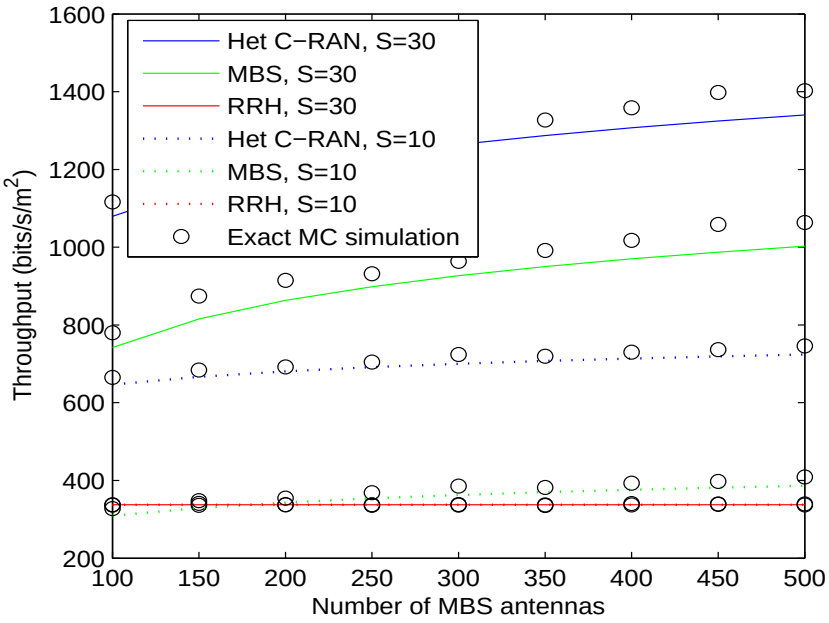

(a) Throughput.

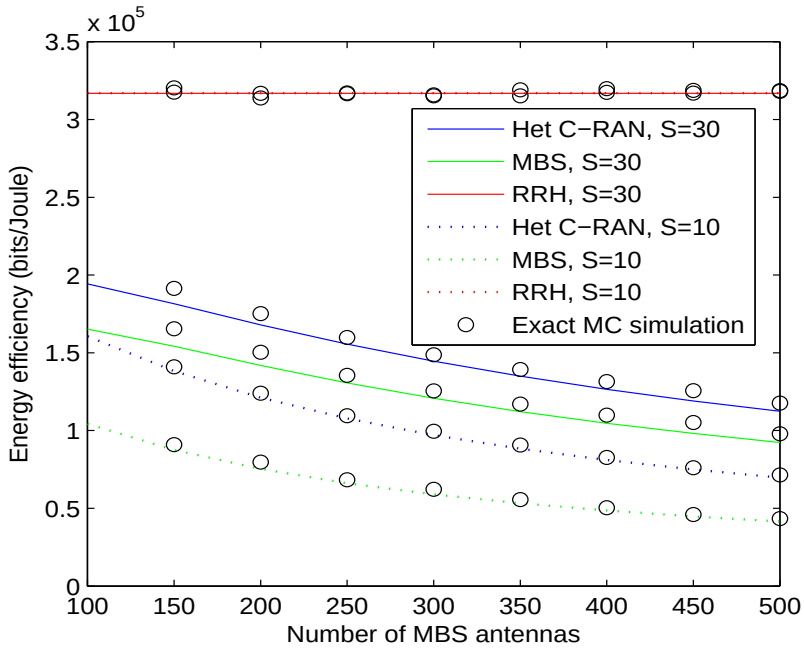

(b) Energy efficiency.

Figure 4.2: Area throughput and average energy efficiency versus number of MBS antennas for different number of users S.

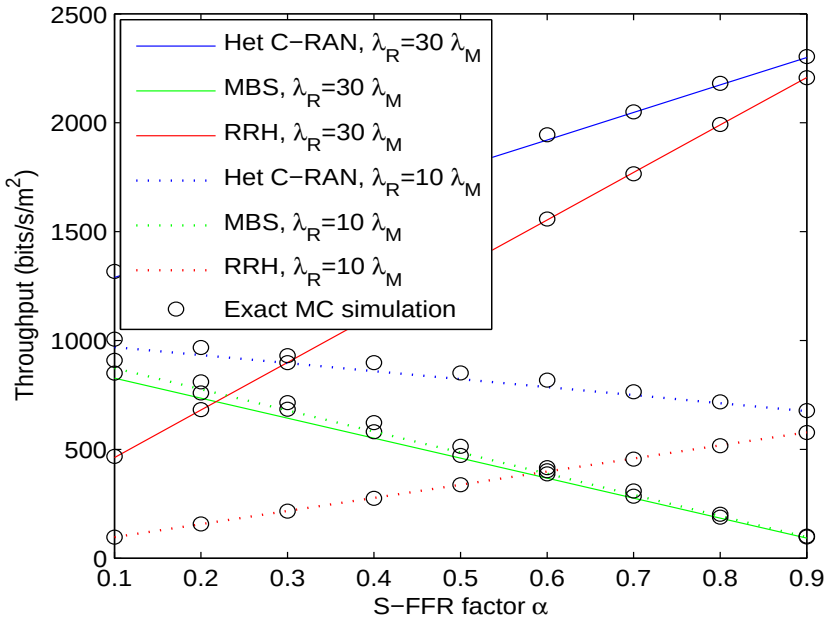

(a) Throughput.

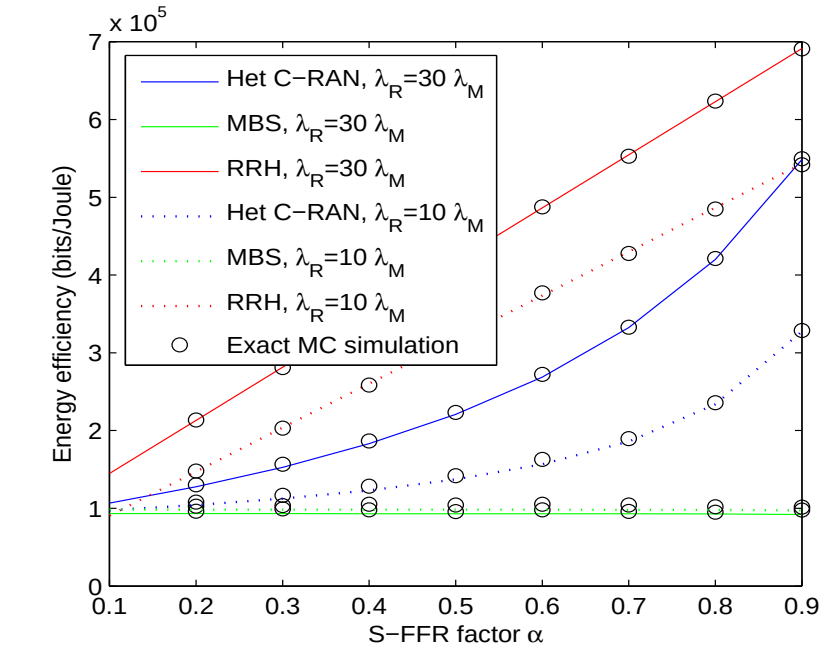

(b) Energy efficiency.

Figure 4.3: Area throughput and average energy efficiency versus S-FFR factor α for different tier density ratio.

point, exceeding which, the throughput achieved by the RRHs tier is higher than that in MBSs tier. In contrast, when the density of RRHs is dense (e.g. $\lambda_{\mathrm{R}} = 30\lambda_{\mathrm{M}}$), the throughput of the HC-RAN increases with α, which can be explained by the fact that the RRHs tier plays a key role in this case, and more number of RBs are allocated to the RRHs tier.

In Figure 4.3(b), it can be seen that RRHs tier achieves higher EE than the MBSs tier, and the EE of the RRHs tier and HC-RAN increases with the S-FFR factor α, given the RRHs tier density. When deploying more RRHs in the network, EE of the HC-RAN significantly improves. There is an interesting phenomenon that the S-FFR factor has negligible impact on the EE of the MBSs tier. The reason is that for massive MIMO empowered MBS, the low power cost for backhaul link and static hardware can be omitted compared with the power cost of massive MIMO precoding as equation (4.32) shows, in this condition, each RB of the MBS has the same EE, which means it is independent of the frequency resource allocation.

4.4.3 The effects of RRHs transmit power and RRH tier density

Figure 4.4 and 4.5 shows the area throughput and energy efficiency versus RRHs transmit power for different RRH tier density. We set the number of MBS antennas as 200 and $S = 15$.

In Figure 4.4(a), it can be seen that the throughput of RRHs tier increases with the RRH transmit power while the throughput of MBSs tier decreases, due to the fact that the dense RRHs shorten their distances to users. Because the MBSs tier dominates the traffic load when the density of RRHs tier is not dense (e.g. $\lambda_{\mathrm{R}} = 10\lambda_{\mathrm{M}}$ in this figure), the throughput of the whole network decreases with the increased RRH transmit power. In contrast, when the density of RRHs is relatively dense (e.g. $\lambda_{\mathrm{R}} = 30\lambda_{\mathrm{M}}$), the throughput of the HC-RAN increases with RRH transmit power. Meanwhile, it is noticeable that the dense deployment of RRHs only slightly degrades the throughput

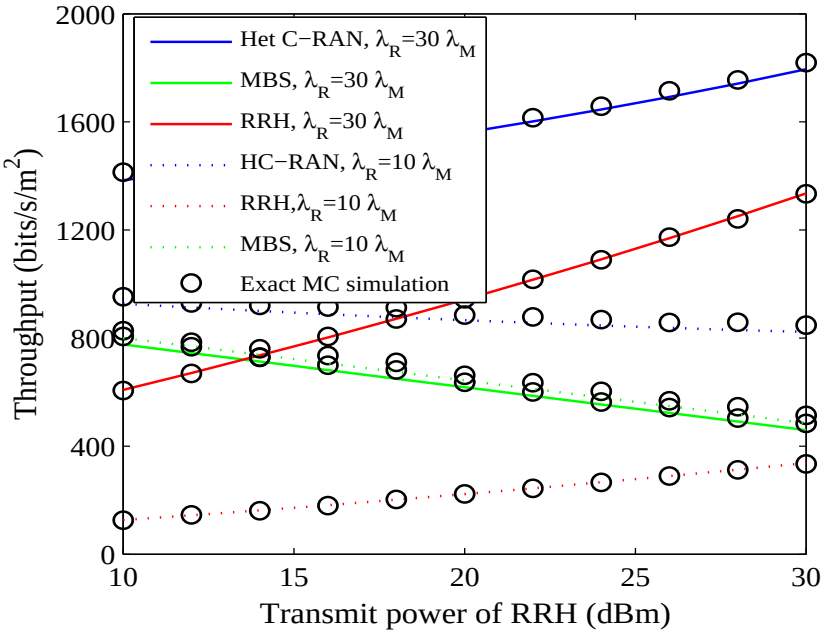

(a) Throughput.

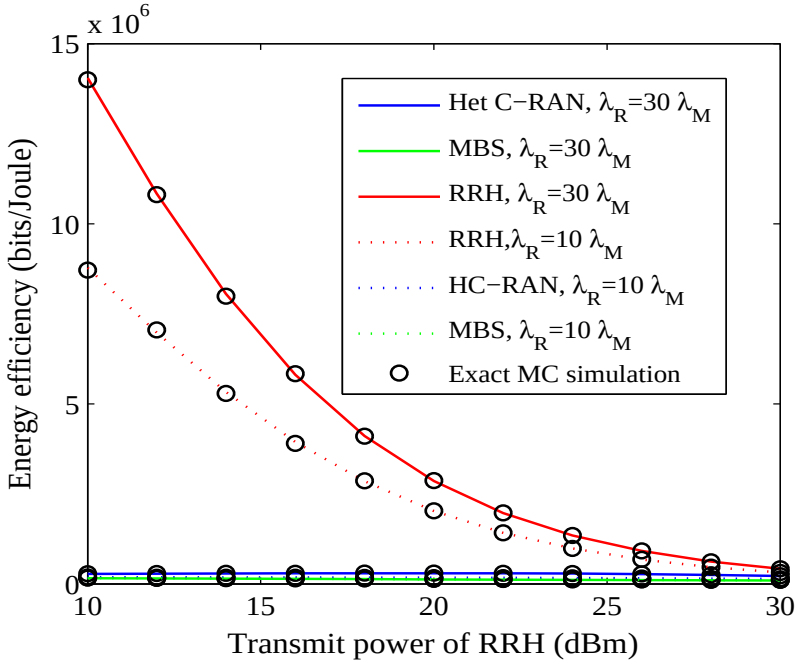

(b) Energy efficiency.

Figure 4.4: Area throughput and average energy efficiency versus RRH transmit power for different tier density ratio.

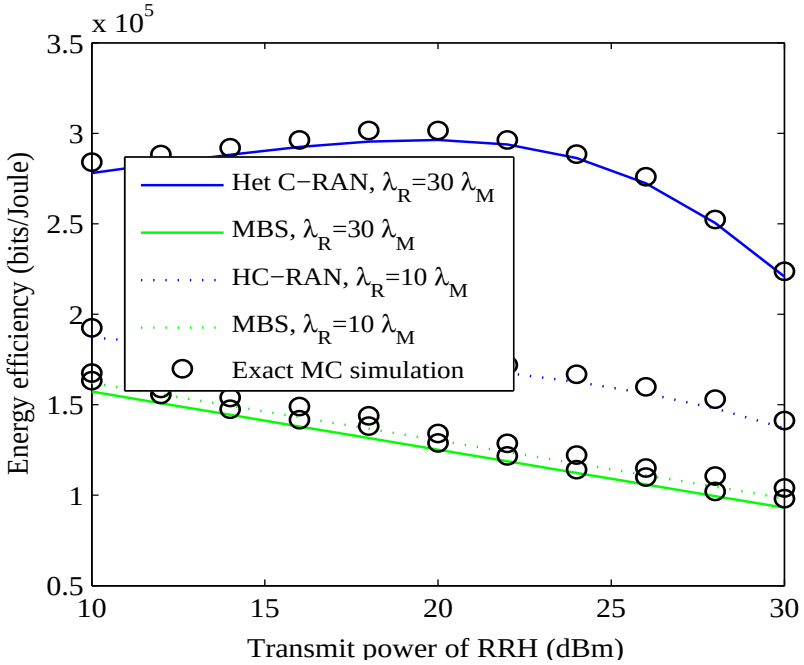

Figure 4.5: Average energy efficiency versus RRH transmit power with different tier density ratio (without RRH tier).

of the MBSs tier which is ascribed to the effectiveness of the C-RAN on interference coordination. Also, there is a critical point, exceeding which, the throughput achieved by the RRHs tier is higher than that in MBSs tier. This observation suggests that when the HC-RAN is dense, the overall network throughput can be improved via increasing the transmit power of RRHs to offload from the MBSs.

In Figure 4.4(b), it can be seen that RRHs tier achieves much higher EE than both MBSs tier and the whole network, and the EE of the RRHs tier decreases with the RRH transmit power, given the same RRHs tier density. That's proves that the EE of RRH tier is almost inversely proportional to the RRH transmit power, as the equation (4.32) shows.

To clearly present the performance of MBSs tier and the overall network, the Figure 4.4(b) is re-plotted but without the RRH tier. As shown in the 4.5, the EE of the MBSs decreases with the increased RRH transmit power. It is observed that the EE of the HetNet decreases with the increasing RRH transmit power when the number of

RRHs is relatively small. The reason is that the power consumption of massive MIMO empowered MBS, including the low power cost for backhaul link and static hardware, dominates the whole network's power consumption. In the dense deployment, however, there is an optimal value of RRH transmit power for the EE of whole network. The reason is that when the RRH tier is dense, the RRH tier, which has a higher EE, plays a more important role in the HetNet and increase the EE of the whole network at the beginning. After a critical point, the strong inter-tier interference has a adverse impact of the network performance, which leads to a decrease of the HetNet EE. This figure shows that deploying more RRHs in a massive MIMO enabled C-RAN can increase the network EE, when an appropriate value of the RRHs transmit power was chosen.

4.5 Summary

This chapter integrated the massive MIMO and HC-RAN into one system to examine the co-effect of the two most envisioned 5G technology candidates. In such a scenario, both remote radio heads (RRHs) and massive MIMO macrocell BSs were deployed to potentially accomplish high throughput and energy efficiency (EE). It is noticeable that one of the most crucial challenges is the physical scarcity of ratio frequency (RF) spectra allocated for cellular communications in the next generation network. Thus, the implementation of the S-FFR was utilised to mitigate the inter-tier interference. It first obtained the exact expressions for the throughput of the RRHs tier. Then, a tight approximation approach for evaluating the throughput of the macrocell base stations tier was presented. Numerical results collaborated the analysis and showed that massive MIMO with dense deployment of RRHs can significantly enhance both throughput and EE of HC-RAN. More frequency resources allocated to the RRHs can improve the network energy efficiency. The S-FFR factor and RRH tier transmit power should be carefully chosen, whose effect depends on the density of the RRHs.

Chapter 5

Uplink Performance Evaluation in Massive MIMO enabled Heterogeneous Cellular Networks with Interference Management

5.1 Overview

In the massive MIMO aided HCNs, downlink transmission has been examined by considering different performance metrics such as spectrum efficiency [XM15] or energy efficiency [LWC+15b]. As the majority of the payload data and network energy consumption are coupled to the downlink, fewer researches are available for uplink transmission. However, more users served by the massive MIMO macrocells and large numbers of small cells result in severer uplink interference. Thus, interference management is critically important for the uplink transmission, since more users served by the massive MIMO macrocells and large numbers of small cells results in severer uplink interference. The work of [JMMY09] adjusted the maximum transmit power of femtocell users for interference mitigation in two-tier femtocell networks, where two schemes were proposed to suppress the cross-tier interference under a fixed threshold and an adaptive threshold. The uplink power control under quality constraints for enhancing network performance in a massive MIMO multicell network was investigated in [YM15].

While the aforementioned literature laid a good foundation in understanding the uplink power control for coordinating interference in the HCNs or massive systems, interference management for a system which integrates both the two key technologies has not been conducted yet. As such, this chapter focuses on the uplink performance evaluation and enhancement in massive MIMO aided HCNs. A joint uplink power control and CRE scheme for uplink interference coordination in a two-tier massive MIMO aided HCN consisting of picocells and massive MIMO macrocells is proposed. Specifically, due to the massive MIMO array gains, the uplink/downlink imbalance is boosted in the massive MIMO aided HCNs. In light of this, CRE is employed to tackle the uplink/downlink imbalance problem. Since users in the massive MIMO macrocells are provided with large array gains, the level of their transmit power can be greatly lowered. Hence, the uplink power control is adopted in the picocells. Finally, the performance of the proposed massive MIMO aided HCNs in terms of area SE and EE are evaluated.

5.2 System Model

This section considers the uplink transmission in a two-tier heterogeneous network (HetNet), in which massive MIMO macrocells are overlaid with picocells.

5.2.1 Spatial Distribution

The locations of macrocell base stations (MBSs) are modelled following a homogeneous Poisson point process (PPP) Φ_{M} with density λ_{M}. The locations of picocell base stations (PBSs) are modeled following an independent homogeneous PPP Φ_{P} with density λ_{P}. Each MBS is equipped with N antennas and receives data streams from S single-antenna users over the same time and frequency band, while each PBS equipped with one single antenna receives one data stream from a single-antenna user in each transmission. It is assumed that the density of users is much greater than that of BSs so that there always will be one active mobile user at each time slot in every small cell and

multiple active mobile users in every macrocell. The zero-forcing beamforming (ZFBF) is employed to cancel the intra-cell interference at the MBS, and the ZFBF matrix at a MBS is $\mathbf{W}=\mathbf{G}^H\left(\mathbf{G}^H\mathbf{G}\right)^{-1}$ with the channel matrix $\mathbf{G}$ [HYA14], where H denotes the Hermitian transpose. All the channels undergo independent and identically distributed (i.i.d.) quasi-static Rayleigh fading.

5.2.2 Uplink Power Control

Owing to the benefits of massive MIMO such as large antenna array gain, users associated with the MBSs can use lower transmit power, hence the uplink power control in the picocells is focused on. Specifically, the open-loop uplink power control is applied in the picocells, and the transmit power for a user associated with the PBS is given by

$$P_{\mathrm{u,P}} = \min\left\{P_{\max}, P_o L\left(|X_\kappa|\right)^{-\eta}\right\}, \tag{5.1}$$

where $P_{\max}$ is the maximum transmit power, P_o is the normalized power density, $L\left(|X_\kappa|\right) = \beta|X_\kappa|^{-\alpha}$ is the path loss with the exponent α, and β is the frequency dependent constant value, $|X_\kappa|$ is the distance between the user and its associated PBS, $\eta \in [0,1]$ is the path loss compensation factor, which controls the picocell user's transmit power. Here $\eta = 1$ represents that the path loss between a user and its serving PBS is fully compensated, and $\eta = 0$ represents that there is no path loss compensation.

5.2.3 User Association

This section considers the downlink-centric user association [1], which means that the user association is determined during the downlink transmission. In the downlink, each MBS transmits S user-streams with equal power assignment. As such, the long-term average downlink receive power P_ℓ^{r} at a macrocell user (MUE) which is connected with the MBS

[1] Although user association for the downlink and uplink can be decoupled in the conventional cellular networks, the main drawback for the decoupling is that channel reciprocity in massive MIMO systems will be lost [B+16].

ℓ ($\ell \in \Phi_{\mathrm{M}}$) is

$$P_{\ell}^{\mathrm{r}} = G_a \frac{P_{\mathrm{M}}}{S} L\left(|X_{\ell}|\right), \tag{5.2}$$

where G_a is the array gain, P_{M} is the MBS's transmit power, $L\left(|X_{\ell}|\right) = \beta |X_{\ell}|^{-\alpha_{\mathrm{M}}}$ is the path loss function, $|X_{\ell}|$ is the distance, and α_{M} is the path loss exponent. The array gain G_a obtained by the ZFBF transmission is $N - S + 1$ [XM15]. In the picocell, considering the effect of picocell range expansion, the long-term average downlink receive power P_{κ}^{r} at a picocell user (PUE) which is connected with the PBS κ ($\kappa \in \Phi_{\mathrm{P}}$) is expressed as

$$P_{\kappa}^{\mathrm{r}} = P_{\mathrm{P}} L\left(|X_{\kappa}|\right) B, \tag{5.3}$$

where P_{P} is the PBS's transmit power and $L\left(|X_{\kappa}|\right) = \beta (|X_{\kappa}|)^{-\alpha_{\mathrm{P}}}$ is the path loss function, and B is the biasing factor, which is useful for offloading the data traffic to small cells in conventional HetNets [JSXA12].

5.2.4 Channel Model

Assuming that a typical serving base station is located at the origin o. Then the receive signal-to-interference-plus-noise ratio (SINR) of a typical serving MBS at a random distance $|X_{o,\mathrm{M}}|$ from its intended MUE is given by

$$\mathrm{SINR}_{\mathrm{M}} = \frac{P_{\mathrm{u,M}} h_{o,\mathrm{M}} L\left(|X_{o,\mathrm{M}}|\right)}{I_{\mathrm{M}} + I_{\mathrm{P}} + \delta^2}, \tag{5.4}$$

where $I_{\mathrm{M}} = \sum_{i \in \Phi_{\mathrm{u,M}} \backslash \mathrm{B}_{o,\mathrm{M}}} P_{\mathrm{u,M}} h_{i,\mathrm{M}} L\left(|X_{i,\mathrm{M}}|\right)$ is the uplink intra-tier interference, $I_{\mathrm{P}} = \sum_{j \in \Phi_{\mathrm{u,P}}} P_{j,\mathrm{P}} h_{j,\mathrm{M}} L\left(|X_{j,\mathrm{M}}|\right)$ is the uplink inter-tier interference, $P_{\mathrm{u,M}}$ and $P_{j,\mathrm{P}}$ are the transmit power of the MUE and PUE $j \in \Phi_{\mathrm{u,P}}$ ($\Phi_{\mathrm{u,P}}$ is the point process corresponding to the interfering PUEs), respectively, $h_{o,\mathrm{M}} \sim \Gamma\left(N - S + 1, 1\right)$ [HYA14] is the small-scale fading channel power gain between the typical serving MBS and its intended user, and $|X_{i,\mathrm{M}}|$ is distance between the typical serving MBS and interfering MUE $i \in \Phi_{\mathrm{u,M}} \backslash \mathrm{B}_{o,\mathrm{M}}$

($\Phi_{\mathrm{u,M}} \backslash \mathrm{B}_{o,\mathrm{M}}$ is the point process corresponding to the interfering MUEs). Different from the downlink transmission, $h_{i,\mathrm{M}} \sim \exp(1)$ is the small-scale fading interfering channel power gain of interfering single antenna MUEs. Then, $h_{j,\mathrm{M}} \sim \exp(1)$ and $|X_{j,\mathrm{M}}|$ are the small-scale fading interfering channel power gain and distance between the typical serving MBS and interfering PUE j, respectively, and δ^2 is the noise power.

The SINR of a typical serving PBS at a random distance $|X_{o,\mathrm{P}}|$ from its intended user is given by

$$\mathrm{SINR}_{\mathrm{P}} = \frac{P_{\mathrm{u,P}} g_{o,\mathrm{P}} L\left(|X_{o,\mathrm{P}}|\right)}{J_{\mathrm{M}} + J_{\mathrm{P}} + \delta^2}, \tag{5.5}$$

where $J_{\mathrm{M}} = \sum_{i \in \Phi_{\mathrm{u,M}}} P_{\mathrm{u,M}} g_{i,\mathrm{P}} L\left(|X_{i,\mathrm{P}}|\right)$, $J_{\mathrm{P}} = \sum_{j \in \Phi_{\mathrm{u,P}} \backslash \mathrm{B}_{o,\mathrm{P}}} P_{j,\mathrm{P}} g_{j,\mathrm{P}} L\left(|X_{j,\mathrm{P}}|\right)$, $g_{o,\mathrm{P}} \sim \exp(1)$ is the small-scale fading channel power gain between the typical serving PBS and its intended user, $g_{i,\mathrm{P}} \sim \exp(1)$ and $|X_{i,\mathrm{P}}|$ are the small-scale fading interfering channel power gain and distance between the typical serving PBS and interfering user $i \in \Phi_{\mathrm{u,M}}$, respectively, $g_{j,\mathrm{P}} \sim \exp(1)$ and $|X_{j,\mathrm{P}}|$ are the small-scale fading interfering channel power gain and distance between the typical serving MBS and interfering user $j \in \Phi_{\mathrm{u,P}} \backslash \mathrm{B}_{o,\mathrm{P}}$ (except the typical PUE), respectively.

5.3 Spectrum Efficiency and Energy Efficiency

5.3.1 Area Uplink Spectrum Efficiency

In this section, the area uplink spectrum efficiency for massive MIMO macrocell tier and picocell tier are evaluated. The area uplink spectrum efficiency is used to examine the impacts of different densities of picocells and massive MIMO macrocells on the uplink spectrum efficiency of different tiers.

Due to the downlink-centric user association is considered, the probability density functions (pdf) of the distance $|X_{o,\mathrm{M}}|$ between a typical MUE and its serving MBS $B_{o,\mathrm{M}}$,

$$f_{|X_{o,\mathrm{M}}|}(x)=\frac{2\pi\lambda_{\mathrm{M}}}{\mathcal{A}_{\mathrm{M}}}x\exp\left\{-\pi\lambda_{\mathrm{M}}x^2-\pi\lambda_{\mathrm{P}}\left(\frac{P_{\mathrm{P}}BSx^{\alpha_{\mathrm{M}}}}{P_{\mathrm{M}}(N-S+1)}\right)^{2/\alpha_{\mathrm{P}}}\right\} \tag{5.6}$$

$$f_{|X_{o,\mathrm{P}}|}(x)=\frac{2\pi\lambda_{\mathrm{P}}}{\mathcal{A}_{\mathrm{P}}}x\exp\left\{-\pi\lambda_{\mathrm{P}}x^2-\pi\lambda_{\mathrm{M}}\left(\frac{P_{\mathrm{M}}(N-S+1)x^{\alpha_{\mathrm{P}}}}{P_{\mathrm{P}}BS}\right)^{2/\alpha_{\mathrm{M}}}\right\} \tag{5.7}$$

where

$$\mathcal{A}_{\mathrm{M}}=2\pi\lambda_{\mathrm{M}}\int_0^{\infty}r\exp\left\{-\pi\lambda_{\mathrm{M}}r^2-\pi\lambda_{\mathrm{P}}\left(\frac{P_{\mathrm{P}}BSr^{\alpha_M}}{P_M(N-S+1)}\right)^{2/\alpha_{\mathrm{P}}}\right\}dr \tag{5.8}$$

$$\mathcal{A}_{\mathrm{P}}=2\pi\lambda_{\mathrm{P}}\int_0^{\infty}r\exp\left\{-\pi\lambda_{\mathrm{P}}r^2-\pi\lambda_{\mathrm{M}}\left(\frac{P_{\mathrm{M}}(N-S+1)r^{\alpha_{\mathrm{P}}}}{P_{\mathrm{P}}BS}\right)^{2/\alpha_{\mathrm{M}}}\right\}dr \tag{5.9}$$

$$\Xi_1(x)=\frac{P_{u,\mathrm{M}}\beta 2\pi S\lambda_{\mathrm{M}}}{\alpha_{\mathrm{M}}-2}x^{2-\alpha_{\mathrm{M}}}, \tag{5.10}$$

$$\Xi_2(x)=\frac{2\pi\lambda_{\mathrm{P}}\beta}{\alpha_{\mathrm{M}}-2}(R_{\mathrm{M}}(x))^{2-\alpha_{\mathrm{M}}}\left(P_o\beta^{-\eta}\int_0^{r_o}t^{\alpha_{\mathrm{P}}\eta}f_{|X_{o,\mathrm{P}}|}(t)\,dt+P_{\max}\int_{r_o}^{\infty}f_{|X_{o,\mathrm{P}}|}(t)\,dt\right) \tag{5.11}$$

---

and the distance $|X_{o,\mathrm{P}}|$ between a typical PUE and its serving PBS $B_{o,\mathrm{P}}$ are obtained as (5.6) and (5.7) at the top of the next page, respectively. Detailed derivation process can be found in chapter 3.

Then, based on the distance statistic properties, the following two theorems can be obtained.

Theorem 8. *The area uplink spectrum efficiency for the macrocell tier is lower bounded as*

$$\mathcal{R}_{\mathrm{M}}^{\mathrm{L}}=S\lambda_{\mathrm{M}}\log_2\left(1+e^{\Delta_1+\Delta_2}\right), \tag{5.12}$$

where

$$\Delta_1 = \ln\left(P_{u,\mathrm{M}}\beta\right) + \psi\left(N-S+1\right) - \alpha_{\mathrm{M}} \int_0^{\infty} \ln\left(x\right) f_{|X_{o,\mathrm{M}}|}\left(x\right) dx, \tag{5.13}$$

and

$$\Delta_2 = -\ln\left(\int_0^{\infty} \Xi_1\left(x\right) f_{|X_{o,\mathrm{M}}|}\left(x\right) dx + \int_0^{\infty} \Xi_2\left(x\right) f_{|X_{o,\mathrm{M}}|}\left(x\right) dx + \delta^2 \right), \tag{5.14}$$

where $\psi\left(\cdot\right)$ *is the digamma function [AS70],* $f_{|X_{o,\mathrm{M}}|}$ *is given by* (5.6)*,* $\Xi_1\left(x\right)$ *and* $\Xi_2\left(x\right)$ *are given by* (5.10) *and* (5.11)*,* $R_{\mathrm{M}}\left(x\right) = \left(\frac{P_{\mathrm{P}}BS}{P_{\mathrm{M}}(N-S+1)}\right)^{1/\alpha_{\mathrm{P}}} x^{\alpha_{\mathrm{M}}/\alpha_{\mathrm{P}}}$*, and* $r_o = \left(\frac{P_{\max}}{P_o}\right)^{1/(\alpha_{\mathrm{P}}\eta)} \beta^{1/\alpha_{\mathrm{P}}}$.

Proof. Based on (5.4), the area uplink spectrum efficiency is calculated as

$$\mathcal{C}_{\mathrm{M}} = S\lambda_{\mathrm{M}} \underbrace{\mathrm{E}\left\{\log_2\left(1+\mathrm{SINR}_{\mathrm{M}}\right)\right\}}_{\Theta_1}. \tag{5.15}$$

By using Jensen's inequality, a lower bound for Θ_1 is

$$\Theta_1^L = \log_2\left(1 + e^{Z_1+Z_2}\right), \tag{5.16}$$

where

$$\begin{cases} Z_1 = \mathrm{E}\left\{\ln\left(P_{u,M}h_{o,M}\beta|X_{o,M}|^{-\alpha_M}\right)\right\}, \\ Z_2 = \mathrm{E}\left\{\ln\left(\dfrac{1}{I_M + I_P + \delta^2}\right)\right\}. \end{cases} \tag{5.17}$$

First calculate Z_1 as

$$Z_1 = \ln\left(P_{u,\mathrm{M}}\beta\right) + \mathrm{E}\left\{\ln\left(h_{o,\mathrm{M}}\right)\right\} - \alpha_{\mathrm{M}}\mathrm{E}\left\{\ln|X_{o,\mathrm{M}}|\right\} \tag{5.18}$$

Considering that $h_{o,\mathrm{M}} \sim \Gamma(N-S+1)$, $\mathrm{E}\left\{\ln\left(h_{o,M}\right)\right\}$ is calculate as $\mathrm{E}\left\{\ln\left(h_{o,\mathrm{M}}\right)\right\} = \psi\left(N-S+1\right)$. The $\mathrm{E}\left\{\ln|X_{o,\mathrm{M}}|\right\}$ is next derived as

$$\mathrm{E}\left\{\ln|X_{o,\mathrm{M}}|\right\} = \int_0^{\infty} \ln\left(x\right) f_{|X_{o,\mathrm{M}}|}\left(x\right) dx \tag{5.19}$$

By using Jensen's inequality, the lower bound on the Z_2 is derived as

$$Z_2 > \overline{Z_2} = \ln\left(\frac{1}{\mathrm{E}\left\{I_{\mathrm{M}}\right\} + \mathrm{E}\left\{I_{\mathrm{P}}\right\} + \delta^2}\right) \tag{5.20}$$

Then,

$$\begin{aligned}\mathrm{E}\left\{I_{\mathrm{M}}\right\} &= \int_0^\infty \mathrm{E}\left\{I_{\mathrm{M}} \,||X_{o,\mathrm{M}}| = x\right\} f_{|X_{o,\mathrm{M}}|}(x)\, dx \\ &\overset{(a)}{=} \int_0^\infty \left(P_{u,\mathrm{M}}\beta 2\pi S\lambda_{\mathrm{M}} \int_x^\infty r^{1-\alpha_{\mathrm{M}}} dr\right) f_{|X_{o,\mathrm{M}}|}(x)\, dx \end{aligned} \tag{5.21}$$

where (a) results from using the Campbell's theorem [BB09]. Similarly, $\mathrm{E}\left\{I_{\mathrm{P}}\right\}$ can also be obtained as follows:

$$\begin{aligned}&\mathrm{E}\left\{I_{\mathrm{P}}\right\} = \int_0^\infty \mathrm{E}\left\{\sum\nolimits_{j\in\Phi_{\mathrm{u,P}}} P_{\mathrm{u,P}} h_{j,\mathrm{M}} L\left(|X_{j,\mathrm{M}}|\right)\right\} f_{|X_{o,\mathrm{M}}|}(x)\, dx \\ &= \int_0^\infty \left(P_{u,\mathrm{P}}\beta 2\pi\lambda_{\mathrm{P}} \int_{R_{\mathrm{M}}(x)}^\infty r^{1-\alpha_{\mathrm{M}}} dr\right) f_{|X_{o,\mathrm{M}}|}(x)\, dx \\ &= \int_0^\infty \left(\min\left\{P_{\max}, P_o L\left(|X_\kappa|\right)^{-\eta}\right\} \beta 2\pi\lambda_{\mathrm{P}} \int_{R_{\mathrm{M}}(x)}^\infty r^{1-\alpha_{\mathrm{M}}} dr\right) f_{|X_{o,\mathrm{M}}|}(x)\, dx \end{aligned} \tag{5.22}$$

Substituting (5.17) and (5.16) into (5.15), (5.12) is got. □

Theorem 9. *The area uplink spectrum efficiency for the picocell tier is given by*

$$\mathcal{R}_{\mathrm{P}} = \frac{\lambda_{\mathrm{P}}}{\ln 2} \int_0^\infty \frac{F_{\mathrm{cov}}^{\mathrm{P}}(\gamma)}{1+\gamma} d\gamma, \tag{5.23}$$

where $F_{\mathrm{cov}}^{\mathrm{P}}(\gamma) = \int_0^\infty F_{\left\{X_{o,\mathrm{P}}=x\right\}}(\gamma)\, f_{|X_{o,\mathrm{P}}|}(x)dx$ *is the complementary cumulative distribution function (CCDF) of* $\mathrm{SINR_P}$*, here* $f_{|X_{o,\mathrm{P}}|}(x)$ *is given by* (5.7) *and* $F_{\left\{X_{o,\mathrm{P}}=x\right\}}(\gamma)$ *is given by* (5.24)*, in which* $P_{o,\mathrm{P}} = \min\left\{P_{\max}, P_o(\beta x^{-\alpha_{\mathrm{P}}})^{-\eta}\right\}$*,* $R_{\mathrm{P}}(x) = \left(\frac{P_{\mathrm{M}}(N-S+1)}{P_{\mathrm{P}}BS}\right)^{1/\alpha_{\mathrm{M}}} x^{\alpha_{\mathrm{P}}/\alpha_{\mathrm{M}}}$*,* ${}_2F_1\left[\cdot,\cdot;\cdot;\cdot\right]$ *is the Gauss hypergeometric function [GR07, (9.142)].*

Proof. By following the similar approach in [JSXA12], the area average uplink spectrum

$$F_{\left\{X_{o,\mathrm{P}}=x\right\}}(\gamma)=\exp\left\{-\frac{\delta^2 x^{\alpha_\mathrm{P}}\gamma}{\beta P_{o,\mathrm{P}}}-S\lambda_\mathrm{M}2\pi\frac{x^{\alpha_\mathrm{P}}\gamma}{P_{o,\mathrm{P}}}P_{u,\mathrm{M}}\frac{\left(R_\mathrm{P}(x)\right)^{2-\alpha_\mathrm{P}}}{\alpha_\mathrm{P}-2}\right.$$
$${}_2F_1\left[\frac{\alpha_\mathrm{P}-2}{\alpha_\mathrm{P}},1;2-\frac{2}{\alpha_\mathrm{P}};-\frac{x^{\alpha_\mathrm{P}}\gamma}{P_{o,\mathrm{P}}}P_{u,\mathrm{M}}\left(R_\mathrm{P}(x)\right)^{-\alpha_\mathrm{P}}\right]-\lambda_\mathrm{P}2\pi\frac{x^{\alpha_\mathrm{P}}\gamma}{P_{o,\mathrm{P}}}P_o\beta^{-\eta}\frac{x^{2-\alpha_\mathrm{P}}}{\alpha_\mathrm{P}-2}\int_0^{r_o}t^{\alpha_\mathrm{P}\eta}$$
$${}_2F_1\left[\frac{\alpha_\mathrm{P}-2}{\alpha_\mathrm{P}},1;2-\frac{2}{\alpha_\mathrm{P}};-\frac{x^{\alpha_\mathrm{P}}\gamma}{P_{o,\mathrm{P}}}P_o\beta^{-\eta}t^{\alpha_\mathrm{P}\eta}x^{-\alpha_\mathrm{P}}\right]f_{|X_{o,\mathrm{P}}|}(t)\,dt$$
$$\left.-\lambda_\mathrm{P}2\pi\frac{x^{\alpha_\mathrm{P}}\gamma}{P_{o,\mathrm{P}}}P_{\max}\frac{x^{2-\alpha_\mathrm{P}}}{\alpha_\mathrm{P}-2}{}_2F_1\left[\frac{\alpha_\mathrm{P}-2}{\alpha_\mathrm{P}},1;2-\frac{2}{\alpha_\mathrm{P}};-\frac{x^{\alpha_\mathrm{P}}\gamma}{P_{o,\mathrm{P}}}P_{\max}x^{-\alpha_\mathrm{P}}\right]\int_{r_o}^{\infty}f_{|X_{o,\mathrm{P}}|}(t)\,dt\right\} \tag{5.24}$$

---

efficiency $\mathcal{R}_\mathrm{P}$ is expressed as:

$$\mathcal{R}_\mathrm{P}=\frac{\lambda_\mathrm{P}}{\ln 2}\int_0^\infty\frac{F_{\mathrm{cov}}^{\mathrm{P}}(\gamma)}{1+\gamma}d\gamma \tag{5.25}$$

where $F_{\mathrm{cov}}^{\mathrm{P}}(\gamma)=\int_0^\infty F_{\left\{X_{o,\mathrm{P}}=x\right\}}(\gamma)\,f_{|X_{o,\mathrm{P}}|}(x)dx$.

Firstly, the CCDF of γ can be provided given a distance $|X_{o,\mathrm{P}}|=x$, which is calculated as

$$\begin{aligned}F_{\left\{X_{\mathrm{o,P=x}}\right\}}(\gamma)&=\mathrm{P}r\left(\frac{P_{o,\mathrm{P}}g_{o,\mathrm{P}}\beta x^{-\alpha_P}}{J_\mathrm{M}+J_\mathrm{P}+\delta^2}>\gamma\right)\\&=\mathrm{P}r\left(g_{o,\mathrm{P}}>\frac{\left(J_\mathrm{M}+J_\mathrm{P}+\delta^2\right)\gamma x^{\alpha_P}}{P_{o,\mathrm{P}}\beta}\right)\\&=\mathrm{E}\left\{\exp\left(-\frac{\left(J_\mathrm{M}+J_\mathrm{P}+\delta^2\right)\gamma x^{\alpha_P}}{P_{o,\mathrm{P}}\beta}\right)\right\}\\&=\exp\left(-\frac{\delta^2\gamma x^{\alpha_P}}{P_{o,\mathrm{P}}\beta}\right)\mathcal{L}_{J_\mathrm{M}}(s)\,\mathcal{L}_{J_\mathrm{P}}(s)\end{aligned} \tag{5.26}$$

where $s=\frac{\gamma x^{\alpha_P}}{P_{o,\mathrm{P}}\beta}$, $\mathcal{L}_{J_\mathrm{M}}(\cdot)$ and $\mathcal{L}_{J_\mathrm{P}}(\cdot)$ are the Laplace transform of the PDF of J_M and J_P, and are given by

$$\begin{aligned}\mathcal{L}_{J_{\mathrm{M}}}(s) &= \prod\nolimits_{j\in\Phi_{u,\mathrm{M}}} \mathrm{E}_{g_{i,\mathrm{P}}}\left\{\exp\left(-sP_{o,\mathrm{M}}g_{i,\mathrm{P}}\beta|X_{i,\mathrm{P}}|^{-\alpha_{\mathrm{P}}}\right)\right\} \\ &= \exp\left(-2\pi\lambda_{\mathrm{M}}S\int_{R_{\mathrm{P}}(x)}^{\infty}\left(1-\mathrm{E}_{g_{i,\mathrm{P}}}\left[\exp\left(-sP_{u,\mathrm{M}}g_{i,\mathrm{P}}\beta r^{-\alpha_{\mathrm{P}}}\right)\right]\right)rdr\right) \\ &= \exp\left(-2\pi\lambda_{M}S\int_{R_{\mathrm{P}}(x)}^{\infty}\left(1-\frac{1}{1+sP_{u,\mathrm{M}}\beta r^{-\alpha_{\mathrm{P}}}}\right)rdr\right) \end{aligned} \tag{5.27}$$

Based on (5.32), the $\mathcal{L}_{J_{\mathrm{P}}}(s)$ can be derived as

$$\begin{aligned}\mathcal{L}_{J_{\mathrm{P}}}(s) &= \prod\nolimits_{j\in\Phi_{M}} \mathrm{E}_{g_{j,\mathrm{P}}}\left\{\exp\left(-sP_{u,\mathrm{P}}g_{j,\mathrm{P}}\beta|X_{j,\mathrm{P}}|^{-\alpha_{P}}\right)\right\} \\ &= \exp\left(-2\pi\lambda_{P}\int_{x}^{\infty}\mathrm{E}_{P_{\mathrm{u,P}}}\left\{\frac{sP_{\mathrm{u,P}}\beta r^{-\alpha_{P}}}{1+sP_{\mathrm{u,P}}\beta r^{-\alpha_{P}}}\right\}rdr\right) \\ &= \exp\Bigg(-2\pi\lambda_{P}\Bigg(\left[\int_{r_o}^{\infty}f_{|X_{j,\mathrm{P}}|}(t)\,dt\right]\left[\int_{x}^{\infty}\frac{sP_{\max}\beta r^{-\alpha_{P}}}{1+sP_{\max}\beta r^{-\alpha_{P}}}rdr\right] \\ &+\left[\int_{x}^{\infty}\left(\int_{0}^{r_o}\frac{sP_{o}\beta^{-\eta}t^{\alpha_{P}\eta}\beta r^{-\alpha_{P}}}{1+sP_{o}\beta^{-\eta}t^{\alpha_{P}\eta}\beta r^{-\alpha_{P}}}f_{|X_{j,\mathrm{P}}|}(t)\,dt\right)rdr\right]\Bigg)\Bigg) \end{aligned} \tag{5.28}$$

Finally, after some manipulations, (5.23) in section 5.3 using Mathematica can be obtained. □

5.3.2 Energy Efficiency

In this subsection, the energy efficiency for massive MIMO macrocell tier and picocell tier are evaluated. According to [Mia13], the average power consumption of a MUE is defined as

$$\mathrm{P}_{\mathrm{M}}^{\mathrm{total}} = P_f + \frac{P_{\mathrm{u,M}}}{\varepsilon}, \tag{5.29}$$

where P_f is the fixed circuit power consumption, the transmit power of MUE is $P_{\mathrm{u,M}}$, and ε is the power amplifier efficiency. Thus, the EE for a typical MUE is lower bounded as

$$\mathrm{EE}_{\mathrm{M}}^{\mathrm{L}} = \frac{\mathcal{R}_{\mathrm{M}}^{\mathrm{L}}}{S\lambda_{\mathrm{M}}\mathrm{P}_{\mathrm{M}}^{\mathrm{total}}}, \tag{5.30}$$

where $\mathcal{R}_{\mathrm{M}}^{\mathrm{L}}$ is the average SE given by (5.12).

Similarly, the average power consumption of a PUE can be defined as

$$\mathrm{P}_{\mathrm{P}}^{\mathrm{total}} = P_f + \frac{\overline{\mathrm{P}}_{\mathrm{u,P}}}{\varepsilon}, \tag{5.31}$$

where the average transmit power $\overline{\mathrm{P}}_{\mathrm{u,P}}$ is derived as following

$$\begin{aligned}
\overline{\mathrm{P}}_{\mathrm{u,P}} &= \int_0^{\infty} \min\left\{P_{\max}, P_o\beta x^{-\eta}\right\} f_{|x_{o,\mathrm{P}}|}(x)\,dx \\
&= \int_0^{x_o} \min\left\{P_{\max}, P_o\beta^{-\eta}x^{\alpha_P\eta}\right\} f_{|x_{o,\mathrm{P}}|}(x)\,dx \\
&= P_o\beta^{-\eta}\int_0^{r_o} x^{\alpha_P\eta} f_{|x_{o,\mathrm{P}}|}(x)\,dx + P_{\max}\int_{r_o}^{\infty} f_{|x_{o,\mathrm{P}}|}(x)\,dx
\end{aligned} \tag{5.32}$$

From equation (5.32), it can be indicated that the PUE average transmit power is dependent on the density of small cells.

Finally, the energy efficiency for a typical PUE is derived as

$$\mathrm{EE}_{\mathrm{P}} = \frac{\mathcal{R}_{\mathrm{P}}}{\lambda_{\mathrm{P}}\mathrm{P}_{\mathrm{P}}^{\mathrm{total}}} \tag{5.33}$$

where $\mathcal{R}_{\mathrm{P}}$ is the average SE given by (5.23).

Parameter	Symbol	Value
Pathloss exponent to MUEs	α_{M}	3.5
Pathloss exponent to PUEs	α_{D}	4
The MBS transmit power	P_{M}	43dBm
The PBS transmit power	P_{P}	30dBm
The MUE transmit power	$P_{\mathrm{u,M}}$	15dBm
The PUE maximum transmit power	$P_{\max}$	23 dBm
Bandwidth	BW	5 MHz
The noise power	σ^2	$-170 + 10 \times log_{10}(BW)$ dBm
The power density [SSP+13]	P_o	-80 dBm
Users static power consumption	P_{fix}	100 mW
Power amplifier efficiency	ε	0.5
Number of antennas	N	200

Table 5-A: Simulation Parameters.

5.4 Numerical Results

In this section, numerical results are presented to evaluate the area uplink spectrum efficiency of MUE and PUE in the massive MIMO aided HCN. Such a network is set to operate at a carrier frequency of 1 GHz. The density of MBSs is $\lambda_{\mathrm{M}} = \left(500^2 \times \pi\right)^{-1} \mathrm{m}^{-2}$ in a circular region with radius 1×10^4 m. Other parameter settings are shown in Table 5.4.

In the figures, Monte Carlo (MC) simulated values of the MUE low bound uplink spectrum efficiency and the PUE exact uplink spectrum efficiency are marked by 'o', while the MUE exact uplink spectrum efficiency are marked by square for tightness analysis. They are all numerically obtained to validate the analysis.

Figure 5.1 shows the area uplink spectrum efficiency versus density ratio between PBS and MBS. Each MBS is equipped with $N = 400$ antennas, the number of users served in each macrocell is $S = 25$ and the biasing factor is $B = 3$ dB. It can be seen that the lower bound curves for area uplink spectrum efficiency of the macrocell tier obtained from Theorem 8 can efficiently predict the performance behaviour. Uplink power control applied in the picocells can significantly affect the area uplink spectrum efficiency of the macrocell tier and picocell tier. Specifically, when the path loss compensation factor is

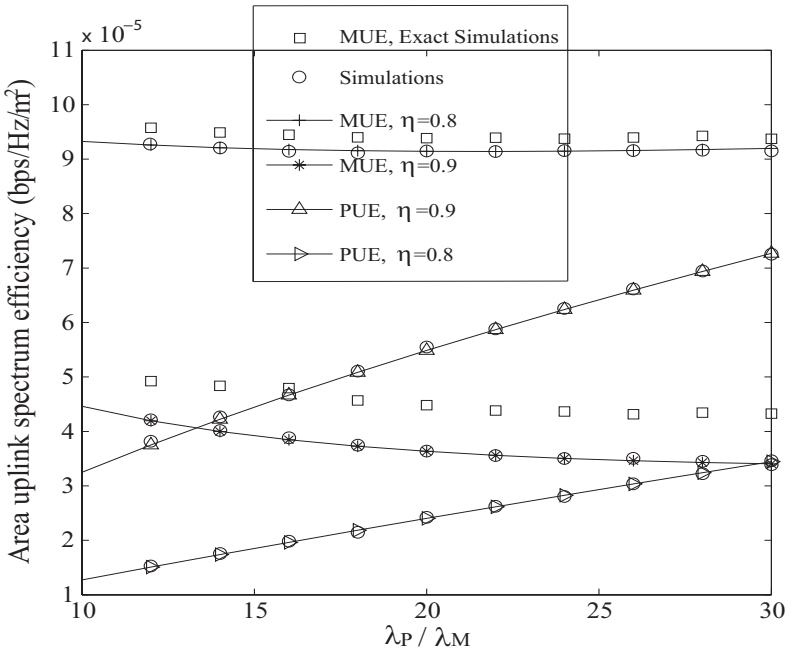

Figure 5.1: The area uplink spectrum efficiency of MUE and PUE versus the tier density ratio for different power compensation factor η.

lower, uplink performance in the macrocells is enhanced, due to the fact that macrocells experience less interference from the uplink transmissions in the picocells. Although users in the picocells can use the maximum transmit power $P_{\max} = 23$ dBm when they are not close to their serving PBSs, the area uplink spectrum efficiency of the picocell tier is declined. The reason is that the transmit power of the users who are very close to their serving PBSs is controlled, and their achievable uplink spectrum efficiency decreases significantly. Deploying more PBSs improves the area uplink spectrum efficiency of picocell tier, however, the uplink performance of the macrocell tier decreases due to more uplink interference from the picocell tier.

Figure 5.2 shows the the area uplink spectrum efficiency versus the power control compensation factor η with different MBS antenna numbers N and maximum PUE transmit power P_{max}. Each MBS serves $S = 25$ MUEs, the density of PBSs is $\lambda_{\rm P} = 30 \times \lambda_{\rm M}$, and the bias factor is $B = 3$ dB. From this figure, it is obviously to see that employing more antennas on MBS can effectively enhance the area uplink spectrum

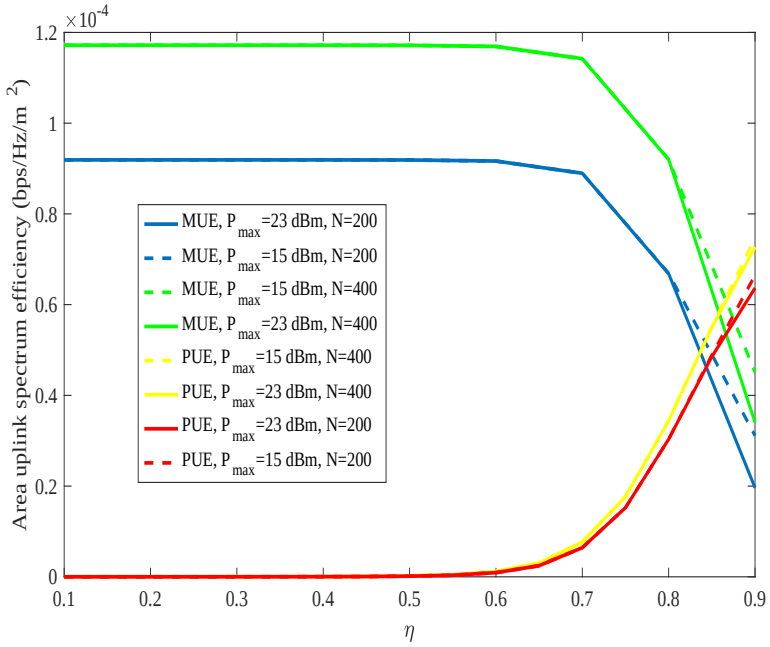

Figure 5.2: The area uplink spectrum efficiency of MUE and PUE versus the power compensation factor η for different MBS antenna numbers N and maximum PUE transmit power P_{max}.

efficiency of MUEs, due to the large array gain. Then, it can be found that the uplink spectrum efficiency of MUEs increases when the PUE transmit power is controlled and converges to a constant value when $\eta \leqslant 0.6$. Besides, when the $P_{\max}$ is lower, the MUEs have higher spectrum efficiency resulting from less interference. But the effect of the $P_{\max}$ can be ignored when $\eta \leqslant 0.7$. Thus, the maximum PUE transmit power can be set as a lower value in order to save energy when power control is applied.

Figure 5.3 shows the the area uplink spectrum efficiency versus number of users served by each MBS. Each MBS is equipped with $N = 200$ antennas, the density of PBSs is $\lambda_{\mathrm{P}} = 30 \times \lambda_{\mathrm{M}}$, and the power control compensation factor $\eta = 0.8$. It can be found that CRE has a substantial effect on the area uplink spectrum efficiency of the macrocell tier, when more users per marcocell are served. However, increasing CRE bias factor degrades the uplink performance of picocell tier, since more faraway users in the picocells are served by PBSs. Obviously, serving more users increases the area spectrum efficiency of the macrocell tier due to more multiplexing gains, and more uplink transmissions in

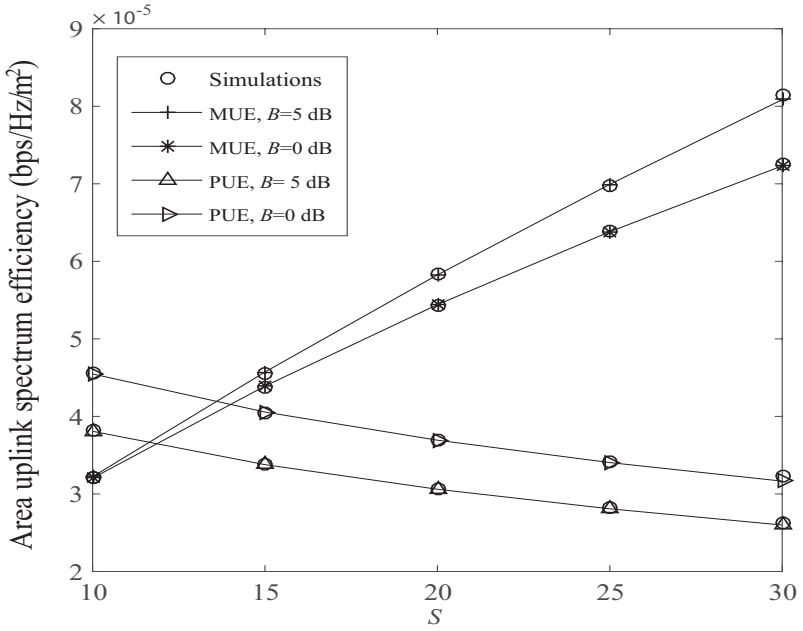

Figure 5.3: The area uplink spectrum efficiency of MUE and PUE versus the number of users S for different bias factor B with unit dB.

the macrocells result in a mild decrease in the area uplink spectrum efficiency of the picocell tier, since interference from MUEs increases.

Figure 5.4 shows the the uplink average energy efficiency of a MUE and a PUE versus density ratio $\lambda_{\mathrm{P}}/\lambda_{\mathrm{M}}$ with different power compensation factor η. Each MBS is equipped with $N = 400$ antennas, the number of users is $S = 25$. It can be seen that a typical PUE has a higher average energy efficiency than MUE when its transmit power is less controlled, due to the shorter distance. However, MUE will have a much higher energy efficiency than PUE when η is lower because the MUE experience less interference and the spectrum efficiency of PUE decreases a lot. Although the average transmit power of each PUE decreases with the increased density ratio, the energy efficiency gain of each PUE cannot offset the loss from its average spectrum efficiency.

Figure 5.5 shows the the average energy efficiency a MUE and a PUE versus the number of users S with different bias factor B with unit dB. Each MBS is equipped with $N = 200$ antennas, the density of PBSs is $\lambda_{\mathrm{P}} = 30 \times \lambda_{\mathrm{M}}$, and the power control

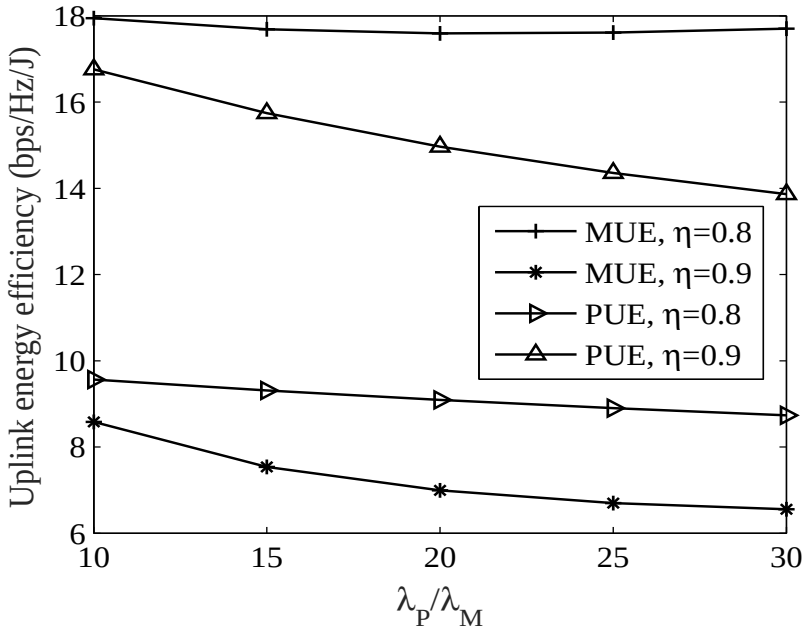

Figure 5.4: The uplink energy efficiency of MUE and PUE versus the tier density ratio for different power compensation factor η.

compensation factor $\eta = 0.8$. From this figure, it can be seen that with the increasing number of users, the uplink energy efficiency of both MUE and PUE are decreasing. Because the power assigned to each user decreases when more users are served by a MBS. Meanwhile, inter-tier interference becomes severer when more users are served, thus the energy efficiency of picocell tier decreases as well. Similar to the Figure 5.3, the effect of CRE on macrocell tier becomes substantial when more users are served.

5.5 Summary

In this chapter, a joint uplink power control and CRE scheme for uplink interference coordination is proposed in a two-tier massive MIMO aided HCN, consisting of picocells and massive MIMO macrocells. Specifically, CRE is employed to tackle the uplink/downlink imbalance problem due to the massive MIMO array gains. The uplink power control is adopted in the picocells to suppress the inter-tier interference. Lower bounds of the

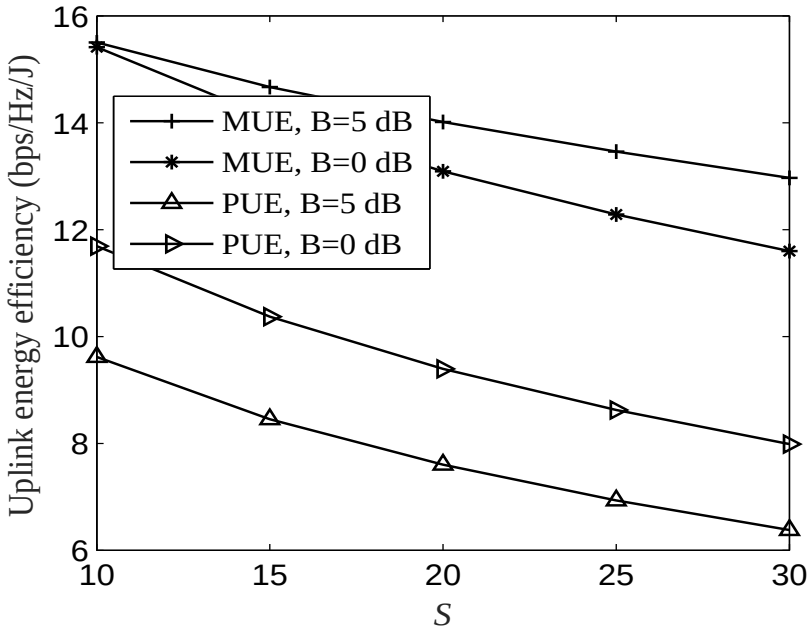

Figure 5.5: The area uplink spectrum efficiency of MUE and PUE versus the number of users S for different bias factor B with unit dB.

spectrum efficiency and energy efficiency of MUE and PUE are derived as mathematical expressions for analysis. Numerical results confirmed that the inter-tier interference can be coordinated by jointly adopting uplink power control and CRE. Hence, the area spectrum efficiency and average energy efficiency of MUEs can be enhanced effectively in a dense small cell deployment.

Chapter 6

Performance Evaluation and Enhancement in D2D Underlaid Massive MIMO enabled Cellular Networks

6.1 Overview

As previous chapters show, massive MIMO can drastically improve the spectral efficiency (SE) by using large number of antennas and accommodating dozens of users in the same radio channel [NLM13a]. However, the circuit power consumption increases with the number of antennas, which may deteriorate the downlink EE of massive MIMO systems. Device to device (D2D) takes advantage of the proximity to support direct transmissions without the aid of base stations (BSs) or the core networks. As a result, D2D can improve both SE and EE, and decrease the delay [AWM14]. However, the D2D distance plays a dominant role in D2D transmission, which significantly affects the D2D performance. When D2D users and cellular users share the same frequency bands in D2D underlaid massive MIMO cellular networks, interference becomes a key issue to be addressed. In such networks, severe co-channel interference exists due to the following two key factors:

- In contrast to the traditional cellular networks, massive MIMO cellular networks enable much more cellular transmissions at the same time and frequency band.

As such, the inter-cell interference and cellular-to-D2D interference will be much higher than ever before.

- D2D users are expected to be dense for offloading the network traffic. As such, the D2D-to-cellular interference will significantly deteriorate the cellular transmissions.

Currently, interference mitigation in such networks remains an open problem.

This chapter focuses on uplink D2D underlaid massive MIMO cellular networks. In order to coordinate the inter-cell interference, cellular-to-D2D interference, and D2D-to-cellular interference, two power control schemes for cellular users and D2D users are considered, respectively. To date, there are few results available for presenting the uplink SE and EE with power control in such networks. Therefore, this chapter reveals design insights into the interplay between massive MIMO and D2D in the uplink cellular setting.

6.2 Related Works and Motivation

The implementation of D2D in the cellular networks is a promising approach to offload cellular traffic and avoid congestion in the core network [FLYW+14]. In [EHA14], D2D and cellular mode selection was considered for achieving better link quality. The work of [MLPH11] assumed that D2D user has a protection zone such that the uplink cellular-to-D2D interference cannot be larger than a threshold, and showed that the capacity of a D2D link can be enhanced while the capacity loss of cellular users is negligible. In [YZD+16], cooperative transmissions in the D2D overlay/underlay cellular networks were studied, and it was verified that the D2D transmission capacity can be enhanced with the assistance of relay. In [MLY+16], a contract-based cooperative spectrum sharing was developed to exploit the transmission opportunities for the D2D links and keep the maximum profit of the cellular links. Nevertheless, the aforementioned literature only considered D2D communications in the traditional cellular networks, and more research efforts are needed to comprehensively understand the D2D communications in the future

cellular networks such as 5G with many disruptive technologies [LWC+16].

Power control has been widely studied in conventional D2D underlaid cellular networks for interference management [GBCC11, AEA15, HNDZ16, LLAH15, ZFJ+15, LOZ16, YHX+16]. In [GBCC11], a dynamic power control mechanism was proposed for controlling the D2D user's transmit power, so as to reduce the D2D-to-cellular interference. In [AEA15], the truncated channel inversion power control was adopted such that the data rate is constant during the transmissions, and D2D and cellular users cannot transmit signals if their transmit power is larger than a predefined value. A centralized power control solution in D2D enabled two-tier cellular networks was proposed by [HNDZ16]. In [LLAH15], power control algorithms were proposed for mitigating the cross-tier interference between the D2D links and one single cellular link. In the work of [LLAH15], centralized power control problem was formulated as a linear-fractional programming and the optimal solution was obtained by using standard convex programming tools. D2D power control in conventional uplink MIMO cellular networks was studied by authors of [ZFJ+15], where a distributed resource allocation algorithm was proposed based on the game-theoretic model. In [LOZ16], joint beamforming and power control was studied in a single cell consisting of one D2D pair and multiple cellular users, and the optimization problem was formulated for minimizing the total transmit power. The work of [YHX+16] also considered a D2D underlaid single cell network and investigated the downlink power control for maximizing the sum rate of D2D pairs. However, these prior works only pay attention to power control problem in the conventional D2D underlaid cellular networks. Moreover, the majority of the existing D2D power control designs such as [ZFJ+15, LOZ16, YHX+16] need the global channel state information (CSI), which is challenging in D2D underlaid massive MIMO cellular networks, since the CSI between the D2D users and massive MIMO enabled BSs cannot be easily obtained.

The opportunities and challenges of the co-existence of the massive MIMO and D2D have recently been investigated in the uplink [LHA15] and downlink transmissions [SBK+15]. In [LHA15], D2D and massive MIMO aided cellular uplink SE were

studied and the interplay between D2D and massive MIMO was exploited, which showed that there is a loss in cellular SE due to D2D underlay. To redeem the cellular performance loss, authors in [LHA15] assumed that the number of canceled D2D interfering signals is scaled with the number of BS antennas. In [SBK$^+$15], downlink sum rate and EE were analyzed in a single massive MIMO cell, where multiple D2D transmitters were randomly located. The work of [SBK$^+$15] utilized equal power allocation without considering interference management, and showed that the benefits of the coexistence of D2D and massive MIMO are limited by the density of D2D users. Particularly when there are vast D2D links and each massive MIMO BS provides services for dozens of users, interference becomes a major issue and needs to be mitigated [LHA15, SBK$^+$15]. Although the existing works [LHA15] and [SBK$^+$15] have respectively investigated the uplink and downlink features of the massive MIMO cellular networks with underlaid D2D, the interference management via power control in such networks has not been conducted yet. To date, no effort has been devoted to analyze the effects of uplink power control on the SE and EE of the D2D underlaid massive MIMO cellular networks.

6.3 System Model

The uplink transmission in a cellular network is considered, where massive MIMO enabled macrocells are underlaid with D2D transceivers, as shown in Fig. 6.3. The locations of macrocell BSs (MBSs) are modeled following a homogeneous Poisson point process (HPPP) Φ_{M} with density λ_{M}. The locations of D2D transmitters are modeled following an independent HPPP Φ_{D} with density λ_{D}. Each MBS is equipped with N antennas and receives data streams from S single-antenna cellular user equipments (CUEs) over the same time and frequency band, while each D2D receiver equipped with one single antenna receives one data stream from a single-antenna D2D transmitter in each transmission. The linear zero-forcing beamforming (ZFBF) is employed to cancel the intra-cell interference at the MBS [HYA14]. It is assumed that the density of CUEs

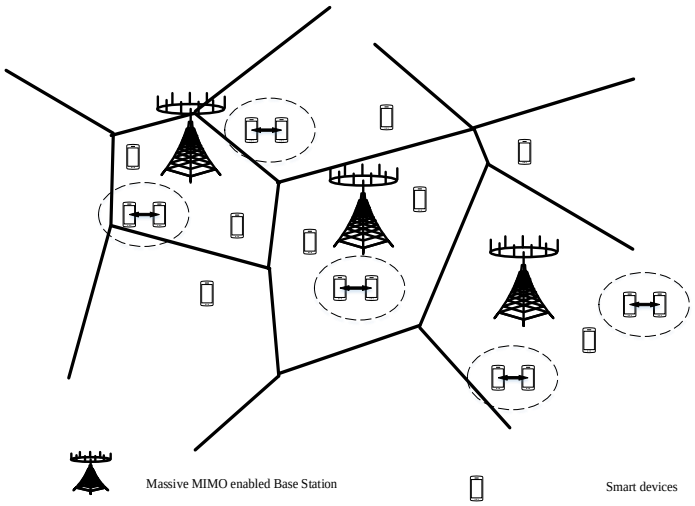

Figure 6.1: An illustration of the D2D underlaid cellular networks equipped with massive MIMO MBSs.

is much greater than that of MBSs so that there always will be multiple active CUEs in every macrocell. All the channels undergo independent and identically distributed (i.i.d.) quasi-static Rayleigh fading. Each CUE is assumed to be connected with its nearest MBS such that the Euclidean plane is divided into Poisson-Voronoi cells.

6.3.1 Power Control Policy

In the macrocells, the open-loop uplink power control is applied such that far-away CUEs can obtain more path loss compensation, and the transmit power for a CUE associated with the MBS is given by [1]

$$P_{\mathrm{C}} = \min\left\{P_{\max}^{\mathrm{C}}, P_o L\left(|X_{\mathrm{C,M}}|\right)^{-\eta}\right\}, \tag{6.1}$$

[1]Note that [NDA13a] also studied the open-loop power control in a single-tier cellular networks without considering the maximum transmit power constraint.

where $P_{\max}^{\mathrm{C}}$ is the maximum CUE transmit power, P_o is the normalized power density, $L\left(|X_{\mathrm{C,M}}|\right) = \beta |X_{\mathrm{C,M}}|^{-\alpha_{\mathrm{M}}}$, α_{M} is the path loss exponent, β is the frequency dependent constant value, $|X_{\mathrm{C,M}}|$ is the distance between the CUE and its associated MBS and $\eta \in [0, 1]$ is the path loss compensation factor, which controls the CUE transmit power. Here $\eta = 1$ represents that the path loss between a CUE and its serving MBS is fully compensated, and $\eta = 0$ represents that there is no path loss compensation. Note that the open-loop uplink power control does not require the instantaneous CSI.

To mitigate the D2D-to-cellular interference, it is considered that the average received interference at the MBS from a D2D transmitter should not exceed a maximum value I_{th}, which is different from [AEA15] where D2D transmitter stops transmissions if its transmit power is larger than a predefined value to achieve a fixed data rate. Therefore, the D2D transmit power is given by

$$P_{\mathrm{D}} = \min \left\{ P_{\max}^{\mathrm{D}}, \frac{I_{\mathrm{th}}}{L\left(|X_{\mathrm{D,M}}|\right)} \right\}, \tag{6.2}$$

where $P_{\max}^{\mathrm{D}}$ is the maximum D2D transmit power, $|X_{\mathrm{D,M}}|$ is the distance between a D2D transmitter and its nearest MBS. If there is no power control on the D2D transmitters, the shorter $|X_{\mathrm{D,M}}|$, the stronger interference power. Here, $I_{\mathrm{th}} = 0$ represents that there is no allowable D2D transmission and the considered network reduces to the one-tier massive MIMO enabled multi-cell network, and $I_{\mathrm{th}} = \infty$ represents that there is no D2D power control. Different from [LHA15] which assumed that MBSs can obtain perfect CSI between the D2D transmitters and themselves, and have the ability of canceling sufficient number of D2D interfering signals, the proposed D2D power control policy does not need the instantaneous CSI and possesses much lower complexity.

6.3.2 Channel Model

It is assumed that a typical serving MBS is located at the origin o. The receive signal-to-interference-plus-noise ratio (SINR) of a typical serving MBS at a random distance

$|X_{o,\mathrm{M}}|$ from its intended CUE [2] is given by

$$\mathrm{SINR}_{\mathrm{M}} = \frac{P_{o,\mathrm{C}} h_{o,\mathrm{M}} L\left(|X_{o,\mathrm{M}}|\right)}{I_{\mathrm{M}} + I_{\mathrm{D}} + \sigma^2}, \tag{6.3}$$

where $P_{o,\mathrm{C}}$ is the transmit power of the typical CUE, $h_{o,\mathrm{M}} \sim \Gamma\left(N - S + 1, 1\right)$ [HYA14] is the small-scale fading channel power gain between the typical serving MBS and its intended CUE, σ^2 is the noise power, I_{M} and I_{D} are the interference from inter-cell CUEs and D2D transmitters, which are found as

$$\begin{cases} I_{\mathrm{M}} = \sum\nolimits_{i \in \Phi_{\mathrm{u,M}} \backslash \mathrm{B}(o)} P_{i,\mathrm{C}} h_{i,\mathrm{M}} L\left(|X_{i,\mathrm{M}}|\right), \\ I_{\mathrm{D}} = \sum\nolimits_{j \in \Phi_{\mathrm{D}}} P_{j,\mathrm{D}} h_{j,\mathrm{M}} L\left(|X_{j,\mathrm{M}}|\right), \end{cases} \tag{6.4}$$

where $P_{i,\mathrm{C}}$ is the transmit power of the interfering CUE $i \in \Phi_{\mathrm{u,M}} \backslash \mathrm{B}\left(o\right)$ ($\Phi_{\mathrm{u,M}} \backslash \mathrm{B}\left(o\right)$ is the point process corresponding to the interfering CUEs), $P_{j,\mathrm{D}}$ is the transmit power of the interfering D2D $j \in \Phi_{\mathrm{D}}$, $h_{i,\mathrm{M}} \sim \exp(1)$ and $|X_{i,\mathrm{M}}|$ are the small-scale fading interfering channel power gain and distance between the typical serving MBS and interfering CUE i, respectively, $h_{j,\mathrm{M}} \sim \exp(1)$ and $|X_{j,\mathrm{M}}|$ are the small-scale fading interfering channel power gain and distance between the typical serving MBS and interfering D2D transmitter j, respectively.

Likewise, the SINR of a typical D2D receiver at a distance d_o [3] from its D2D transmitter is given by

$$\mathrm{SINR}_{\mathrm{D}} = \frac{P_{o,\mathrm{D}} g_{o,\mathrm{D}} L\left(d_o\right)}{J_{\mathrm{M}} + J_{\mathrm{D}} + \sigma^2}, \tag{6.5}$$

where $g_{o,\mathrm{D}} \sim \exp(1)$ and $L\left(d_o\right) = \beta (d_o)^{-\alpha_{\mathrm{D}}}$ is the small-scale fading channel power gain and path loss between the typical D2D receiver and its corresponding D2D transmitter,

[2] Since the cellular and D2D users may experience similar shadow fading conditions which are not independent, to be tractable, the effect of shadow fading is not examined in this paper.

[3] Since there is no well-recognized D2D distance distribution, in this paper, we consider d_o as a constant parameter, which can be arbitrary values.

respectively, α_{D} is the path loss exponent, J_{M} and J_{D} are the interference from the CUEs and interfering D2D transmitters, respectively, given by

$$\begin{cases} J_{\mathrm{M}} = \sum\nolimits_{i\in\Phi_{\mathrm{u,M}}} P_{i,\mathrm{C}} g_{i,\mathrm{D}} L\left(|X_{i,\mathrm{D}}|\right), \\ J_{\mathrm{D}} = \sum\nolimits_{j\in\Phi_{\mathrm{D}}\backslash o} P_{j,\mathrm{D}} g_{j,\mathrm{D}} L\left(|X_{j,\mathrm{D}}|\right), \end{cases} \tag{6.6}$$

where $g_{i,\mathrm{D}} \sim \exp(1)$ and $|X_{i,\mathrm{D}}|$ are the small-scale fading interfering channel power gain and distance between the typical D2D receiver and interfering CUE $i \in \Phi_{\mathrm{u,M}}$, respectively, $g_{j,\mathrm{D}} \sim \exp(1)$ and $|X_{j,\mathrm{D}}|$ are the small-scale fading interfering channel power gain and distance between the typical D2D receiver and interfering D2D transmitter $j \in \Phi_{\mathrm{D}}\backslash o$, respectively.

6.4 Spectrum Efficiency and Energy Efficiency

By addressing the effects of power control, the SE and EE are examined for the cellular and D2D transmissions. Firstly, the following probability density function (PDF) of the D2D transmit power is needed to be derived based on (6.2).

6.4.1 D2D Transmit Power Distribution

Lemma 5. *The PDF of a typical D2D transmit power is given by*

$$f_{P_{\mathrm{D}}}(x) = \begin{cases} \frac{2\pi\lambda_{\mathrm{M}}}{\alpha_{\mathrm{M}}} \left(\frac{\beta}{I_{\mathrm{th}}}\right)^{2/\alpha_{\mathrm{M}}} x^{2/\alpha_{\mathrm{M}}-1} \bar{\Delta}(x), & x < P_{\max}^{\mathrm{D}} \\ \delta\left(x - P_{\max}^{\mathrm{D}}\right) \bar{\Delta}\left(P_{\max}^{\mathrm{D}}\right), & x \geq P_{\max}^{\mathrm{D}} \end{cases}, \tag{6.7}$$

where $\bar{\Delta}(x) = \exp\left(-\pi\lambda_{\mathrm{M}}\left(\frac{\beta x}{I_{\mathrm{th}}}\right)^{2/\alpha_{\mathrm{M}}}\right)$ *and* $\delta(\cdot)$ *is the Dirac delta function.*

Proof. Based on (6.2), the cumulative distribution function (CDF) of P_{D} is written as

$$\begin{aligned} F_{P_{\mathrm{D}}}(x) &= \Pr\left(P_{\mathrm{D}} \leq x\right) \\ &= \Pr\left(\min\left\{\frac{I_{\mathrm{th}}}{L\left(|X_{\mathrm{D,M}}|\right)}, P_{\max}^{\mathrm{D}}\right\} \leq x\right) \\ &= \begin{cases} 1, & x \geq P_{\max}^{\mathrm{D}} \\ \Delta(x), & x < P_{\max}^{\mathrm{D}} \end{cases} \\ &= \mathrm{U}\left(x - P_{\max}^{\mathrm{D}}\right)\left(1 - \Delta(x)\right) + \Delta(x), \end{aligned} \tag{6.8}$$

where $\mathrm{U}(\cdot)$ is the unit step function denoted as $\mathrm{U}(x) = \begin{cases} 1, & x \geq 0 \\ 0, & x < 0 \end{cases}$, and $\Delta(x)$ is calculated as

$$\begin{aligned} \Delta(x) &= \Pr\left(\frac{I_{\mathrm{th}}}{L(|X_{\mathrm{D,M}}|)} \leq x\right) \\ &= \Pr\left(|X_{\mathrm{D,M}}| \leq \left(\frac{\beta x}{I_{\mathrm{th}}}\right)^{1/\alpha_{\mathrm{M}}}\right). \end{aligned} \tag{6.9}$$

Since the PDF of the distance $|X_{\mathrm{D,M}}|$ between a D2D transmitter and its nearest MBS is given by [JSXA12]

$$f_{|X_{\mathrm{D,M}}|}(r) = 2\pi\lambda_{\mathrm{M}} r \exp\left(-\pi\lambda_{\mathrm{M}} r^2\right). \tag{6.10}$$

Then, (6.9) is further derived as

$$\begin{aligned} \Delta(x) &= \int_0^{\left(\frac{\beta x}{I_{\mathrm{th}}}\right)^{1/\alpha_{\mathrm{M}}}} f_{|X_{\mathrm{D,M}}|}(r) dr \\ &= 1 - \exp\left(-\pi\lambda_{\mathrm{M}}\left(\frac{\beta x}{I_{\mathrm{th}}}\right)^{2/\alpha_{\mathrm{M}}}\right). \end{aligned} \tag{6.11}$$

Substituting (6.11) into (6.8),

$$F_{P_{\mathrm{D}}}(x) = 1 - \mathrm{U}\left(P_{\max}^{\mathrm{D}} - x\right) \exp\left(-\pi\lambda_{\mathrm{M}}\left(\frac{\beta x}{I_{\mathrm{th}}}\right)^{2/\alpha_{\mathrm{M}}}\right). \tag{6.12}$$

$$\Xi_1(t) = \int_0^{\infty} \left(1 - e^{-tP_{o,\mathrm{C}}(N-S+1)\beta(\frac{x}{\pi\lambda_{\mathrm{M}}})^{-\frac{\alpha_{\mathrm{M}}}{2}}}\right) \exp\Big(-2\pi S\lambda_{\mathrm{M}} \int_x^{\infty} (1-\Upsilon_1) r dr - x\Big) dx \tag{6.14}$$

with

$$\Upsilon_1 = \left(1 + tP_{\max}^{\mathrm{C}} \beta r^{-\alpha_{\mathrm{M}}}\right)^{-1} e^{-\pi\lambda_{\mathrm{M}} r_o^2} + \int_0^{\pi\lambda_{\mathrm{M}} r_o^2} \left(e^{\nu} + e^{\nu} tP_o \beta^{1-\eta} (\frac{\nu}{\pi\lambda_{\mathrm{M}}})^{\frac{\eta\alpha_{\mathrm{M}}}{2}} r^{-\alpha_{\mathrm{M}}}\right)^{-1} d\nu$$

$$\Xi_2(t) = \exp\Big\{ -\pi\lambda_{\mathrm{D}} \beta^{\frac{2}{\alpha_{\mathrm{M}}}} \Big[\frac{\left(P_{\max}^{\mathrm{D}}\right)^{\frac{2}{\alpha_{\mathrm{M}}}}}{\varpi_0}(1 - e^{-\varpi_0} - \varpi_0 e^{-\varpi_0}) + \left(P_{\max}^{\mathrm{D}}\right)^{\frac{2}{\alpha_{\mathrm{M}}}} \bar{\Delta}\left(P_{\max}^{\mathrm{D}}\right)\Big]$$
$$\Gamma(1 + \frac{2}{\alpha_{\mathrm{M}}})\Gamma(1 - \frac{2}{\alpha_{\mathrm{M}}}) t^{\frac{2}{\alpha_{\mathrm{M}}}} \Big\} \tag{6.15}$$

Taking the derivative of $F_{P_{\mathrm{D}}}(x)$ in (6.12), the PDF of P_{D} in (6.7) is obtained and the proof is completed. □

From **Lemma** 5, it can be seen that the level of the D2D transmit power is dependent on the massive MIMO enabled MBS density and the interference threshold I_{th}.

6.4.2 Spectrum Efficiency

With the assistance of **Lemma** 5, the SE for a typical CUE can be obtained in the following theorem.

Theorem 10. *The achievable SE under power control for a typical CUE is given by*

$$\overline{R}_{\mathrm{C}} = 1/\ln(2) \int_0^{\infty} \frac{\Xi_1(t)}{t} \Xi_2(t)\, e^{-\sigma^2 t} dt, \tag{6.13}$$

where $\Xi_1(t)$ *and* $\Xi_2(t)$ *is given by* (6.14) *and* (6.15) *at the top of next page, in which* $r_o = \left(\frac{P_{\max}^{\mathrm{C}}}{P_o}\right)^{1/(\alpha_{\mathrm{M}}\eta)} \beta^{1/\alpha_{\mathrm{M}}}$ *and* $\varpi_0 = \pi\lambda_{\mathrm{M}} \left(\frac{\beta P_{\max}^{\mathrm{D}}}{I_{\mathrm{th}}}\right)^{2/\alpha_{\mathrm{M}}}$.

Proof. Based on (6.3), the SE for a typical CUE is written as

$$\begin{aligned}\overline{R}_{\mathrm{C}} &= \mathbb{E}\left\{\log_2\left(1+\mathrm{SINR}_{\mathrm{M}}\right)\right\} \\ &= \mathbb{E}\left\{\log_2\left(1+\frac{Z_1}{I_{\mathrm{M}}+I_{\mathrm{D}}+\sigma^2}\right)\right\},\end{aligned} \tag{6.16}$$

where $Z_1 = P_{o,\mathrm{C}} h_{o,\mathrm{M}} L\left(|X_{o,\mathrm{M}}|\right)$. Using [Ham08, Lemma 1], (6.16) can be equivalently transformed as

$$\begin{aligned}\overline{R}_{\mathrm{C}} &= \frac{1}{\ln(2)}\mathbb{E}\left\{\int_0^\infty \frac{1}{t}\left(1-e^{-tZ_1}\right)e^{-t\left(I_{\mathrm{M}}+I_{\mathrm{D}}+\sigma^2\right)}dt\right\} \\ &= \frac{1}{\ln(2)}\int_0^\infty \frac{1}{t}\underbrace{\mathbb{E}\left\{\left(1-e^{-tZ_1}\right)e^{-tI_{\mathrm{M}}}\right\}}_{\Xi_1(t)}\underbrace{\mathbb{E}\left\{e^{-tI_{\mathrm{D}}}\right\}}_{\Xi_2(t)}e^{-t\sigma^2}dt.\end{aligned} \tag{6.17}$$

Firstly, $\Xi_1(t)$ is calculated as

$$\begin{aligned}\Xi_1(t) &= \int_0^\infty \mathbb{E}_{|X_{o,\mathrm{M}}|=x}\left\{\left(1-e^{-tZ_1}\right)e^{-tI_{\mathrm{M}}}\right\} f_{|X_{o,\mathrm{M}}|}(x)\,dx \\ &\overset{(a)}{\approx} \int_0^\infty \left(1-e^{-tP_{o,\mathrm{C}}(N-S+1)\beta x^{-\alpha_{\mathrm{M}}}}\right)\mathbb{E}_{|X_{o,\mathrm{M}}|=x}\left\{e^{-tI_{\mathrm{M}}}\right\} \\ &\qquad \times f_{|X_{o,\mathrm{M}}|}(x)\,dx,\end{aligned} \tag{6.18}$$

where step (a) is obtained due to the fact that $h_{o,\mathrm{M}} \approx N-S+1$ for large N, $f_{|X_{o,\mathrm{M}}|}(x)$ is the PDF of the nearest distance between the typical CUE and its serving MBS, as seen in (6.10), and $\mathbb{E}_{|X_{o,\mathrm{M}}|=x}\left\{e^{-tI_{\mathrm{M}}}\right\}$ in (6.18) can be derived as

$$\begin{aligned}&\mathbb{E}_{|X_{o,\mathrm{M}}|=x}\left\{e^{-tI_{\mathrm{M}}}\right\} \\ &\overset{(b)}{=} \exp\left\{-S\lambda_{\mathrm{M}}\int_{\mathcal{R}^2\setminus \mathrm{B}(o)}\left(1-\mathbb{E}\left\{e^{-tP_{i,\mathrm{C}}h_{i,\mathrm{M}}\beta r^{-\alpha_{\mathrm{M}}}}\right\}\right)rdr\right\} \\ &= \exp\left\{-2\pi S\lambda_{\mathrm{M}}\int_x^\infty \left(1-\mathbb{E}\left\{e^{-tP_{i,\mathrm{C}}h_{i,\mathrm{M}}\beta r^{-\alpha_{\mathrm{M}}}}\right\}\right)rdr\right\} \\ &\overset{(c)}{=} \exp\left\{-2\pi S\lambda_{\mathrm{M}}\int_x^\infty \left(1-\underbrace{\mathbb{E}_{P_{i,\mathrm{C}}}\left\{\frac{1}{1+tP_{i,\mathrm{C}}\beta r^{-\alpha_{\mathrm{M}}}}\right\}}_{\Upsilon_1}\right)rdr\right\},\end{aligned} \tag{6.19}$$

where step (b) is the generating functional of the PPP, and step (c) is given by considering $h_{i,\mathrm{M}} \sim \exp(1)$. Based on the power control given in (6.1), Υ_1 is given by

$$\begin{aligned}\Upsilon_1 = &\left(1 + tP_{\max}^{\mathrm{C}} \beta r^{-\alpha_{\mathrm{M}}}\right)^{-1} \int_{r_o}^{\infty} f_{|X_{i,\mathrm{M}}|}(\nu)\, d\nu \\ &+ \int_0^{r_o} \left(1 + tP_o \beta^{1-\eta} \nu^{\eta\alpha_{\mathrm{M}}} r^{-\alpha_{\mathrm{M}}}\right)^{-1} f_{|X_{i,\mathrm{M}}|}(\nu)\, d\nu, \end{aligned} \tag{6.20}$$

where $r_o = \left(\frac{P_{\max}^{\mathrm{C}}}{P_o}\right)^{1/(\alpha_{\mathrm{M}}\eta)} \beta^{1/\alpha_{\mathrm{M}}}$ represents the distance such that the path loss compensation reaches the maximum value under power constraint, and $f_{|X_{i,\mathrm{M}}|}(\nu)$ is the PDF of the nearest distance between the interfering CUE i and its serving MBS. Substituting (6.20) and (6.19) into (6.18), after some manipulations, (6.14) is obtained. Then,

$$\begin{aligned}\Xi_2(t) &= \mathbb{E}\left\{e^{-t\sum_{j\in\Phi_{\mathrm{D}}} P_{j,\mathrm{D}} h_{j,\mathrm{M}} L(|X_{j,\mathrm{M}}|)}\right\} \\ &= \exp\left\{-2\pi\lambda_{\mathrm{D}} \int_0^{\infty} \left(1 - \mathbb{E}\left\{e^{-tP_{j,\mathrm{D}} h_{j,\mathrm{M}} L(|X_{j,\mathrm{M}}|)}\right\}\right) r dr\right\}. \end{aligned} \tag{6.21}$$

After some manipulations, the above can be derived as [HAB+09]

$$\Xi_2(t) = \exp\left(-\pi\lambda_{\mathrm{D}} \beta^{\frac{2}{\alpha_{\mathrm{M}}}} \mathbb{E}\left\{(P_{j,\mathrm{D}})^{\frac{2}{\alpha_{\mathrm{M}}}}\right\} \Gamma(1 + \frac{2}{\alpha_{\mathrm{M}}}) \Gamma(1 - \frac{2}{\alpha_{\mathrm{M}}}) t^{\frac{2}{\alpha_{\mathrm{M}}}}\right), \tag{6.22}$$

where $\Gamma(\cdot)$ is the Gamma function [GR07]. By using **Lemma** 5 , $\mathbb{E}\left\{(P_{j,\mathrm{D}})^{\frac{2}{\alpha_{\mathrm{M}}}}\right\}$ is given by

$$\begin{aligned}\mathbb{E}\left\{(P_{j,\mathrm{D}})^{\frac{2}{\alpha_{\mathrm{M}}}}\right\} &= \int_0^{\infty} x^{\frac{2}{\alpha_{\mathrm{M}}}} f_{P_{\mathrm{D}}}(x)\, dx \\ &= \frac{(P_{\max}^{\mathrm{D}})^{\frac{2}{\alpha_{\mathrm{M}}}}}{\varpi_0}(1 - e^{-\varpi_0} - \varpi_0 e^{-\varpi_0}) + \left(P_{\max}^{\mathrm{D}}\right)^{\frac{2}{\alpha_{\mathrm{M}}}} \bar{\Delta}\left(P_{\max}^{\mathrm{D}}\right), \end{aligned} \tag{6.23}$$

where $f_{P_{\mathrm{D}}}(x)$ is given by (6.7), $\varpi_0 = \pi\lambda_{\mathrm{M}}\left(\frac{\beta P_{\max}^{\mathrm{D}}}{I_{\mathrm{th}}}\right)^{2/\alpha_{\mathrm{M}}}$. Substituting (6.23) into (6.22), (6.15) is obtained. □

Based on **Theorem** 10, the area SE (bits/s/Hz/m^2) achieved by the cellular is cal-

culated as

$$\mathcal{A}_{\mathrm{C}} = \overline{R}_{\mathrm{C}} S \lambda_{\mathrm{M}}. \tag{6.24}$$

It is confirmed in **Theorem 10** that the achievable SE of a typical CUE $\overline{R}_{\mathrm{C}}$ is an increasing function of N, since add more massive MIMO antennas will increase power gains. It is a decreasing function of S, since serving more CUEs in each cell will decrease the power gain and increase the inter-cell interference. In addition, $\overline{R}_{\mathrm{C}}$ is also a decreasing function of λ_{D}, since more D2D transmissions will give rise to severer D2D-to-cellular interference.

Based on **Theorem** 10, the area SE (bps/Hz/m^2) achieved by the cellular is calculated as

$$\mathcal{A}_{\mathrm{C}} = \overline{R}_{\mathrm{C}} S \lambda_{\mathrm{M}}. \tag{6.25}$$

D2D density plays a dominant role in the level of D2D-to-cellular interference, which has a big effect on the cellular SE. Thus, the following important scale property can be achieved.

Scale Property 1. *Given an expected SE $\overline{R}_{\mathrm{C}}^{\mathrm{th}}$ of the CUE, it is achievable when the D2D density satisfies*

$$\lambda_{\mathrm{D}} \leq \left((N - S + 1) \frac{X_1}{2^{\overline{R}_{\mathrm{C}}^{\mathrm{th}}} - 1} - X_2 \right) (X_3)^{-1}, \tag{6.26}$$

$$\bar{P}_C = P_o \beta^{-\eta} (\pi \lambda_{\mathrm{M}})^{-\frac{\eta \alpha_{\mathrm{M}}}{2}} \left(\Gamma \left(1 + \frac{\eta \alpha_{\mathrm{M}}}{2} \right) - \Gamma \left(1 + \frac{\eta \alpha_M}{2}, \pi \lambda_{\mathrm{M}} \sqrt{r_o} \right) \right) + P_{\max}^{C} \exp \left(-\pi \lambda_{\mathrm{M}} r_o^2 \right) \tag{6.29}$$

$$\bar{P}_D = \int_0^{P_{\max}^{\mathrm{D}}} \left(\mathbf{1} \left(x < \frac{D_o^{\alpha_{\mathrm{M}}} I_{\mathrm{th}}}{\beta} \right) \left(1 - \exp \left(-\pi \lambda_{\mathrm{M}} D_o^2 \right) \right) + \exp \left(-\pi \lambda_{\mathrm{M}} (\varpi_1(x))^2 \right) \right) dx \tag{6.30}$$

---

where

$$X_1 = \exp \Bigg\{ \ln \left(\frac{P_{\max}^{\mathrm{C}}}{P_o \beta^{-\eta}} \right) \exp \left(-\pi \lambda_{\mathrm{M}} r_o^2 \right) + \ln \left(P_o \beta^{-\eta+1} \right) - \frac{\alpha_{\mathrm{M}}}{2} \psi(1) + \frac{\alpha_{\mathrm{M}}}{2} \ln (\pi \lambda_{\mathrm{M}}) + \frac{\eta \alpha_{\mathrm{M}}}{2} \Bigg(\ell + \Gamma \left(0, r_o^2 \pi \lambda_{\mathrm{M}} \right) + 2 e^{-r_o^2 \pi \lambda_{\mathrm{M}}} \ln(r_o) + \ln(\pi \lambda_{\mathrm{M}}) \Bigg) \Bigg\} \tag{6.27}$$

with the digmma function $\psi(\cdot)$ and Euler-Mascheroni constant $\ell \approx 0.5772$, and

$$\begin{cases} X_2 = 2\pi \lambda_{\mathrm{M}} \displaystyle\int_0^{\infty} \beta 2\pi S \lambda_{\mathrm{M}} \bar{P}_C \frac{x^{2-\alpha_{\mathrm{M}}}}{\alpha_{\mathrm{M}} - 2} x \exp \left(-\pi \lambda_{\mathrm{M}} x^2 \right) dx + \sigma^2, \\ X_3 = 2\pi\beta \left(\dfrac{D_o^{2-\alpha_{\mathrm{M}}}}{2} + \dfrac{D_o^{2-\alpha_{\mathrm{M}}}}{\alpha_{\mathrm{M}} - 2} \right) \bar{P}_D, \end{cases} \tag{6.28}$$

where $\bar{P}_C$ and $\bar{P}_D$ are given by (6.29) *and* (6.30)*, and represent the average transmit powers of CUE and D2D transmitter, respectively, $\mathbf{1}(A)$ is the indicator function that returns one if the condition A is satisfied, $\varpi_1(x) = \max \left\{ D_o, \left(\frac{\beta x}{I_{\mathrm{th}}} \right)^{1/\alpha_{\mathrm{M}}} \right\}$, and D_o is the reference distance, which is utilized to avoid singularity caused by proximity [HL14][4].*

[4]Note that the reference distance can also represent the minimum distance between a D2D transmitter and the typical serving MBS in the practical scenario [HK12].

Proof. Based on (6.16), the SE for a CUE can be tightly lower bounded as [WNE+15]

$$\overline{R}_{\mathrm{C}}^{\mathrm{L}} = \log_2\left(1 + X_1 e^{Y_2}\right), \tag{6.31}$$

where $X_1 = e^{Y_1}$, and

$$\begin{cases} Y_1 = \mathrm{E}\left\{\ln\left(P_{o,\mathrm{C}} h_{o,\mathrm{M}} \beta |X_{o,\mathrm{M}}|^{-\alpha_{\mathrm{M}}}\right)\right\} \\ Y_2 = \mathrm{E}\left\{\ln\left(\frac{1}{I_{\mathrm{M}}+I_{\mathrm{D}}+\sigma^2}\right)\right\} \end{cases} \tag{6.32}$$

Firstly, Y_1 is calculated as

$$Y_1 = \mathrm{E}\left\{\ln\left(P_{o,\mathrm{C}}\right)\right\} - \alpha_{\mathrm{M}}\mathrm{E}\left\{\ln\left(|X_{o,\mathrm{M}}|\right)\right\} + \mathrm{E}\left\{\ln\left(h_{o,\mathrm{M}}\right)\right\} + \ln\left(\beta\right). \tag{6.33}$$

Based on the uplink power control given in (6.1), $\mathrm{E}\left\{\ln\left(P_{o,\mathrm{C}}\right)\right\}$ can be obtained as

$$\begin{aligned} \mathrm{E}\left\{\ln\left(P_{o,\mathrm{C}}\right)\right\} &= \int_0^{\infty} \mathrm{E}_{|X_{o,\mathrm{M}}|=x}\left\{\ln\left(P_{o,\mathrm{C}}\right)\right\} f_{|X_{o,\mathrm{M}}|}\left(x\right) dx \\ &= \int_0^{r_o} \left(\ln\left(P_o \beta^{-\eta}\right) + \eta\alpha_{\mathrm{M}} \ln\left(x\right)\right) f_{|X_{o,\mathrm{M}}|}\left(x\right) dx + \int_{r_o}^{\infty} \ln\left(P_{\max}^{\mathrm{C}}\right) f_{|X_{o,\mathrm{M}}|}\left(x\right) dx \\ &= \ln\left(P_o \beta^{-\eta}\right)\left(1 - \exp\left(-\pi\lambda_{\mathrm{M}} r_o^2\right)\right) + \ln\left(P_{\max}^{\mathrm{C}}\right)\exp\left(-\pi\lambda_{\mathrm{M}} r_o^2\right) \\ &+ \frac{\eta\alpha_{\mathrm{M}}}{2}\left(\ell + \Gamma\left(0, r_o^2\pi\lambda_{\mathrm{M}}\right) + 2e^{-r_o^2\pi\lambda_{\mathrm{M}}}\ln(r_o) + \ln(\pi\lambda_{\mathrm{M}})\right), \end{aligned} \tag{6.34}$$

where $\ell \approx 0.5772$ is the Euler-Mascheroni constant.

Then, the $\mathrm{E}\left\{\ln\left(|X_{o,\mathrm{M}}|\right)\right\}$ is derived as

$$\begin{aligned} \mathrm{E}\left\{\ln\left(|X_{o,\mathrm{M}}|\right)\right\} &= \int_0^{\infty} \ln\left(x\right) f_{|X_{o,\mathrm{M}}|}\left(x\right) dx \\ &= \int_0^{\infty} \ln\left(x\right) 2\pi\lambda_{\mathrm{M}} x \exp\left(-\pi\lambda_{\mathrm{M}} x^2\right) dx \\ &= \frac{1}{2}\psi\left(1\right) - \frac{1}{2}\ln\left(\pi\lambda_M\right). \end{aligned} \tag{6.35}$$

Considering that $h_{o,\mathrm{M}} \sim \Gamma\left(N - S + 1, 1\right)$, $\mathrm{E}\left\{\ln\left(h_{o,\mathrm{M}}\right)\right\} = \psi\left(N - S + 1\right)$ can be

obtained. Thus, $X_1 = e^{Y_1}$ can be obtained given in (6.27).

By using Jensen's inequality, the lower bound on the Y_2 can be derived as

$$Y_2 > \overline{Y}_2 = \ln\left(\frac{1}{\mathrm{E}\left\{I_{\mathrm{M}}\right\} + \mathrm{E}\left\{I_{\mathrm{D}}\right\} + \sigma^2}\right). \tag{6.36}$$

Firstly,

$$\mathrm{E}\left\{I_{\mathrm{M}}\right\} = \int_0^{\infty} \mathrm{E}_{|X_{o,\mathrm{M}}|=x}\left\{I_{\mathrm{M}}\right\} f_{|X_{o,\mathrm{M}}|}(x)\, dx, \tag{6.37}$$

where $\mathrm{E}_{|X_{o,\mathrm{M}}|=x}\left\{I_{\mathrm{M}}\right\}$ is given by

$$\begin{aligned}\mathrm{E}_{|X_{o,\mathrm{M}}|=x}\left\{I_{\mathrm{M}}\right\} &= \mathrm{E}\left\{\sum\nolimits_{i\in\Phi_{u,\mathrm{M}}\setminus B(o)} P_{i,\mathrm{C}} h_{i,\mathrm{M}} \beta r^{-\alpha_{\mathrm{M}}}\right\} \\ &\overset{(a)}{=} \beta 2\pi S \lambda_{\mathrm{M}} \mathbb{E}\left\{P_{i,\mathrm{C}}\right\} \frac{x^{2-\alpha_{\mathrm{M}}}}{\alpha_{\mathrm{M}} - 2},\end{aligned} \tag{6.38}$$

in which (a) results from Campbell's theorem, and the average transmit power of the CUE is calculated as

$$\begin{aligned}&\mathbb{E}\left\{P_{i,\mathrm{C}}\right\} = \int_0^{\infty} \mathrm{E}_{|X_{i,\mathrm{M}}|=x}\left\{P_{i,C}\right\} f_{|X_{i,\mathrm{M}}|}(x)\, dx \\ &= \int_0^{r_o} \left(P_o \beta^{-\eta} x^{\eta\alpha_{\mathrm{M}}}\right) f_{|X_{i,\mathrm{M}}|}(x)\, dx + \int_{r_o}^{\infty} P_{\max}^{C} f_{|X_{i,\mathrm{M}}|}(x)\, dx \\ &= P_o \beta^{-\eta} (\pi\lambda_{\mathrm{M}})^{-\frac{\eta\alpha_{\mathrm{M}}}{2}} \left(\Gamma\left(1 + \frac{\eta\alpha_{\mathrm{M}}}{2}\right) - \Gamma\left(1 + \frac{\eta\alpha_M}{2}, \pi\lambda_{\mathrm{M}}\sqrt{r_o}\right)\right) + P_{\max}^{C} \exp\left(-\pi\lambda_{\mathrm{M}} r_o^2\right).\end{aligned} \tag{6.39}$$

Likewise, $\mathbb{E}\left\{I_{\mathrm{D}}\right\}$ is derived as

$$\begin{aligned}\mathbb{E}\left\{I_{\mathrm{D}}\right\} &= 2\pi\lambda_{\mathrm{D}} \beta \mathbb{E}\left\{P_{j,\mathrm{D}}\right\} \int_0^{\infty} \left(\max\left(D_o, r\right)\right)^{-\alpha_{\mathrm{M}}} r dr \\ &= 2\pi\lambda_{\mathrm{D}} \beta \mathbb{E}\left\{P_{j,\mathrm{D}}\right\} \left(\frac{D_o^{2-\alpha_{\mathrm{M}}}}{2} + \frac{D_o^{2-\alpha_{\mathrm{M}}}}{\alpha_{\mathrm{M}} - 2}\right)\end{aligned} \tag{6.40}$$

where D_o is the minimum distance between a D2D transmitter and the typical serving

MBS in practice, and $\mathrm{E}\{P_{j,\mathrm{D}}\}$ is given by

$$\mathrm{E}\{P_{j,\mathrm{D}}\} = \int_0^{\infty} \bar{F}_{P_{j,\mathrm{D}}}(x)\, dx, \tag{6.41}$$

where $\bar{F}_{P_{j,\mathrm{D}}}(x)$ is the complementary cumulative distribution function. Based on (6.7),

$$\begin{aligned}\bar{F}_{P_{j,\mathrm{D}}}(x) &= \Pr(P_{j,\mathrm{D}} > x) = \Pr\left(\min\left\{\frac{I_{\mathrm{th}}}{L(|X_{\mathrm{D,M}}|)}, P_{\max}^{\mathrm{D}}\right\} > x\right) \\ &= \begin{cases} 0, & x \geq P_{\max}^{\mathrm{D}} \\ \widetilde{\Delta}(x), & x < P_{\max}^{\mathrm{D}} \end{cases},\end{aligned} \tag{6.42}$$

where $\widetilde{\Delta}(x)$ is

$$\begin{aligned}\widetilde{\Delta}(x) &= \Pr\left(\frac{I_{\mathrm{th}}}{L(|X_{\mathrm{D,M}}|)} > x\right) \\ &= \mathbf{1}\left(x < \frac{D_o^{\alpha_{\mathrm{M}}} I_{\mathrm{th}}}{\beta}\right) \int_0^{D_o} f_{|X_{\mathrm{D,M}}|}(r)\, dr + \int_{\varpi_1}^{\infty} f_{|X_{\mathrm{D,M}}|}(r)\, dr \\ &= \mathbf{1}\left(x < \frac{D_o^{\alpha_{\mathrm{M}}} I_{\mathrm{th}}}{\beta}\right)\left(1 - \exp\left(-\pi\lambda_{\mathrm{M}} D_o^2\right)\right) + \exp\left(-\pi\lambda_{\mathrm{M}}(\varpi_1(x))^2\right)\end{aligned} \tag{6.43}$$

where $\varpi_1(x) = \max\left\{D_o, \left(\frac{\beta x}{I_{\mathrm{th}}}\right)^{1/\alpha_{\mathrm{M}}}\right\}$. By substituting (6.42) into (6.41), $\mathrm{E}\{P_{j,\mathrm{D}}\}$ is derived as

$$\mathrm{E}\{P_{j,\mathrm{D}}\} = \int_0^{P_{\max}^{\mathrm{D}}} \widetilde{\Delta}(x)\, dx. \tag{6.44}$$

Substituting (6.37) and (6.40) into the right-hand-side of (6.36), $\overline{Y}_2$ is obtained. According to (6.31), the expected $\overline{R}_{\mathrm{C}}^{\mathrm{th}}$ can be satisfied when $\overline{R}_{\mathrm{C}}^{\mathrm{th}} \leq \log_2\left(1 + X_1 e^{\overline{Y}_2}\right)$. Therefore, $\bar{Y}_2 \geq \ln\left(\frac{2^{\bar{R}_{\mathrm{C}}^{\mathrm{th}}} - 1}{X_1}\right)$ can be achieved, after some manipulations, the desired result is obtained given in (6.26). □

From **Scale Property 1**, it can be found that given an targeted SE, the number of D2D links needs to be lower than a critical value, to limit the D2D-to-cellular interference. Adding more massive MIMO antennas can allow cellular networks to accommodate more

$$\Xi_3(t) = \int_0^{\varpi_0} \frac{1}{1 + tI_{\rm th}(\frac{x}{\pi\lambda_{\rm M}})^{\frac{\alpha_{\rm M}}{2}} d_o^{-\alpha_{\rm D}}} e^{-x} dx + \frac{\bar{\Delta}\left(P_{\max}^{\rm D}\right)}{1 + tP_{\max}^{\rm D}\beta d_o^{-\alpha_{\rm D}}} \tag{6.46}$$

$$\Xi_4(t) = \exp\Big(- \pi\beta^{\frac{2}{\alpha_{\rm D}}}\Gamma(1 + \frac{2}{\alpha_{\rm D}})\Gamma(1 - \frac{2}{\alpha_{\rm D}})t^{\frac{2}{\alpha_{\rm D}}}(S\lambda_{\rm M}\Omega_1 + \lambda_{\rm D}\Omega_2)\Big), \tag{6.47}$$

where

$$\Omega_1 = (P_o\beta^{-\eta})^{\frac{2}{\alpha_{\rm D}}}(\pi\lambda_{\rm M})^{-\frac{\eta\alpha_{\rm M}}{\alpha_{\rm D}}}\Big(\Gamma(1 + \frac{\eta\alpha_{\rm M}}{\alpha_{\rm D}}) - \Gamma(1 + \frac{\eta\alpha_{\rm M}}{\alpha_{\rm D}}, \pi\lambda_{\rm M} r_o^2)\Big) + \left(P_{\max}^{\rm C}\right)^{\frac{2}{\alpha_{\rm D}}} e^{-\pi\lambda_{\rm M} r_o^2} \tag{6.48}$$

$$\Omega_2 = \left(\pi\lambda_{\rm M}(\frac{\beta}{I_{\rm th}})^{\frac{2}{\alpha_{\rm M}}}\right)^{-\frac{\alpha_{\rm M}}{\alpha_{\rm D}}}\Big(\Gamma(1 + \frac{\alpha_{\rm M}}{\alpha_{\rm D}}) - \Gamma(1 + \frac{\alpha_{\rm M}}{\alpha_{\rm D}}, \varpi_0)\Big) + \left(P_{\max}^{\rm D}\right)^{\frac{2}{\alpha_{\rm D}}} \bar{\Delta}\left(P_{\max}^{\rm D}\right) \tag{6.49}$$

---

underlaid D2D links.

For a typical D2D link, its SE can be obtained as follows.

Theorem 11. *The SE for a typical D2D link with a given distance d_o is given by*

$$\overline{R}_{\rm D} = 1/\ln(2)\int_0^{\infty} \frac{1}{t}\left(1 - \Xi_3(t)\right)\Xi_4(t)\, e^{-t\sigma^2} dt, \tag{6.45}$$

where $\Xi_3(t)$ and $\Xi_4(t)$ are given by (6.46) *and* (6.47).

Proof. Based on (6.5), $\overline{R}_{\rm D}$ is given by

$$\begin{aligned}
\overline{R}_{\rm D} &= \mathbb{E}\left\{\log_2\left(1 + {\rm SINR}_{\rm D}\right)\right\} \\
&\overset{(a)}{=} 1/\ln(2)\int_0^{\infty} \frac{1}{t}\left(1 - \underbrace{\mathbb{E}\left\{e^{-tZ_2}\right\}}_{\Xi_3(t)}\right)\underbrace{\mathbb{E}\left\{e^{-t(J_{\rm M}+J_{\rm D})}\right\}}_{\Xi_4(t)} e^{-t\sigma^2} dt,
\end{aligned} \tag{6.50}$$

where $Z_2 = P_{o,{\rm D}} g_{o,{\rm D}} L\left(d_o\right)$, and step (a) is obtained by following the similar approach in

(6.17). Using **Lemma** 5, the $\Xi_3(t)$ is first derived as

$$\Xi_3(t) = \mathbb{E}_{P_{o,\mathrm{D}}}\left\{\mathbb{E}_{g_{o,\mathrm{D}}}\left\{e^{-tZ_2}\right\}\right\} = \mathbb{E}_{P_{o,\mathrm{D}}}\left\{\frac{1}{1+tP_{o,\mathrm{D}}\beta d_o^{-\alpha_\mathrm{D}}}\right\}$$
$$= \int_0^\infty \left(1+tx\beta d_o^{-\alpha_\mathrm{D}}\right)^{-1} f_{P_\mathrm{D}}(x)\,dx. \tag{6.51}$$

Substituting (6.7) into (6.51), (6.46) is obtained.

Considering that the cellular interference J_M and D2D interference J_D are independent, $\Xi_4(t)$ is calculated as

$$\Xi_4(t) = \mathbb{E}\left\{e^{-tJ_\mathrm{M}}\right\}\mathbb{E}\left\{e^{-tJ_\mathrm{D}}\right\}. \tag{6.52}$$

Similar to (6.22), $\mathbb{E}\left\{e^{-tJ_\mathrm{M}}\right\}$ is derived as

$$\mathbb{E}\left\{e^{-tJ_\mathrm{M}}\right\} = \exp\left(-\pi S\lambda_\mathrm{M}\beta^{\frac{2}{\alpha_\mathrm{D}}}\Omega_1\Gamma(1+\frac{2}{\alpha_\mathrm{D}})\Gamma(1-\frac{2}{\alpha_\mathrm{D}})t^{\frac{2}{\alpha_\mathrm{D}}}\right), \tag{6.53}$$

where $\Omega_1 = \mathbb{E}\left\{(P_{i,\mathrm{C}})^{\frac{2}{\alpha_\mathrm{D}}}\right\}$ is given by

$$\Omega_1 = \int_0^{r_o}\left(P_o\beta^{-\eta}\nu^{\eta\alpha_\mathrm{M}}\right)^{\frac{2}{\alpha_\mathrm{D}}} f_{|X_{i,\mathrm{M}}|}(\nu)\,d\nu$$
$$+\left(P_{\max}^{\mathrm{C}}\right)^{\frac{2}{\alpha_\mathrm{D}}}\int_{r_o}^\infty f_{|X_{i,\mathrm{M}}|}(\nu)\,d\nu. \tag{6.54}$$

After some manipulations, Ω_1 is derived as (6.48). Likewise, $\mathbb{E}\left\{e^{-tJ_\mathrm{D}}\right\}$ is derived as

$$\mathbb{E}\left\{e^{-tJ_\mathrm{D}}\right\} = \exp\left(-\pi\lambda_\mathrm{D}\beta^{\frac{2}{\alpha_\mathrm{D}}}\Omega_2\Gamma(1+\frac{2}{\alpha_\mathrm{D}})\Gamma(1-\frac{2}{\alpha_\mathrm{D}})t^{\frac{2}{\alpha_\mathrm{D}}}\right), \tag{6.55}$$

where $\Omega_2 = \mathbb{E}\left\{(P_{j,\mathrm{D}})^{\frac{2}{\alpha_\mathrm{D}}}\right\}$, using **Lemma** 5, Ω_2 is given by

$$\Omega_2 = \int_0^{P_{\max}^{\mathrm{D}}} x^{\frac{2}{\alpha_\mathrm{D}}} f_{P_\mathrm{D}}(x)\,dx + \left(P_{\max}^{\mathrm{D}}\right)^{\frac{2}{\alpha_\mathrm{D}}}\bar{\Delta}\left(P_{\max}^{\mathrm{D}}\right). \tag{6.56}$$

After some manipulations, Ω_2 is derived as (6.49). Then, (6.47) is attained by substituting (6.53) and (6.55) into (6.52). □

It is confirmed in **Theorem 11** that the SE for a typical D2D link is independent of massive MIMO antennas, and is a decreasing function of S due to the fact that more uplink transmissions will result in severer cellular-to-D2D interference. Moreover, it is also a decreasing function of λ_{D}, since more inter-D2D interference deteriorates the typical D2D transmission.

Based on **Theorem** 11, the area SE achieved by the D2D tier is

$$\mathcal{A}_{\mathrm{D}} = \overline{R}_{\mathrm{D}}\lambda_{\mathrm{D}}. \tag{6.57}$$

Since D2D density also has a substantial effect on the level of inter-D2D interference, which greatly affects the SE of D2D. Thus, the following important scale property is attained.

Scale Property 2. *The expected SE $\overline{R}_{\mathrm{D}}^{\mathrm{th}}$ of the D2D transmitter can be achieved when the D2D density satisfies*

$$\lambda_{\mathrm{D}} \leq \left(\frac{X_4}{2^{\overline{R}_{\mathrm{D}}^{\mathrm{th}}}-1} - S\lambda_{\mathrm{M}}X_5\right)(X_6)^{-1}, \tag{6.58}$$

where

$$X_4 = \exp\left\{ \int_0^{P_{\max}^{\mathrm{D}}} \ln(x)\, f_{P_{\mathrm{D}}}(x)\, dx + \ln\left(P_{\max}^{\mathrm{D}}\right) \right.$$
$$\left. \bar{\Delta}\left(P_{\max}^{\mathrm{D}}\right) + \ln\left(\beta {d_o}^{-\alpha_{\mathrm{D}}}\right) + \ell \right\}, \tag{6.59}$$

$$X_5 = 2\pi \left(P_o \beta^{-\eta} (\pi\lambda_{\mathrm{M}})^{-\frac{\eta\alpha_{\mathrm{M}}}{2}} \left(\Gamma\left(1 + \frac{\eta\alpha_{\mathrm{M}}}{2}\right) \right.\right.$$
$$\left. - \Gamma\left(1 + \frac{\eta\alpha_M}{2}, \pi\lambda_{\mathrm{M}}\sqrt{r_o}\right) \right) + P_{\max}^{\mathrm{C}}$$
$$\left. \exp\left(-\pi\lambda_{\mathrm{M}} r_o^2\right) \right) \beta \left(\frac{D_1^{2-\alpha_{\mathrm{D}}}}{2} + \frac{D_1^{2-\alpha_{\mathrm{M}}}}{\alpha_{\mathrm{D}} - 2} \right), \tag{6.60}$$

$$X_6 = 2\pi\beta \left(\frac{D_2^{2-\alpha_{\mathrm{D}}}}{2} + \frac{D_2^{2-\alpha_{\mathrm{D}}}}{\alpha_{\mathrm{D}} - 2} \right) \bar{P}_{\mathrm{D}}, \tag{6.61}$$

where D_1 and D_2 are the reference distances, $\bar{P}_{\mathrm{D}}$ is given by (6.30)*.*

Proof. Similar to (6.50), the SE for a D2D link can be tightly lower bounded as

$$\bar{\mathrm{R}}_{\mathrm{D}}^{\mathrm{L}} = \log_2\left(1 + X_4 e^{Y_4}\right) \tag{6.62}$$

where $X_4 = e^{Y_3}$, and

$$\begin{cases} Y_3 = \mathrm{E}\left\{\ln\left(P_{o,\mathrm{D}} g_{o,\mathrm{D}} \beta {d_o}^{-\alpha_{\mathrm{D}}}\right)\right\} \\ Y_4 = \mathrm{E}\left\{\ln\left(\frac{1}{J_{\mathrm{M}} + J_{\mathrm{D}} + \sigma^2}\right)\right\} \end{cases}$$

Firstly, Y_3 is calculated as

$$Y_3 = \mathrm{E}\left\{\ln\left(P_{o,\mathrm{D}}\right)\right\} + \mathrm{E}\left\{\ln\left(g_{o,\mathrm{D}}\right)\right\} - \alpha_{\mathrm{D}} \ln\left(d_o\right) + \ln\left(\beta\right) \tag{6.63}$$

Based on the D2D power control given in (6.2) and **Lemma** 5, $\mathrm{E}\left\{\ln\left(P_{o,\mathrm{D}}\right)\right\}$ is

obtained as

$$\begin{aligned}\mathrm{E}\left\{\ln\left(P_{o,\mathrm{D}}\right)\right\} &= \int_0^{\infty} \ln\left(x\right) f_{P_{\mathrm{D}}}\left(x\right) dx \\ &= \int_0^{P_{\max}^{\mathrm{D}}} \ln\left(x\right) f_{P_{\mathrm{D}}}\left(x\right) dx + \ln\left(P_{\max}^{\mathrm{D}}\right)\bar{\Delta}\left(P_{\max}^{\mathrm{D}}\right)\end{aligned} \tag{6.64}$$

Considering that $g_{o,\mathrm{D}} \backsim \exp(1)$, $\mathrm{E}\left\{\ln\left(g_{o,\mathrm{D}}\right)\right\} = \int_0^{\infty} \ln(x) e^{-x} dx = \ell = 0.5772$ is got. Thus, $X_4 = e^{Y_3}$ can be obtained given in (6.59).

By using Jensen's inequality, the lower bound on the Y_4 can be derived as

$$Y_4 > \bar{Y}_4 = \ln\left(\frac{1}{\mathrm{E}\left\{J_{\mathrm{M}}\right\} + \mathrm{E}\left\{J_{\mathrm{D}}\right\} + \sigma^2}\right). \tag{6.65}$$

$\mathrm{E}\left\{J_{\mathrm{M}}\right\}$ is first derived as

$$\begin{aligned}\mathrm{E}\left\{J_{\mathrm{M}}\right\} &= \mathrm{E}\left\{\sum\nolimits_{i\in\Phi_{u,\mathrm{M}}} P_{i,C} g_{i,\mathrm{D}} L\left(\left|X_{i,\mathrm{D}}\right|\right)\right\} \\ &= 2\pi S \lambda_M \mathrm{E}\left\{P_{i,\mathrm{C}}\right\} \beta \int_0^{\infty} \left(\max\left(D_1, r\right)\right)^{1-\alpha_{\mathrm{D}}} dr \\ &= 2\pi S \lambda_M \mathrm{E}\left\{P_{i,\mathrm{C}}\right\} \beta \left(\frac{D_1^{2-\alpha_{\mathrm{D}}}}{2} + \frac{D_1^{2-\alpha_{\mathrm{M}}}}{\alpha_{\mathrm{D}} - 2}\right),\end{aligned} \tag{6.66}$$

where $\mathrm{E}\left\{P_{i,\mathrm{C}}\right\}$ is given by (6.39), and D_1 is the reference distance to avoid singularity.

Similar to (6.40), $\mathrm{E}\left\{J_{\mathrm{D}}\right\}$ is calculated as

$$\mathrm{E}\left\{J_{\mathrm{D}}\right\} = 2\pi\lambda_{\mathrm{D}}\beta\mathbb{E}\left\{P_{j,\mathrm{D}}\right\}\left(\frac{D_2^{2-\alpha_{\mathrm{D}}}}{2} + \frac{D_2^{2-\alpha_{\mathrm{D}}}}{\alpha_{\mathrm{D}} - 2}\right), \tag{6.67}$$

where $\mathbb{E}\left\{P_{j,\mathrm{D}}\right\}$ is given by (6.44), and D_2 is the reference distance.

Substituting (6.66) and (6.67) into the right-hand-side of (6.65), $\overline{Y}_4$ is obtained. Based on (6.62) and (6.65), $\overline{R}_{\mathrm{D}}^{\mathrm{th}} \leq \log_2\left(1 + X_4 e^{\overline{Y}_4}\right) \Rightarrow \bar{Y}_4 \geq \ln\left(\frac{2^{\bar{R}_{\mathrm{D}}^{\mathrm{th}}} - 1}{X_4}\right)$, after some manipulations, (6.58) can be obtained and complete the proof. □

From **Scale Property 2**, it can be found that given an targeted SE, the number of

D2D links needs to be lower than a critical value, to limit the inter-D2D interference. The number of D2D links that achieves the targeted SE decreases when each MBS serves more users at the same time and frequency band, due to severer cellular-to-D2D interference.

6.4.3 Energy Efficiency

In this subsection, the EE of cellular and D2D transmissions is evaluated, which is of paramount importance in 5G systems due to the fact that one of key performance indicators (KPIs) in 5G is ten times lower energy consumption per service than the today's networks [5GP]. The EE is defined as the ratio of the SE to the average power consumption.

The average power consumption of a CUE is calculated

$$\overline{P}_C^{total} = P_f + \frac{\overline{P}_{\mathrm{C}}}{\varepsilon}, \tag{6.68}$$

where P_f is the fixed circuit power consumption, $\overline{\mathrm{P}}_{\mathrm{C}}$ is the average transmit power given by (6.29), and ε is the power amplifier efficiency. Thus, the EE for a typical CUE is derived as

$$\overline{\mathrm{EE}}_{\mathrm{C}} = \frac{\overline{R}_{\mathrm{C}}}{\overline{P}_C^{total}}, \tag{6.69}$$

where $\overline{R}_{\mathrm{C}}$ is the average SE given by (6.13). For uplink transmission, the average power consumption for a CUE is only dependent on the maximum transmit power level and the path loss compensation, as shown in (6.68). Therefore, $\overline{\mathrm{EE}}_{\mathrm{C}}$ is an increasing function of N and a decreasing function of S, since $\overline{R}_{\mathrm{C}}$ increases with N and decreases with increasing S.

Likewise, the average power consumption of a D2D transmitter is calculated as

$$\overline{P}_{\mathrm{D}}^{total} = P_f + \frac{\overline{\mathrm{P}}_{\mathrm{D}}}{\varepsilon}, \tag{6.70}$$

where $\overline{\mathrm{P}}_{\mathrm{D}}$ is the average transmit power. Based on (6.23), $\overline{\mathrm{P}}_{\mathrm{D}}$ is given by

$$\overline{\mathrm{P}}_{\mathrm{D}} = \frac{(P_{\max}^{\mathrm{D}})^2}{\varpi_2}(1 - e^{-\varpi_2} - \varpi_2 e^{-\varpi_2}) + \left(P_{\max}^{\mathrm{D}}\right)^2 \bar{\Delta}\left(P_{\max}^{\mathrm{D}}\right) \tag{6.71}$$

with $\varpi_2 = \pi\lambda_{\mathrm{M}}\left(\frac{\beta P_{\max}^{\mathrm{D}}}{I_{\mathrm{th}}}\right)^2$. Thus, the EE for a typical D2D pair is derived as

$$\overline{\mathrm{EE}}_{\mathrm{D}} = \frac{\overline{R}_{\mathrm{D}}}{\overline{P}_D^{total}} \tag{6.72}$$

where $\overline{R}_{\mathrm{D}}$ is the average SE given by (6.45). Similarly, the EE for a typical D2D pair is independent of massive MIMO antennas, and is a decreasing function of S, since more cellular-to-D2D interference decreases the SE.

6.5 Numerical Results

In this section, numerical results are presented to evaluate the area average SE and average EE of the cellular and D2D in the D2D underlaid massive MIMO cellular network. Such a network is assumed to operate at a carrier frequency of 1 GHz. The results show the effect of massive MIMO in terms of user number S, the effect of D2D in terms of its density λ_D and the effect of power control in terms of the compensation factor η and interference threshold I_{th}. The basic parameters are summarized in Table **6-A**, and it is assumed that the density of MBSs is $\lambda_{\mathrm{M}} = \left(500^2 \times \pi\right)^{-1} \mathrm{m}^{-2}$ in a circular region with radius 1×10^4 m.

In the figures, the analytical area SE curves for the cellular and D2D are obtained from (6.25) and (6.57), respectively, and the analytical EE curves for a CUE or D2D transmitter are obtained from (6.69) and (6.72), respectively. Monte Carlo simulated values of the uplink spectrum efficiency marked by 'o' are numerically obtained to validate the analysis.

Parameter	Symbol	Value
Pathloss exponent to MBSs	α_{M}	3.5
Pathloss exponent to D2Ds	α_{D}	4
The maximum transmit power of MUEs	$P^{C}_{\max}$	23 dBm
The maximum transmit power of DUEs	$P^{D}_{\max}$	15 dBm
Bandwidth	BW	5 MHz
The noise power	σ^2	$-170 + 10 \times log_{10}(BW)$ dBm
The power density [SSP+13]	P_o	-80 dBm
Users static power consumption	P_{fix}	100 mW
Power amplifier efficiency	ε	0.5
Number of antennas	N	400

Table 6-A: Simulation Parameters.

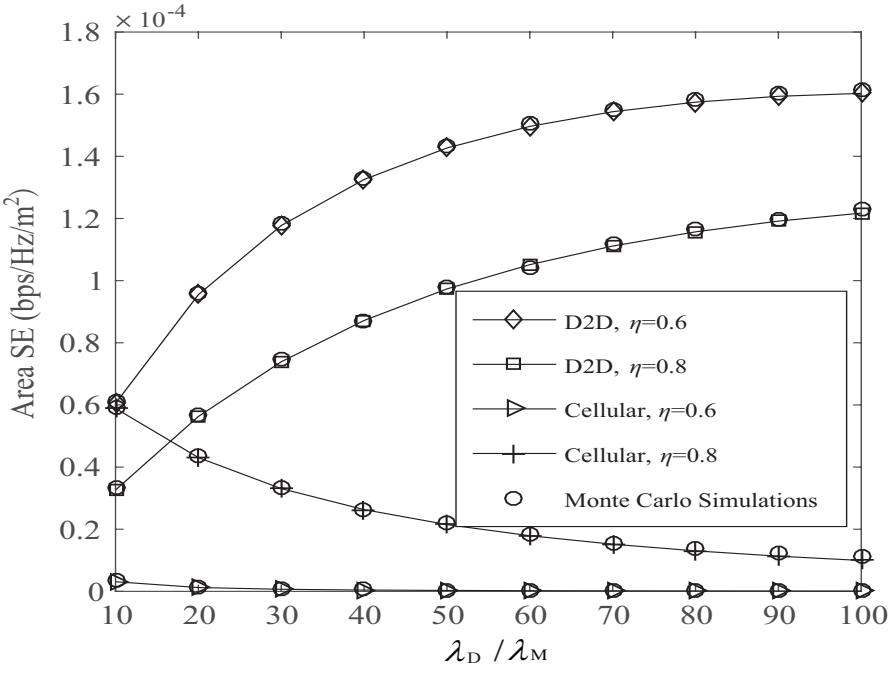

Figure 6.2: Effects of D2D density with the variation of cellular power control on SE: $d_o = 35$ m, $S = 20$ and $I_{\mathrm{th}}/\sigma^2 = 10$ dB.

6.5.1 Power Control Effect

In this subsection, the effects of power control on the area SE and EE are illustrated, to demonstrate the effectiveness of the proposed power control solution.

Figure 6.2 shows the effects of D2D density with the variation of cellular power control. It can be seen that uplink power control applied in the massive MIMO macrocells

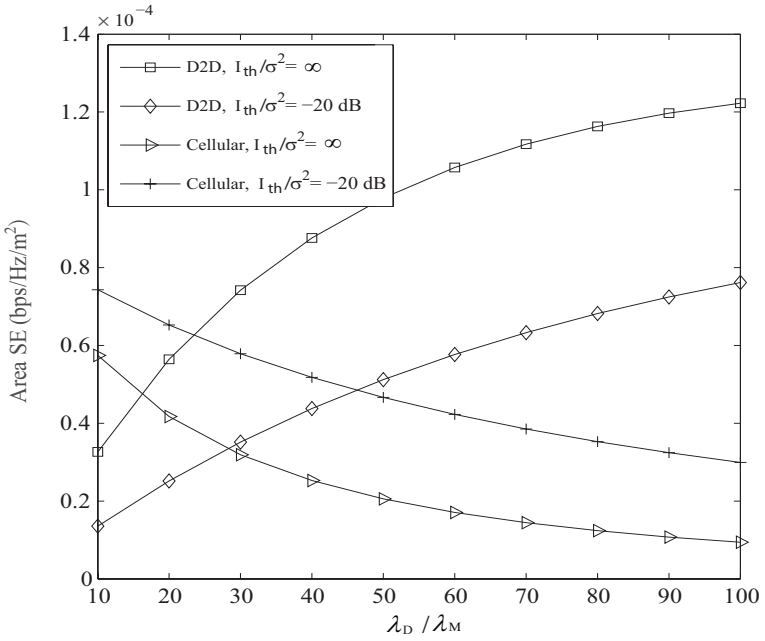

Figure 6.3: Effects of D2D density with the variation of D2D power control on SE: $d_o = 35$ m, $S = 20$ and $\eta = 0.8$.

can significantly affect the area average SE of the D2D and the cellular. Specifically, when the transmit power of the CUE is controlled at a low level, the area average SE of the D2D is improved, because D2D receivers experience less interference from the CUEs. In contrast, the area average SE of the cellular decreases with the CUE transmit power. The performance of the cellular is greatly degraded when the D2Ds are ultra dense, due to the severe interference from the D2D transmitters, which reveals that D2D interference mitigation is required for ensuring the uplink quality of service in the cellular networks.

Figure 6.3 shows the effects of D2D density with the variation of D2D power control on the area SE. We observe that without D2D power control (i.e., $I_{\text{th}}/\sigma^2 = \infty$), the area SE of D2D tier is much higher than the massive MIMO aided cellular when D2D density is large. In particular, the area SE of the cellular is drastically deteriorated by the severe D2D-to-cellular interference. The implementation of the proposed D2D power control policy (e.g., $I_{\text{th}}/\sigma^2 = -20$ dB in this figure.) can efficiently mitigate the D2D-to-cellular interference, and thus improve the cellular performance.

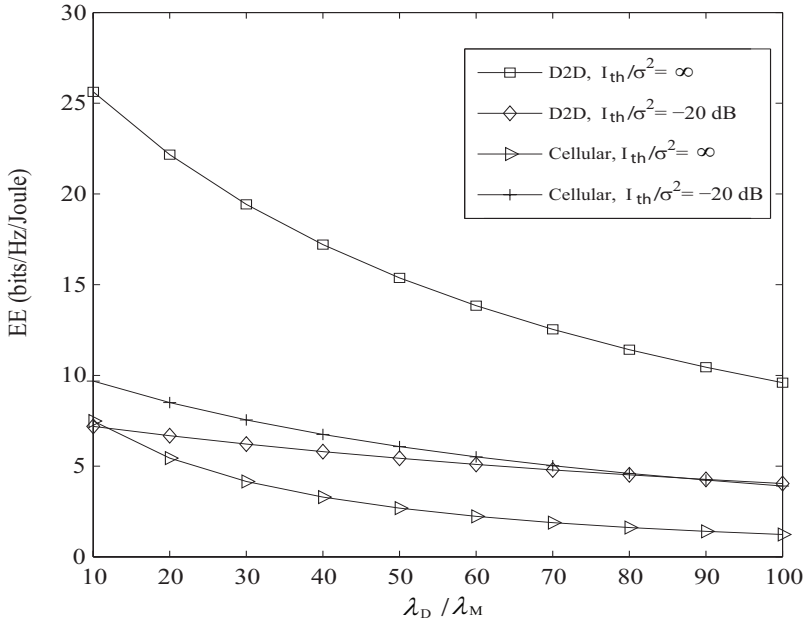

Figure 6.4: Effects of D2D density with the variation of D2D power control on EE: $d_o = 35$ m, $S = 20$ and $\eta = 0.8$.

Figure 6.4 shows the effects of D2D density with the variation of D2D power control on the EE. Without D2D power control, the EE of a D2D link is much higher than that of a cellular uplink, owing to the proximity. The interference increases with the D2D links, which harms both the EE of the cellular user and D2D user. The use of D2D power control enhances the EE of the cellular user, due to its SE improvement. Moreover, by properly coordinating the D2D-to-cellular interference, the uplink EE of a massive MIMO aided cellular is comparable to that of a D2D link.

Figure 6.5 shows the effects of D2D distance with the impact of massive MIMO on the area SE. It is obvious that when the distance between the D2D transmitter and its receiver grows large, the area SE of the D2D decreases, and it has no effect on the cellular performance. As more CUEs are served in each massive MIMO aided macrocell, there is a substantial increase in the area SE of the cellular, due to more multiplexing gains achieved by massive MIMO. However, when more CUEs are served in the uplink, the interference from CUEs is exacerbated, which degrades the D2D performance. Therefore, the cellular-

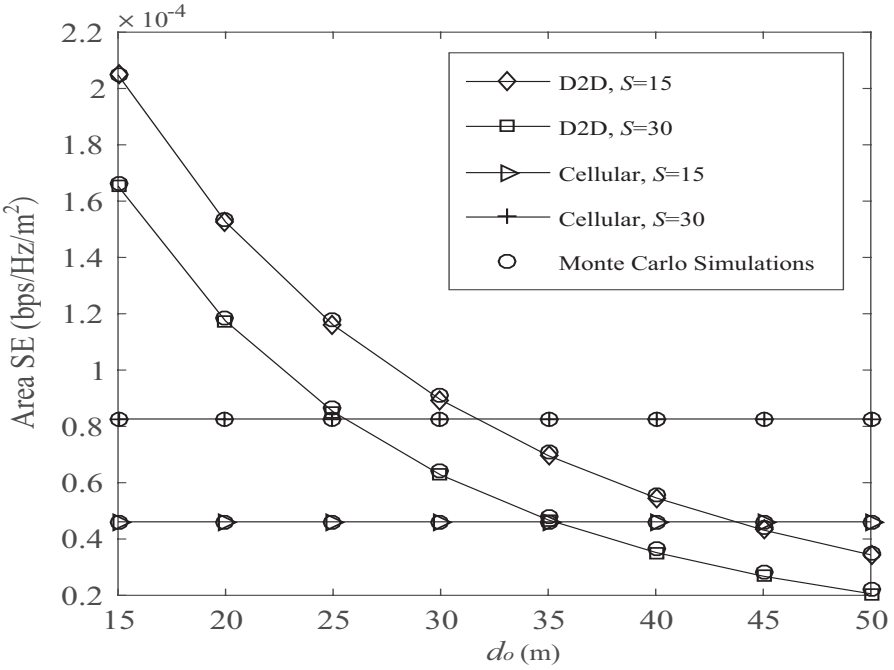

Figure 6.5: Effects of D2D distance with the impact of massive MIMO on SE: $\lambda_{\mathrm{D}} = 30 \times \lambda_{\mathrm{M}}$ m, $\eta = 0.9$ and $I_{\mathrm{th}}/\sigma^2 = 5$ dB.

to-D2D interference also needs to be coordinated. In addition, massive MIMO cellular can achieve better performance than D2D when the D2D distance is large.

6.5.2 Massive MIMO Antennas Effect

In this subsection, we illustrate the effects of massive MIMO antennas on the area SE and EE. In the simulations, we set $d_o = 50$ m, $S = 20$, $\lambda_{\mathrm{D}} = 30 \times \lambda_{\mathrm{M}}$, $\eta = 0.8$ and $I_{\mathrm{th}}/\sigma^2 = 0$ dB.

Fig. 6.6 shows the effects of massive MIMO antennas with the variation of maximum D2D transmit power on the area SE. As confirmed in **Theorem 1**, the area SE increases with N because of obtaining more power gains. As confirmed in **Theorem 2**, increasing massive MIMO antennas has no effect on the D2D SE. When larger maximum D2D transmit power is allowed, the area SE of the D2D is enhanced. However, the area SE of the cellular decreases due to the severer D2D-to-cellular interference.

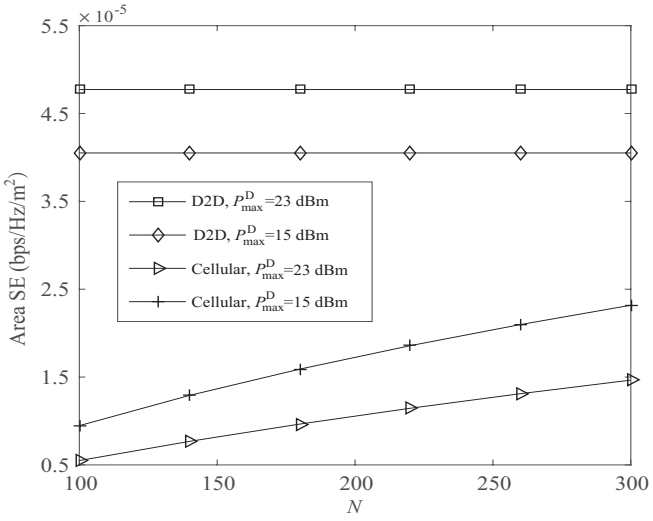

Figure 6.6: Effects of massive MIMO antennas with the variation of maximum D2D transmit power on the area SE.

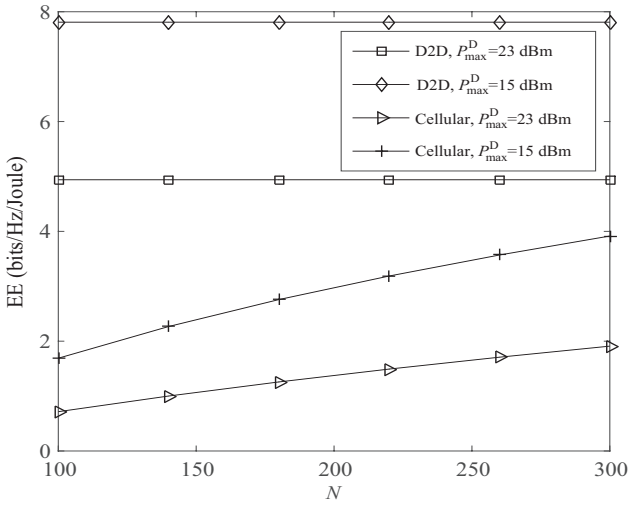

Figure 6.7: Effects of massive MIMO antennas with the variation of maximum D2D transmit power on the EE.

Fig. 6.7 shows the effects of massive MIMO antennas with the variation of maximum D2D transmit power on the EE. As mentioned in Section III-C, the EE of a CUE increases with N because of larger SE. Increasing N has no effect on the EE of a D2D transmitter. Although Fig. 6.6 shows that larger maximum D2D transmit power can improve the SE of the D2D, the EE of the D2D can be reduced because of more D2D power consumption. In addition, the EE of a CUE decreases due to larger D2D-to-cellular interference.

6.5.3 Interplay between Massive MIMO and D2D

In this subsection, the interplay between massive MIMO and D2D is illustrated. Specifically, massive MIMO allows MBS to accommodate more uplink information transmissions, and D2D links can be dense. Therefore, it is crucial to identify their combined effect. In the simulations, we set $d_o = 50$ m, $\eta = 0.9$ and $I_{\text{th}}/\sigma^2 = 0$ dB.

Figure 6.8(a) shows the effects of different S and D2D densities on area SE of the cellular. Serving more CUEs can improve the area SE of the cellular, due to the large multiplexing gains provided by massive MIMO. However, when D2D links grow large (e.g., $\lambda_{\text{D}} = 100 \times \lambda_{\text{M}}$ in this figure.), increasing S will not result in a big improvement of area SE. The reason is that D2D-to-cellular interference becomes severe in the dense D2D scenarios, which reduces the SE of a CUE. Figure 6.8(b) shows the effects of different S and D2D densities on area SE of the D2D. We see that more cellular uplink transmissions will deteriorate the area SE of the D2D, due to the increase of cellular-to-D2D interference. More importantly, there exists the optimal D2D density value for maximizing the area SE of the D2D, beyond which, the area SE of the D2D decreases since a D2D user also suffers severe interference from other D2D transmissions.

In order to compare the performance of massive MIMO and D2D on SE, the SE versus λ_d in a 2-D plot with $S = 20$ and $S = 40$ is displayed. As seen in Figure6.9, when CUE number is relatively small, the D2D tier can achieve a better performance when its density is around 60 times MBS' density; while when CUE number is doubled under the same circumstance, the D2D tier cannot outperform the cellular tier until the density ratio between D2D and MBS rises to 200. This result proves the effectiveness of massive MIMO on enhancing network SE.

Figure 6.10(a) shows the effects of different S and D2D densities on EE of a cellular user. We see that serving more CUEs will decrease the EE, which can be explained by two-fold: 1) The massive MIMO array gain allocated to each CUE decreases; and 2) the interference increases since there are more cellular transmissions. The D2D-to-

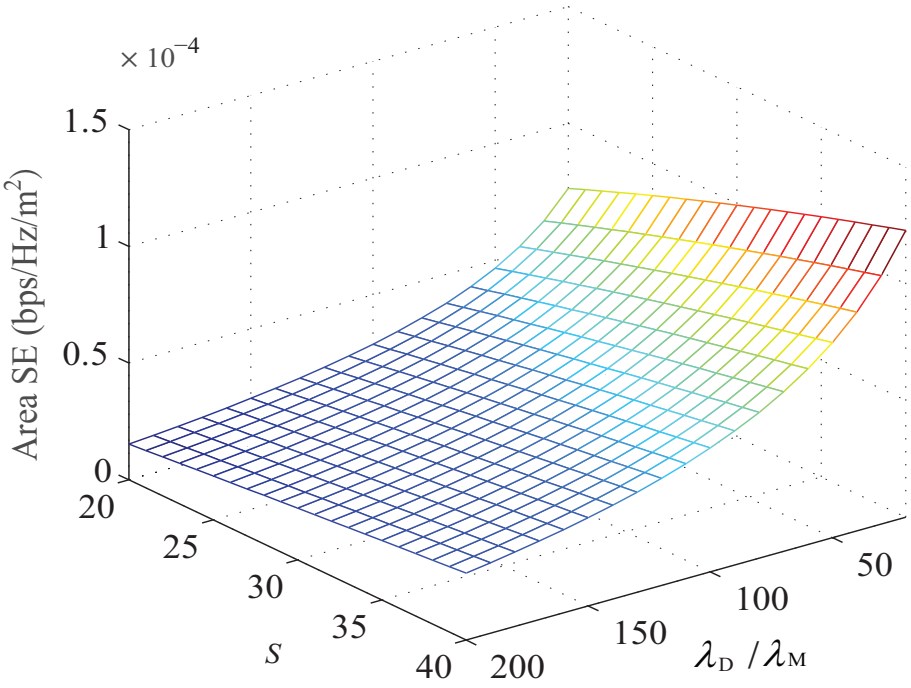

(a) Area SE of the cellular.

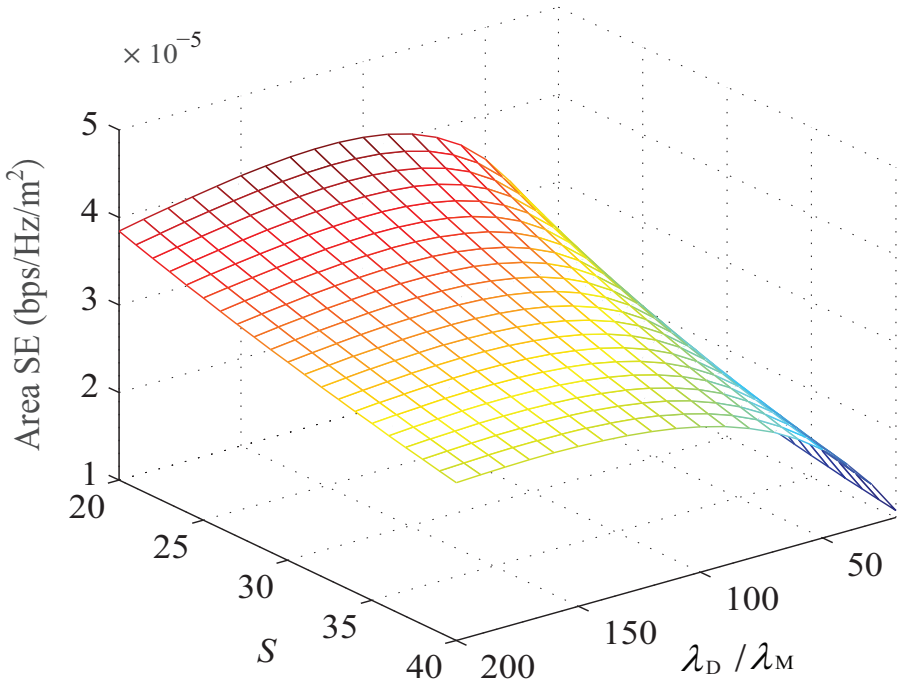

(b) Area SE of the D2D.

Figure 6.8: Effects of different S and D2D densities on area SE.

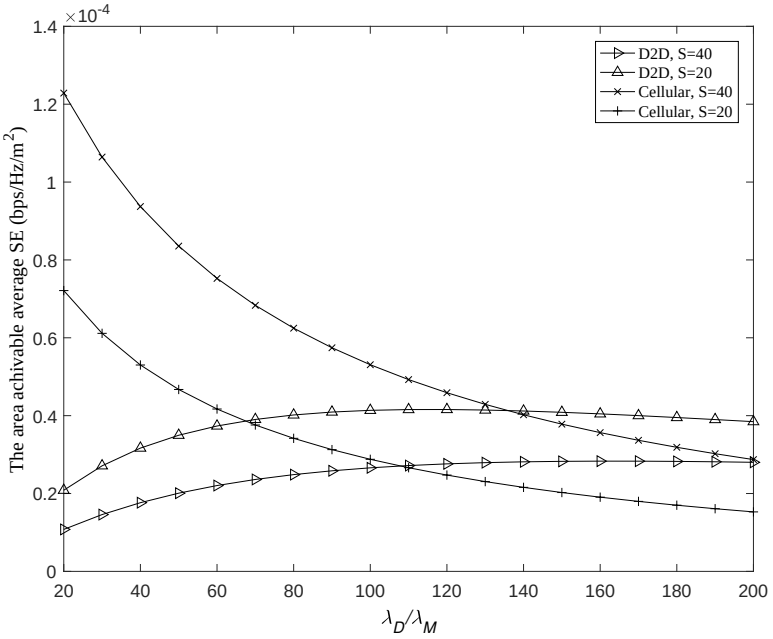

Figure 6.9: Effects of D2D density with the variation of number of cellular users on SE.

cellular interference has a big adverse effect on the EE of a CUE. Figure 6.10(b) shows the effects of different S and D2D densities on EE of a D2D transmitter. When more uplink transmissions are supported by massive MIMO aided cellular, the cellular-to-D2D interference increases, which has a detrimental effect on the EE of a D2D transmitter. The interference from other D2D transmissions also degrades the D2D performance. Moreover, it is indicated from Figure 6.10(a) and Figure 6.10(b) that the EE of a CUE can be comparable to that of a D2D transmitter.

Similarly, to clearly compare the EE of the CUE and D2D transmitter, the EE versus λ_d in a 2-D plot with $S = 20$ and $S = 40$ is displayed. From the Figure 6.11 it can be observed that when the CUE number is small, each D2D transmitter outperforms CUE in terms of EE. However, when the S is doubled, CUE has a much higher average EE than D2D transmitters even though both EE decrease. This means that when the network is dense, more users should connect to the massive MIMO enabled MBSs for higher EE.

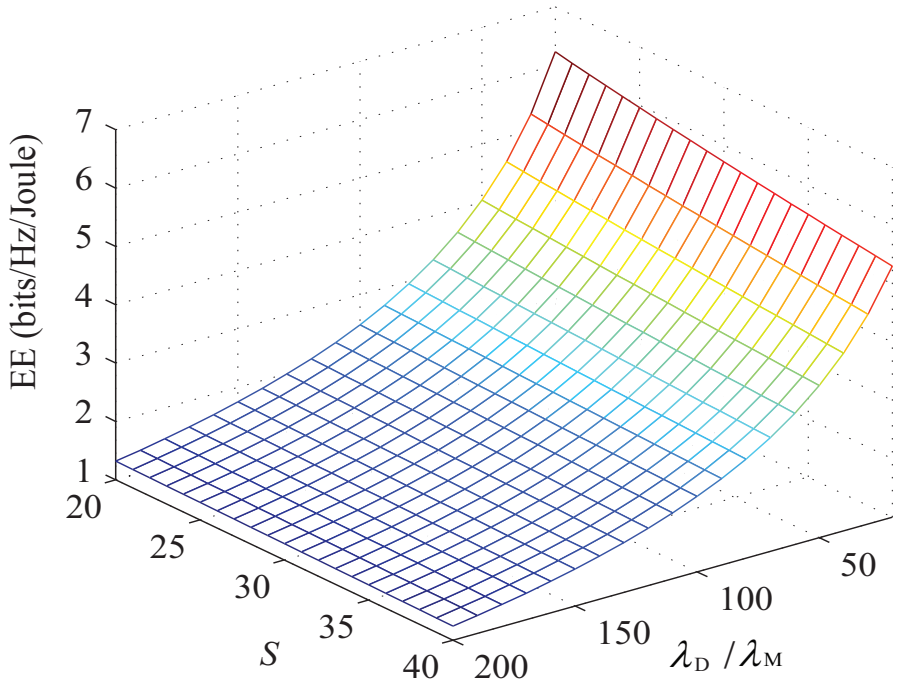

(a) Area EE of the cellular.

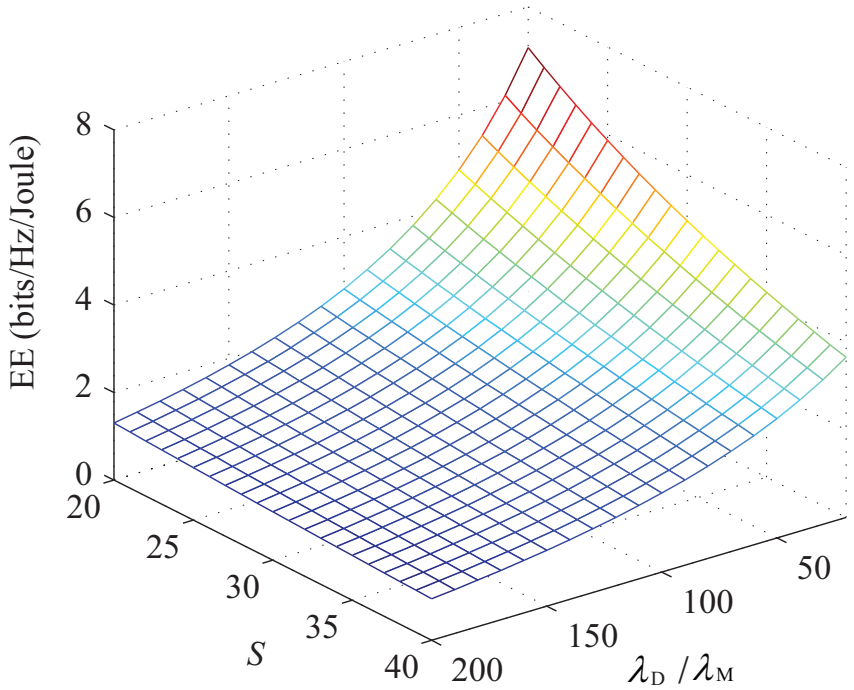

(b) Area EE of the D2D.

Figure 6.10: Effects of different S and D2D densities on area EE.

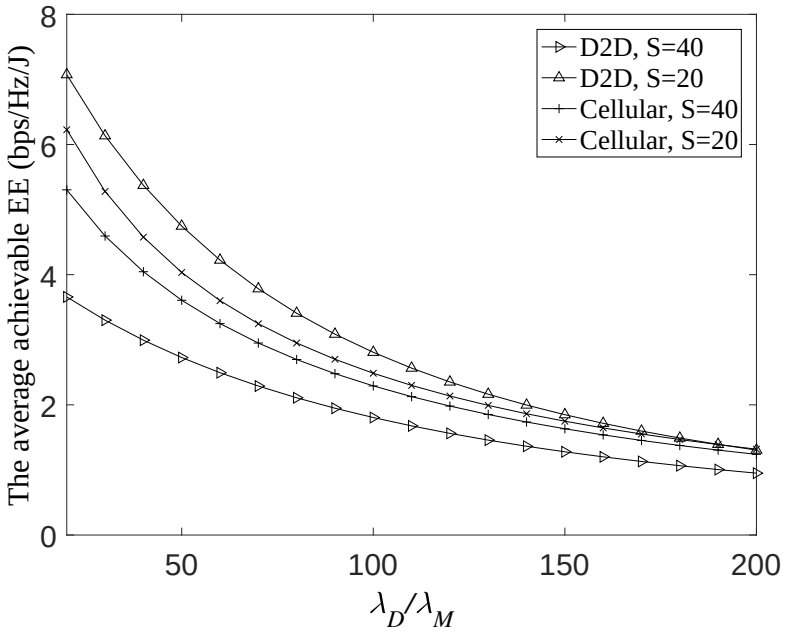

Figure 6.11: Effects of D2D density with the variation of number of cellular users on EE.

6.6 Summary

This chapter concentrated on the uplink power control in the D2D underlaid massive MIMO cellular networks. Specifically, the open-loop power control was applied in the cellular networks for controlling the cellular user's transmit power, to mitigate the cellular-to-D2D interference. A low-complexity D2D power control is adopted, in which D2D transmit power should be controlled such that the interfering signal power received by its closest cellular BS should not exceed than a threshold, to mitigate the D2D-to-cellular interference. The area average SE expressions for the cellular and D2D are derived to characterize the effects of power control, massive MIMO and D2D density. The results confirmed that the implementation of power control in both the cellular and D2D is necessary for guaranteeing the quality of services of the cellular users and D2D receivers. For the ultra-dense D2Ds case, cellular performance degradation can be relieved by using the considered D2D power control. For the case that massive MIMO enabled BSs serve large numbers of cellular users, the D2D performance can be significantly deteriorated,

which indicates that cellular power control is required for suppressing the cellular-to-D2D interference.

Chapter 7

Conclusions and Future Work

7.1 Conclusions

This research work quantified and evaluated the network efficiency gain achieved by the integration of multiple 5G candidate architectures and technologies such as heterogeneous networks (HetNets), cloud radio access network (C-RAN), massive multiple input multiple output (MIMO) transmission and device-to-device (D2D) communication. Interference management mechanisms such as soft fractional frequency reuse (S-FFR) and open loop power control (OLPC) were applied accordingly to mitigate interference. As the analysis was dedicated to evaluating and enhancing the network performance, related key performance indicators (KPIs) such as spectrum efficiency (SE) and energy efficiency (EE) were derived as tractable expressions with the help of mathematical tools from stochastic geometry.

The downlink performance of a k-tier HetNet equipped with massive MIMO enabled macro base stations (MBSs) was evaluated in Chapter 3. The exact expressions for the probability of a user being associated with a macro cell or a small cell was derived in Section 3.2. Based on the user association probability functions, analytical expressions for the KPIs in terms of coverage, SE and EE in the proposed network were derived as well. Compared with conventional HetNets, the implementation of massive MIMO in the macro cell can decrease the demands for small cells while improve the SE, which

simplified the network deployment during the network planning. Section 3.3 considered the impact of applying cell range expansion (CRE) in small cells, which allowed tier selection for cell load balancing. The results proved that the EE of HetNets can be improved via offloading suitable data traffic to small cells. However, too much macro cell users associated with the small cell will degrade the HetNets SE and EE.

The co-effects of massive MIMO and C-RAN on the HetNet performance were comprehensively analysed in Chapter 4. Asymptotic expressions for the throughput and EE of the remote radio heads (RRHs) tier and the macrocell tier were derived for quantifying the network performance. Meanwhile, the S-FFR was employed to mitigate the inter-tier interference. In such a highly integrative network, it is proven that massive MIMO with dense deployment of RRHs can significantly enhance the throughput while more frequency resources allocated to the RRHs can enhance the EE of a HC-RAN. Note that the S-FFR factor should be carefully chosen, since its effect depends on the density of the RRHs.

Due to the fact that more and more users are served in the massive MIMO equipped HetNets, the uplink inter cell interference was well managed via power control in Chapter 5 and its impact on network performance was analysed. After applying an OLPC mechanism in picocells, a tight lower bound of the area uplink SE for the massive MIMO macrocell tier and the exact area uplink SE for the picocell tier were derived. Results shown that the network performance in the macrocells can be significantly improved through applying OLPC in the small cells, while more uplink transmissions in the macrocells had mild adverse effect on the uplink performance in the small cells. In addition, the uplink performance of the massive MIMO macrocells can be improved by expanding the small cell range when dozens of users are served in the macro cells.

A tractable approach to analyse the tight lower bound expressions for the area SE and EE of the cellular and D2D tier was developed in Chapter 6. Two obtained important properties related to the D2D density were regarded as sufficient conditions for satisfying the expected SE. The average power consumption for a cellular user or D2D transmitter

was derived to evaluate EE. The effectiveness of the proposed power control design were confirmed to be able to mitigate the D2D-to-cellular interference.

In summary, the derived KPI expressions from this thesis can be used directly to obtain a good estimation on the performance of various wireless technologies in different network scenarios. The in-depth analysis on the key influencing factors can help network operators and wireless engineers choose appropriate technology and parameters in 5G network planning.

7.2 Future Work

7.2.1 Performance analysis for QoS metrics in HetNets

5G network is expected to deliver high quality of service (QoS) for assuring user experience in addition to high network SE and EE. Meanwhile, QoS requirements have changed according to the emerging applicaitons. Instead of context and audio, streaming video dominates the data traffic now and future, which means higher data rate and lower delay are urgently needed. Therefore, quality of service (QoS) related metrics such as error rates and transmission delay needs to be quantitatively measured in 5G HetNets. Moreover, as pointed in [ARS16], traditional QoS model and parameters may not be sufficient to address new challenges imposed by emerging 5G applications and services. Therefore, investigations into quantifying QoS metrics and proposing novel QoS metrics in HetNets are waited to be conducted.

7.2.2 Performance analysis for cell-edge users in user-centric dense network

As mentioned in [IHX+16], the new paradigm of the 5G networks will shift from the BS-centric to the user-centric. The motivaiton behind it is that the dense deployment

of small cells is regarded as a key technology enabler to meet the exponential growth of data traffic. In such a network, the cell edge users are particularly vulnerable as they experience more severe and complex interference compared to cell center users. To enhance the cell-edge users performance, there are several advanced physical layer technologies are proposed in conventional BS-centric networks. For example, coordinated multi-point (CoMP) can achieve high cell-edge user SE and improve coverage when multiple base stations coordinate their transmission to the same receiver [IDM+11]; the use of milli-meter wave (mmWave) frequencies, which is in 30GHz-300GHz, has been proposed as a strong candidate approach to achieve high performance gain in terms of SE and EE [RSM+13]; as D2D SINR is better when the D2D pair is farther away from the MBSs [YTDR09], deploying D2D pairs at the cell-edge has potentials to improve the cell-edge user experience. However, designing a user-centric ultra-dense small cell network for enhancing cell-edge user performance is still an open issue.

To complement the above mentioned theoretical modelling in the future works, stochastic geometry can still be employed to analyse network performance accurately. Exact or approximation expressions for KPIs are worth be derived. Monte Carlo simulation should be developed for validating the network design and performance analysis. Finally, the impact of different technologies on QoS or cell edge users needs to be scrutinized to lay a solid base for leading up the 5G network research works.

Appendix A

Rayleigh Fading

Rayleigh fading is a commonly used statistical model for the effect of a propagation environment on a radio signal in wireless network. When the multiple reflective paths are large in number and there is no line-of-sight signal component, the envelope of the received signal τ is statistically described by a Rayleigh probability density function (PDF) [Skl97], which can be expressed as:

$$f(\tau) = \frac{2\tau}{\sigma} e^{-\tau^2/\sigma} \tag{A.1}$$

where σ is the scale parameter of the distribution. Rayleigh fading is often classified as the worst case fading type.

Appendix B

Proofs in Chapter 3

B.1 Faà di Bruno's Formula

The Faà di Bruno's Formula is defined as [Cra05]

$$\frac{d^{\mathrm{n}}}{dx^{\mathrm{n}}} f\left(g(x)\right) = \sum \frac{\mathrm{n}!}{\mathrm{m}_1!1!^{\mathrm{m}_1}\mathrm{m}_2!2!^{\mathrm{m}_2}\cdots \mathrm{m}_{\mathrm{n}}!\mathrm{n}!^{\mathrm{m}_{\mathrm{n}}}} \cdot f^{(\mathrm{m}_1+\cdots+\mathrm{m}_{\mathrm{n}})}\left(g\left(x\right)\right) \cdot \prod_{j=1}^{\mathrm{n}} \left(g^{(j)}\left(x\right)\right)^{\mathrm{m}_j} \tag{B.1}$$

where the sum is over all n-tuples of non-negative integers $(\mathrm{m}_1, \cdots, \mathrm{m}_{\mathrm{n}})$ satisfying the constraint

$$1 \cdot \mathrm{m}_1 + 2 \cdot \mathrm{m}_2 + 3 \cdot \mathrm{m}_3 + \cdots + \mathrm{n} \cdot \mathrm{m}_{\mathrm{n}} = \mathrm{n} \tag{B.2}$$

In section 3.2.3.1, $\exp\left(-\frac{\gamma Sz\left(\tau+\delta^2\right)}{P_M\beta}\right)$ is set as $f\left(g(x)\right)$, $-\frac{\gamma Sz\left(\tau+\delta^2\right)}{P_M\beta}$ is set as $g(x)$. Then according to the properties of exponential function, (3.20) can be obtained.

B.2 Integration by Parts

The spectrum efficiency between a typical user and its serving base station is commonly expressed as

$$\text{Throughput} = \mathrm{E}\left\{\log_2(1+\text{SINR})\right\} \tag{B.3}$$

which is a function of SINR. To convert this expression into a function of the coverage probability, we have the following steps

$$\begin{aligned}
\text{Throughput} &= \mathrm{E}\left\{\log_2(1+\text{SINR})\right\} \\
&= \mathrm{E}\left\{\ln(1+\text{SINR})/\ln 2\right\} \\
&\overset{(a)}{=} \frac{1}{\ln 2}\int_0^\infty \ln(1+x)f(x)dx \\
&\overset{(b)}{=} \frac{1}{\ln 2}\left(F(x)\ln(1+x)|_0^\infty - \int_0^\infty \frac{F(x)}{1+x}dx\right) \\
&= \frac{1}{\ln 2}\left(\int_0^\infty \frac{1}{1+x}dx - \int_0^\infty \frac{F(x)}{1+x}dx\right) \\
&= \frac{1}{\ln 2}\left(\int_0^\infty \frac{1-F(x)}{1+x}dx\right) \\
&\overset{(c)}{=} \frac{1}{\ln 2}\int_0^\infty \frac{\mathrm{P}(\text{SINR}>x)}{1+x}dx
\end{aligned} \tag{B.4}$$

where SINR is set as x in (a), (b) is using integration by parts and (c) is due to that the coverage probability of a user is equal to the complementary cumulative distribution function of its SINR.

References

[5GP] 5G-PPP 5G Vision. [Online]. Available: https://5g-ppp.eu/flayer-brochure/.

[ABC+14] J. G. Andrews, S. Buzzi, Wan Choi, S.V. Hanly, A. Lozano, A.C.K. Soong, and J.C. Zhang. What will 5G be? *IEEE J. Sel. Areas Commun.*, 32(6):1065–1082, June 2014.

[ABG11] J. G. Andrews, F. Baccelli, and R.K. Ganti. A tractable approach to coverage and rate in cellular networks. *IEEE Trans. Commun.*, 59(11):3122–3134, November 2011.

[AEA15] K. S. Ali, H. ElSawy, and M. S. Alouini. On mode selection and power control for uplink D2D communication in cellular networks. In *IEEE Int. Conf. on Commun. Workshop (ICCW)*, pages 620–626, 2015.

[AGD+11] G. Auer, V. Giannini, C. Desset, I. Godor, P. Skillermark, M. Olsson, M.A. Imran, D. Sabella, M.J. Gonzalez, O. Blume, and A. Fehske. How much energy is needed to run a wireless network? *IEEE Wireless Commun.*, 18(5):40–49, Oct. 2011.

[And13] J. G. Andrews. Seven ways that HetNets are a cellular paradigm shift. *IEEE Commun. Mag.*, 51(3):136–144, March 2013.

[ARS16] M. Agiwal, A. Roy, and N. Saxena. Next generation 5g wireless networks: A comprehensive survey. *IEEE Commun. Surveys & Tutorials*, 18(3):1617–1655, thirdquarter 2016.

[AS70] M. Abramowitz and I. A. Stegun. *Handbook of Mathematical Functions with Formulas, Graphs, and Mathematical Tables.* Dover Publications, New York, 9th edition, 1970.

[AWM14] A. Asadi, Qing Wang, and V. Mancuso. A survey on device-to-device communication in cellular networks. *IEEE Commun. Surveys & Tutorials*, 16(4):1801–1819, 2014.

[B+16] Federico Boccardi et al. Why to decouple the uplink and downlink in cellular networks and how to do it. *IEEE Commun. Mag.*, March 2016.

[BB09] F. Baccelli and B. Błszczyszyn. *Stochastic Geometry and Wireless Net-*

works, Volume I: Theory. Now Publishers Inc. Hanover, MA, USA, 2009.

[BBPC16] Dilip Bethanabhotla, Ozgun Y. Bursalioglu, Haralabos C. Papadopoulos, and Giuseppe Caire. Optimal user-cell association for massive MIMO wireless networks. *IEEE Trans. Wireless Commun.*, March 2016.

[BHL+14] F Boccardi, R. W. Heath, A. Lozano, T. L. Marzetta, and P. Popovski. Five disruptive technology directions for 5G. *IEEE Commun. Mag.*, 52(2):74–80, February 2014.

[BKLZ97] François Baccelli, Maurice Klein, Marc Lebourges, and Sergei Zuyev. Stochastic geometry and architecture of communication networks. *Telecommunication Systems*, 7(1):209–227, 1997.

[BPG+09] G. Boudreau, J. Panicker, N. Guo, R. Chang, N. Wang, and S. Vrzic. Interference coordination and cancellation for 4G networks. *IEEE Commun. Mag.*, 47(4):74–81, April 2009.

[BSHD14] E. Björnson, L. Sanguinetti, J. Hoydis, and M. Debbah. Designing multi-user MIMO for energy efficiency: When is massive MIMO the answer? In *IEEE Int. Wireless. Commun. Networks.Conf. (WCNC)*, April 2014.

[BSHD15] Emil Bjornson, Luca Sanguinetti, Jakob Hoydis, and Mérouane Debbah. Optimal design of energy-efficient multi-user MIMO systems: Is massive MIMO the answer? *IEEE Trans. Wireless Commun.*, 14(6):3059–3075, 2015.

[BTAS14] Boyd Bangerter, Shilpa Talwar, Reza Arefi, and Kyle Stewart. Networks and devices for the 5G era. *IEEE Commun. Mag.*, 52(2):90–96, 2014.

[CCY+15] Aleksandra Checko, Henrik L Christiansen, Ying Yan, Lara Scolari, Georgios Kardaras, Michael S Berger, and Lars Dittmann. Cloud RAN for mobile networks : a technology overview. *IEEE Commun. Surveys & Tutorials,*, 17(1):405–426, 2015.

[CLRH+14] I Chih-Lin, Corbett Rowell, Shuangfeng Han, Zhikun Xu, Gang Li, and Zhengang Pan. Toward green and soft: a 5G perspective. *IEEE Commun. Mag.*, 52(2):66–73, 2014.

[Cra05] Alex D. D. Craik. Prehistory of Faà di bruno's formula. *The American*

Mathematical Monthly, 112(2):119–130, 2005.

[CZXL11] Yan Chen, Shunqing Zhang, Shugong Xu, and Geoffrey Ye Li. Fundamental trade-offs on green wireless networks. *IEEE Commun. Mag.*, 49(6):30–37, 2011.

[DGBA12a] H. S. Dhillon, R. K. Ganti, F. Baccelli, and J. G. Andrews. Modeling and analysis of K-tier downlink heterogeneous cellular networks. *IEEE J. Sel. Areas Commun.*, 30(3):550–560, April 2012.

[DGBA12b] Harpreet S Dhillon, Radha Krishna Ganti, Francois Baccelli, and Jeffrey G Andrews. Modeling and analysis of K-tier downlink heterogeneous cellular networks. *IEEE J. Sel. Areas Commun.*, 30(3):550–560, 2012.

[DHL12] L. Ding, J. He, and Z. Liu. A novel open loop power control method in LTE uplink. In *Int. Conf. on Wireless Commun. Networking and Mobile Computing (WiCOM)*, pages 1–4, Sept 2012.

[DP13] Zhiguo Ding and H.V. Poor. The use of spatially random base stations in cloud radio access networks. *IEEE Signal Process. Lett.*, 20(11):1138–1141, Nov. 2013.

[DRG14] M. Di Renzo and Peng Guan. Stochastic geometry modeling of coverage and rate of cellular networks using the Gil-Pelaez inversion theorem. *IEEE Commun. Lett.*, 18(9):1575–1578, 2014.

[DRGC13] Marco Di Renzo, Alessandro Guidotti, and Giovanni Emanuale Corazza. Average rate of downlink heterogeneous cellular networks over generalized fading channels: a stochastic geometry approach. *IEEE Trans. Commun.*, 61(7):3050–3071, 2013.

[EHA14] H. ElSawy, E. Hossain, and M. S. Alouini. Analytical modeling of mode selection and power control for underlay D2D communication in cellular networks. *IEEE Trans. Commun.*, 62(11):4147–4161, November 2014.

[EHH13] H. ElSawy, E. Hossain, and M. Haenggi. Stochastic geometry for modeling, analysis, and design of multi-tier and cognitive cellular wireless networks: A survey. *IEEE Commun. Surveys & Tutorials*, 15(3):996–1019, 2013.

[FLYW+14] D. Feng, L. Lu, Y. Yuan-Wu, G. Y. Li, S. Li, and G. Feng. Device-to-device communications in cellular networks. *IEEE Commun. Mag.*, 52(4):49–55, 2014.

[GBCC11] Jaheon Gu, Sueng Jae Bae, Bum-Gon Choi, and Min Young Chung. Dynamic power control mechanism for interference coordination of device-to-device communication in cellular networks. In *Int. Conf. on Ubiquitous and Future Networks (ICUFN)*, pages 71–75, June 2011.

[GJ15] A. Gupta and R. K. Jha. A survey of 5G network: Architecture and emerging technologies. *IEEE Access 3:1206-1232*, 3:1206–1232, 8 2015.

[Gol05] Andrea Goldsmith. *Wireless communications*. Cambridge university press, 2005.

[GR07] I. S. Gradshteyn and I. M. Ryzhik. *Table of Integrals, Series and Products*. Academic Press, San Diego, C.A., 7th edition, 2007.

[GWLH14] W. Gong, X. Wang, M. Li, and Z. Huang. Round-robin resource sharing algorithm for device-to-device multicast communications underlying single frequency networks. In *Int. Conf. on Telecommun. (ICT)*, pages 191–195, May 2014.

[HAB+09] M. Haenggi, J. G. Andrews, F. Baccelli, O. Dousse, and M. Franceschetti. Stochastic geometry and random graphs for the analysis and design of wireless networks. *IEEE J. Sel. Areas Commun.*, 27(7):1029–1046, Sept 2009.

[Hae12] Martin Haenggi. *Stochastic geometry for wireless networks*. Cambridge University Press, 2012.

[Ham08] K. A. Hamdi. Capacity of MRC on correlated rician fading channels. *IEEE Trans. Commun.*, 56(5):708–711, May 2008.

[HH15a] E. Hossain and M. Hasan. 5G cellular: Key enabling technologies and research challenges. *IEEE Instrumentation Measurement Mag.*, 18(3):11–21, June 2015.

[HH15b] E. Hossain and M. Hasan. 5G cellular: Key enabling technologies and research challenges. *IEEE Instrumentation Measurement Mag.*, 18(3):11–

21, Jun. 2015.

[HK12] R. W. Heath and M. Kountouris. Modeling heterogeneous network interference. In *Information Theory and Applications Workshop (ITA)*, pages 17–22, 2012.

[HKB13] Robert W Heath, Marios Kountouris, and Tianyang Bai. Modeling heterogeneous network interference using poisson point processes. *IEEE Trans. Signal Process.*, 61(16):4114–4126, 2013.

[HL14] Kaibin Huang and V. K. N. Lau. Enabling wireless power transfer in cellular networks: Architecture, modeling and deployment. *IEEE Trans. Wireless Commun.*, 13(2):902–912, February 2014.

[HNDZ16] Y. Huang, A. A. Nasir, S. Durrani, and X. Zhou. Mode selection, resource allocation, and power control for D2D-enabled two-tier cellular network. *IEEE Trans. Commun.*, 64(8):3534–3547, August 2016.

[HQ14] Rose Hu and Yi Qian. An energy efficient and spectrum efficient wireless heterogeneous network framework for 5G systems. *IEEE Commun. Mag.*, 52(5):94–101, 2014.

[HTBD13] Jakob Hoydis, Stephan Ten Brink, and Mérouane Debbah. Massive MIMO in the UL/DL of cellular networks: How many antennas do we need? *IEEE J. Sel. Areas Commun.*, 31(2):160–171, 2013.

[HTC12] Hoon Huh, A. M. Tulino, and G. Caire. Network MIMO with linear zero-forcing beamforming: Large system analysis, impact of channel estimation, and reduced-complexity scheduling. *IEEE Trans. Inf. Theory*, 58(5):2911–2934, May 2012.

[HYA14] K. Hosseini, Wei Yu, and R. S. Adve. Large-scale MIMO versus network MIMO for multicell interference mitigation. *IEEE J. Sel. Areas Commun.*, 8(5):930–941, October 2014.

[IDM+11] R. Irmer, H. Droste, P. Marsch, M. Grieger, G. Fettweis, S. Brueck, H. P Mayer, L. Thiele, and V. Jungnickel. Coordinated multipoint: Concepts, performance, and field trial results. *IEEE Commun. Mag.*, 49(2):102–111, February 2011.

[IHX+16] C. L. I, S. Han, Z. Xu, S. Wang, Q. Sun, and Y. Chen. New paradigm of 5G wireless internet. *IEEE J. Sel. Areas Commun.*, 34(3):474–482, March 2016.

[JMMY09] Han-Shin Jo, Cheol Mun, June Moon, and Jong-Gwan Yook. Interference mitigation using uplink power control for two-tier femtocell networks. *IEEE Trans. Wireless Commun.*, 8(10):4906–4910, 2009.

[JMZ+14] V. Jungnickel, K. Manolakis, W. Zirwas, B. Panzner, V. Braun, M. Lossow, M. Sternad, R. Apelfrojd, and T. Svensson. The role of small cells, coordinated multipoint, and massive MIMO in 5G. *IEEE Commun. Mag.*, 52(5):44–51, May 2014.

[JSXA12] Han-Shin Jo, Young Jin Sang, Ping Xia, and J.G. Andrews. Heterogeneous cellular networks with flexible cell association: A comprehensive downlink SINR analysis. *IEEE Trans. Wireless Commun.*, 11(10):3484–3495, October 2012.

[Jun15] Xu Jun. Progress on 5G radio link enhancement. *ZTE Technologies No.3 Special Topic on 5G*, 2015.

[KHXR15] F.A. Khan, Huasen He, Jiang Xue, and T. Ratnarajah. Performance analysis of cloud radio access networks with distributed multiple antenna remote radio heads. *IEEE Trans. Signal Process.*, 63(18):4784–4799, September 2015.

[KTV12] C. Khirallah, J.S. Thompson, and D. Vukobratovic. Energy efficiency of heterogeneous networks in LTE-advanced. *J. Signal Process.*, 69(1):105–113, 2012.

[LETM14] Erik G Larsson, Ove Edfors, Fredrik Tufvesson, and Thomas L Marzetta. Massive MIMO for next generation wireless systems. *IEEE Commun. Mag.*, 52(2):186–195, 2014.

[LHA15] Xingqin Lin, Robert W Heath, and Jeffrey G Andrews. The interplay between massive MIMO and underlaid D2D networking. *IEEE Trans. Wireless Commun.*, 14(6):3337–3351, 2015.

[LLAH15] Namyoon Lee, Xingqin Lin, Jeffrey G Andrews, and RW Heath. Power

control for D2D underlaid cellular networks: Modeling, algorithms, and analysis. *IEEE J. Sel. Areas Commun.*, 33(1):1–13, 2015.

[LOZ16] Min Lin, Jian Ouyang, and Wei-Ping Zhu. Joint beamforming and power control for device-to-device communications underlaying cellular networks. *IEEE J. Sel. Areas Commun.*, 34(1):138–150, 2016.

[LPGdlR+11] D. Lopez-Perez, I. Guvenc, G. de la Roche, M. Kountouris, T. Q. S. Quek, and J. Zhang. Enhanced intercell interference coordination challenges in heterogeneous networks. *IEEE Wireless Communi.*, 18(3):22–30, June 2011.

[LSZ+10] Y. Lin, L. Shao, Z. Zhu, Q. Wang, and R. K. Sabhikhi. Wireless network cloud: Architecture and system requirements. *IBM J. of Research and Development*, 54(1):4:1–4:12, January 2010.

[LWC+15a] D. Liu, L. Wang, Y. Chen, T. Zhang, K. Chai, and M. Elkashlan. Distributed energy efficient fair user association in massive MIMO enabled hetnets. *IEEE Commun. Lett.*, PP(99):1–4, 2015.

[LWC+15b] D. Liu, L. Wang, Y. Chen, T. Zhang, K. Chai, and M. Elkashlan. Distributed energy efficient fair user association in massive MIMO enabled hetnets. *IEEE Commun. Lett.*, PP(99):1–4, 2015.

[LWC+16] D. Liu, L. Wang, Y. Chen, M. Elkashlan, K. K. Wong, R. Schober, and L. Hanzo. User association in 5G networks: A survey and an outlook. *IEEE Commun. Surveys & Tutorials*, pages 1–27, 2016.

[Mad13] Joe Madden. Cloud ran or small cells? *Fierce Broadband Wireless Online Mag.*, 2013.

[Mar10] T. L. Marzetta. Noncooperative cellular wireless with unlimited numbers of base station antennas. *IEEE Trans. Wireless Commun.*, 9(11):3590–3600, November 2010.

[Mia13] Guowang Miao. Energy-efficient uplink multi-user MIMO. *IEEE Trans. Wireless Commun.*, 12(5):2302–2313, 2013.

[MLPH11] H. Min, J. Lee, S. Park, and D. Hong. Capacity enhancement using an interference limited area for device-to-device uplink underlaying cellular

networks. *IEEE Trans. Wireless Commun.*, 10(12):3995–4000, December 2011.

[MLY+16] C. Ma, Y. Li, H. Yu, X. Gan, X. Wang, Y. Ren, and J. J. Xu. Cooperative spectrum sharing in D2D-enabled cellular networks. *IEEE Trans. Commun.*, 64(10):4394–4408, October 2016.

[Mob11] China Mobile. C-RAN: the road towards green RAN. *White Paper, ver*, 2, 2011.

[NAS+10] T. Novlan, J. G. Andrews, I. Sohn, R. K. Ganti, and A. Ghosh. Comparison of fractional frequency reuse approaches in the OFDMA cellular downlink. In *IEEE Global Telecommun. Conf.(GLOBECOM)*, pages 1–5, Dec 2010.

[NDA13a] T. D. Novlan, H. S. Dhillon, and J. G. Andrews. Analytical modeling of uplink cellular networks. *IEEE Trans. Wireless Commun.*, 12(6):2669–2679, June 2013.

[NDA13b] Thomas D Novlan, Harpreet S Dhillon, and Jeffrey G Andrews. Analytical modeling of uplink cellular networks. *IEEE Trans. Wireless Commun.*, 12(6):2669–2679, 2013.

[NLM13a] H. Q. Ngo, E. G. Larsson, and T. L. Marzetta. Energy and spectral efficiency of very large multiuser MIMO systems. *IEEE Trans. Commun.*, 61(4):1436–1449, April 2013.

[NLM13b] H. Q. Ngo, E. G. Larsson, and T. L. Marzetta. The multicell multiuser MIMO uplink with very large antenna arrays and a finite-dimensional channel. *IEEE Trans. Commun.*, 61(6):2350–2361, June 2013.

[PLJ+14a] Mugen Peng, Yuan Li, Jiamo Jiang, Jian Li, and Chonggang Wang. Heterogeneous cloud radio access networks: A new perspective for enhancing spectral and energy efficiencies. *IEEE Wireless Commun.*, 21(6):126–135, 2014.

[PLJ+14b] Mugen Peng, Yuan Li, Jiamo Jiang, Jian Li, and Chonggang Wang. Heterogeneous cloud radio access networks: a new perspective for enhancing spectral and energy efficiencies. *IEEE Wireless Commun.*, 21(6):126–135,

2014.

[PLZW15] Mugen Peng, Yong Li, Zhongyuan Zhao, and Chonggang Wang. System architecture and key technologies for 5G heterogeneous cloud radio access networks. *IEEE Network*, 29(2):6–14, 2015.

[PTHX13] Jinlin Peng, Hao Tang, Peilin Hong, and Kaiping Xue. Stochastic geometry analysis of energy efficiency in heterogeneous network with sleep control. *IEEE Wireless Commun. Letters*, 2(6):615–618, 2013.

[PWLP15] Mugen Peng, Chonggang Wang, V. Lau, and H.V. Poor. Fronthaul-constrained cloud radio access networks: Insights and challenges. *IEEE Wireless Commun.*, 22(2):152–160, April 2015.

[PZJ+15] M. Peng, K. Zhang, J. Jiang, J. Wang, and W. Wang. Energy-efficient resource assignment and power allocation in heterogeneous cloud radio access networks. *IEEE Trans. Veh. Technol.*, pages 1–13, 2015.

[QCK11] Tony QS Quek, Wang Chi Cheung, and Marios Kountouris. Energy efficiency analysis of two-tier heterogeneous networks. In *European Wireless Conf. Sustainable Wireless Technol. (European Wireless)*, pages 1–5. VDE, 2011.

[QdlRGK13] Tony QS Quek, Guillaume de la Roche, İsmail Güvenç, and Marios Kountouris. *Small cell networks: Deployment, PHY techniques, and resource management*. Cambridge University Press, 2013.

[R1-11] 3GPP R1-112381. Uplink co-channel HetNet performance and PC optimization. *3GPP TSG RAN WG1 No.66*, August 22-26 2011.

[RPL+13] Fredrik Rusek, Daniel Persson, Buon Kiong Lau, Erik G Larsson, Thomas L Marzetta, Ove Edfors, and Fredrik Tufvesson. Scaling up MIMO: Opportunities and challenges with very large arrays. *IEEE Signal Process. Mag.*, 30(1):40–60, 2013.

[RSM+13] Theodore S Rappaport, Shu Sun, Rimma Mayzus, Hang Zhao, Yaniv Azar, Kevin Wang, George N Wong, Jocelyn K Schulz, Mathew Samimi, and Felix Gutierrez. Millimeter wave mobile communications for 5G cellular: It will work! *IEEE access*, 1:335–349, 2013.

[SBK+15] Serveh Shalmashi, Emil Björnson, Marios Kountouris, Ki Won Sung, and Mérouane Debbah. Energy efficiency and sum rate tradeoffs for massive MIMO systems with underlaid device-to-device communications. *EURASIP J. Wireless Commun. Netw.*, 2015.

[She15] X. Shen. Device-to-device communication in 5G cellular networks: Challenges, solutions and future directions. *IEEE Network*, 29(2):2–3, March 2015.

[Skl97] B. Sklar. Rayleigh fading channels in mobile digital communication systems .I. characterization. *IEEE Commun. Mag.*, 35(7):90–100, Jul 1997.

[SQKS13] Yong Sheng Soh, T. Q. S. Quek, M. Kountouris, and Hyundong Shin. Energy efficient heterogeneous cellular networks. *IEEE J. Sel. Areas Commun.*, 31(5):840–850, May 2013.

[SSD+09] Lene Tolstrup Sørensen, Knud Erik Skouby, Daniel Dietterle, Ashok Jhunjhunwala, Xiaozhen Fu, and Xiaochun Wang. User scenarios 2020: a worldwide wireless future. *WWRF Outlook*, (4), 2009.

[SSP+13] Krystian Safjan, Stanislaw Strzyz, Klaus Pedersen, Jens Steiner, Claudio Rosa, et al. Open loop power control parameter settings impact on LTE HetNet uplink performance. In *IEEE Int. Conf. Commun. (ICC) Workshops*, pages 1134–1138, 2013.

[TSAJ14] Ralph Tanbourgi, Sushil Singh, Jeffrey G Andrews, and Friedrich K Jondral. A tractable model for non-coherent joint-transmission base station cooperation. *IEEE Trans. Wireless Commun.*, 13(9):4959–4973, 2014.

[WHG+14] Cheng-Xiang Wang, Fourat Haider, Xiqi Gao, Xiao-Hu You, Yang Yang, Dongfeng Yuan, Hadi Aggoune, Harald Haas, Sam Fletcher, and Erol Hepsaydir. Cellular architecture and key technologies for 5G wireless communication networks. *IEEE Commun. Mag.*, 52(2):122–130, 2014.

[WNE+15] L. Wang, H. Q. Ngo, M. Elkashlan, T. Q. Duong, and K. K. Wong. Massive MIMO in spectrum sharing networks: Achievable rate and power efficiency. *IEEE Systems Journal*, PP(99), July 2015.

[XM15] Yi Xu and Shiwen Mao. User association in massive MIMO hetnets.

IEEE System Journal, pages 1–13, Sept 2015.

[YHX+16] Z. Yang, N. Huang, H. Xu, Y. Pan, Y. Li, and M. Chen. Downlink resource allocation and power control for device-to-device communication underlaying cellular networks. *IEEE Commun. Lett.*, 20(7):1449–1452, July 2016.

[YM15] Hong Yang and T. L. Marzetta. On existence of power controls for massive MIMO. *IEEE Int. Symposium Inf. Theory (ISIT)*, pages 2608–2612, 2015.

[YTDR09] C. H. Yu, O. Tirkkonen, K. Doppler, and C. Ribeiro. On the performance of device-to-device underlay communication with simple power control. In *IEEE Vehi. Technol. Conf. Fall (VTC)*, pages 1–5, April 2009.

[YZD+16] Y. Yang, Y. Zhang, L. Dai, J. Li, S. Mumtaz, and J. Rodriguez. Transmission capacity analysis of relay-assisted device-to-device overlay/underlay communication. *IEEE Trans. Industrial Informatics*, pages 1–9, 2016.

[ZDO+14] Zhenyu Zhou, Mianxiong Dong, Kaoru Ota, Jun Wu, and Takao Sato. Energy efficiency and spectral efficiency tradeoff in device-to-device (D2D) communications. *IEEE Wireless Commun. Lett.*, 3(5):485–488, 2014.

[ZFJ+15] W. Zhong, Y. Fang, S. Jin, K. K. Wong, S. Zhong, and Z. Qian. Joint resource allocation for device-to-device communications underlaying uplink MIMO cellular networks. *IEEE J. Sel. Areas Commun.*, 33(1):41–54, January 2015.